博 士 学 位 論 文

氏 名（本 籍）	PHILIPUS NGHILUKUNANYE HISHIMONE(NAMIBIA)
学 位 の 種 類	博　士（工学）
学 位 記 番 号	博　甲　第　153　号
学位授与年月日	平成 31 年 3 月 31 日
学位授与の要件	学位規則第４条第 1 項
学 位 論 文 題 目	THE SPRAY METHOD FOR FABRICATION OF FUNCTIONAL THIN FILMS BY DESIGNED MOLECULAR PRECURSORS IN AQUEOUS SOLUTIONS

論 文 審 査 委 員	主 査	佐 藤　光 史
	副 査	大 倉　利 典
	〃	阿 相　英 孝
	〃	工 藤　一 秋（東 京 大 学）
	〃	
	〃	
	〃	

工 学 院 大 学 大 学 院

SUMMARY OF THE THESIS

THE SPRAY METHOD FOR FABRICATION OF FUNCTIONAL THIN FILMS BY DESIGNED MOLECULAR PRECURSORS IN AQUEOUS SOLUTIONS

Applied Chemistry and Chemical Engineering Program

PHILIPUS NGHILUKUNANYE HISHIMONE

The main subjects studied in this thesis involve the application of the spray method to fabricate thin films for metallic copper (Cu) and lithium cobalt oxide (LCO) from chemical precursors of designed metal complexes, both thin films on non-crystalline quartz glass substrates and spray-coating in the air at ambient temperature and pressure. As the field of nanotechnology continues to evolve, the preference of functional thin films over their corresponding bulk counterparts is clear. For a sustainable society, the continued search for simple and cost-effective routes for the fabrication of functional thin films is, therefore, an important issue for researchers and industries alike.

CHAPTER 1: INTRODUCTION AND BACKGROUND

Chapter 1 presents the general introduction and background on the importance of functional materials with an emphasis on functional thin films. The importance of metallic copper and layered-rock-salt LCO, and their corresponding thin films is discussed. A brief review of the common deposition methods employed to fabricate thin films of metallic copper and layered LCO is presented. Deposition methods such as magnetron sputtering, pulsed laser deposition (PLD), atomic layer deposition (ALD) and chemical vapor deposition (CVD) have been established for the fabrication of high-quality thin films on both amorphous and crystalline, thermally stable substrates. However, the reactions at the atomic level are in the gaseous phase which implies that ultrahigh vacuum systems, complicated and expensive machines are

required. Although CVD does not require ultrahigh vacuum systems, the used chemical precursors with high vapor pressure are often hazardous and toxic.

In counteraction, the liquid phase deposition methods have been developed as cost-effective alternatives to the gas phase methods and, they involve the reactions between the surface of the substrate and the chemical species, in the liquid phase. The MPM was developed in our laboratory and proved to be capable of effectively fabricating nanocrystalline thin films of metals and, metal oxides and phosphates. It is based on the designing of metal complexes in coating solutions with many practical advantages such as excellent stability, homogeneity, coatability, miscibility, etc., and functional thin films are obtained after the heat-treatment of precursor films obtained by coating these coating solutions onto various thermally-stable substrates. In order to obtain precursor films that transform into functional thin films after the heat-treating procedure, the MPM is compatible with various coating methods. The Spin-coating method has been successfully used for the fabrication of various metal oxides, metal phosphates, and metal thin films, including LCO or Cu. Although spin-coating is simple, the associated limits to the size and shape of the usable substrates cannot be ignored. The spin-coating method is generally ideal with solutions employing volatile organic compounds (VOCs) as solvents. However, the use of VOC-based solutions in industries is discouraged due to concerns related to flammability and, the negative effects on human health and the ecosystem.

Presently, spray-coating and related spray-on methods are gaining momentum as preferred solution-based coating methods for industrial coatings and paintings. This is due to the associated advantages of simple instrumentation, reduced material loss and the ability to be scaled up of mass production whereby films can be produced in a Roll-to-Roll and high throughput process, in comparison to other coating procedures such as the spin-coating method. Although, a broad range of solutions which includes the aqueous-based solutions has been successfully used to obtain various kinds of thin films, scientific reports on the formation of

the precursor films necessary for the fabrication of thin films of metallic Cu and thin films of metal oxides such as LCO on amorphous substrates such as quartz glass are lacking. This is the main motivation of the present work and, the aims and objectives of this thesis are given in the concluding section of **Chapter 1**.

CHAPTER 2: METHODOLOGY

The general methodology of the study is outlined in this chapter. All chemical reagents used have been listed along with the suppliers. The experimental procedures, analyses, and measurements used to characterize the precursor solutions and the resultant thin films are discussed. In this thesis, the concept of the MPM was applied. Metal(II) complexes were prepared by reacting the metal salts with 25–28% ammonia solution in water and the obtained precursor solutions involving metal(II) complexes were spray-coated onto non-crystalline quartz glass substrates preheated at 180°C, to form the as-sprayed films. The as-sprayed films were then heat-treated under appropriate conditions to obtain thin films of metallic Cu and layered-rock-salt LCO. For each analysis and measurement, the operating principle is discussed briefly and precisely.

CHAPTER 3: FABRICATION OF HIGHLY CONDUCTIVE AND WELL-ADHERED COPPER THIN FILM ON A QUARTZ GLASS SUBSTRATE BY HEAT-TREATMENT OF A PRECURSOR FILM OBTAINED VIA SPRAY-COATING OF AN AQUEOUS SOLUTION INVOLVING COPPER(II) COMPLEXES

Chapter 3 presents the results and discussions on the fabrication of a highly conductive and well-adhered copper thin film by using MPM with the spray method. The Cu thin film on a quartz glass substrate was fabricated by a procedure involving heat-treatment of a precursor film spray-coated with an aqueous ammonia solution containing Cu(II) complexes. Under this study, the importance of designing metal(II) complexes in the aqueous coating solutions was confirmed by using different types of Cu(II) complexes. With a solution made up of a Cu(II)

complex of ethylenediamine- *N*,*N*,*N*'*N*'-tetraacetic acid ([Cu(H_2edta)]), an amorphous precursor film was obtained right after the spray-coating procedure. Heat-treatment of this film gave a non-conductive film with crystallized metallic copper. It was later confirmed *via* field-emission scanning electron microscopy (FE-SEM) and atomic-force microscopy (AFM) that the copper grains are formed as isolated agglomerates on the surface of the substrate.

However, this reaction process could be modified by using a solution with a mixture of the large [Cu(H_2edta)] complex and the smaller $[Cu(NH_3)_4]^{2+}$ complexes derived from Cu(II) formate and ammonia. The identity of the crystal structure of the film right after spray-coating changes from amorphous to crystallized phases of copper oxides, with increasing content of Cu(II) formate. In this study, the precursor solution with a 1:4 of [Cu(edta)]:Cu(II) formate ratio gave the best results with good reproducibility, among several attempts with varying the ratios. The precursor film that formed on the substrate at 180°C in the air was heat-treated at 350°C and post-annealed at 400°C by placing an identical-sized glass on top, under Ar gas flow in a tubular furnace. X-ray diffraction (XRD) pattern of the resultant film showed only peaks of Cu. The resultant film of 100 nm thickness has an adhesion strength and electrical resistivity of 37(7) MPa and 3.8(6) × 10^{-5} Ω cm, respectively. The images of AFM and FE-SEM revealed a film of well-connected Cu grains with an average surface roughness of 11 nm. The reflectance of the thin film is more than 90% in the far-infrared region. The film's chemical composition was examined by using Auger electron spectroscopy (AES) and the results indicated the presence of neutral carbon atoms, uniformly distributed throughout the film.

CHAPTER 4: THIN FILM FABRICATION AND CHARACTERIZATION OF LAYERED-ROCK-SALT $LiCoO_2$ ON QUARTZ GLASS SPRAY-COATED WITH AN AQUEOUS SOLUTION INVOLVING METAL ACETATES

Chapter 4 gives a detailed discussion on the fabrication of a thin film of layered-rock-salt LCO by using MPM with the spray method. Prior to the thin film fabrication, precursor

solutions involving $LiCH_3COO$ and $Co(CH_3COO)_2$ were prepared. Firstly, an aqueous-based solution was prepared by reacting $LiCH_3COO$ and $Co(CH_3COO)_2$ in aqueous ammonia. Secondly, an ethanol-based solution was prepared by mixing a solution of $LiCH_3COO$ reacted with butylamine in ethanol with another solution of $Co(CH_3COO)_2$ reacted with butylamine, in a 1:1 Li^+:Co^{2+} mole ratio. UV-vis analysis of both the aqueous and ethanol-based solutions confirmed the presence of Co^{2+} which indicates that coordination complexes are present in the solutions, and this is the basis of the MPM.

The heat-treatment of two different precursor film formed onto the quartz substrate *via* different coating methods gave different results. Heat-treating precursor films obtained by spin-coating either of the two solutions onto a non-crystalline quartz glass substrate at 500°C in air for 0.5 h resulted in a film of cobalt oxide (Co_3O_4). On the other hand, the heat-treatment of a precursor film formed *via* spray-coating at 500°C in air for 0.5 h, a thin film with a crystal phase of layered-rock-salt LCO was obtained. The XRD pattern of this resultant film showed only peaks assignable to the layered-rock-salt structure of $LiCoO_2$. From the FE-SEM images of these two resultant thin films, the thin film obtained via spin coating had smaller and well-connected grains, presumably of Co_3O_4. In the case of the thin film obtained via spray-coating, a plurality of elongated and isolated grains measuring about 0.1 μm could be observed. Due to the poor connectivity between the grains of the spray-coated film, the Li^+ diffusion within the matrix was very low which affect the electrical conductivity of the thin film. Therefore, Hall-effect measurements of this thin film of layered-rock-salt LCO were not successful.

Based on earlier work in our laboratory, the formation of layered-rock-salt LCO, on a crystalline substrate can be achieved by a wet-chemical process employing spin-coating. Additionally, from the surface morphology of the thin film obtained after heat-treating the spin-coated precursor film in the present work, it's clearly imaginable that a thin film of layered-rock-salt LCO with much smaller and well-connected grains, can be easily formed by spin-

coating and heat-treating a new precursor film on top of the already formed thin film obtained via spray-coating. On this basis, the thin film obtained after heat-treating the spray-coated precursor film was spin-coated further with an ethanol-based precursor solution containing the identical metal acetates and heat-treated at 500°C in air, for 0.5 h. The XRD pattern of the resultant film showed peaks assignable to the layered-rock-salt structure of $LiCoO_2$. Raman spectroscopy measurements revealed the vibrational modes assignable to layered-rock-salt $LiCoO_2$, with minor content less than 5 mol% of spinel-type Co_3O_4. The image of FE-SEM indicated that the resultant film of a 0.21 μm thickness, has no voids and is a combination of small rounded grains of ca. 10 nm in diameter and hexagonal grains larger than 0.2 μm in length. The Hall-effect measurements indicated that the resultant thin film is a *p*-type semiconductor with an electrical resistivity of 35(2) Ω cm, and a carrier concentration and carrier mobility of 8(2) × 10^{16} cm^{-3} and 2(1) cm^{-2} V^{-1} s^{-1}, respectively.

With these results, a clear distinction between spin-coating and spray-coating in ensuring the fabrication of LCO on a non-crystalline quartz glass substrate was made. The ability to fabricate LCO thin films was attributable to the mechanism of the spray-coating methods through the formation of very-fine, rigid and concentrated precursors having the Li/Co ratio of LCO. Therefore, avoiding the undesirable reaction of Li^+ ions with the non-crystalline quartz glass substrate which is suspected to be the case encountered in the spin-coating method.

CHAPTER 5: FABRICATION AND CHARACTERIZATION OF MWCNT/Cu COMPOSITE THIN FILMS VIA SPRAY-COATING OF AN AQUEOUS SOLUTION CONTAINING COPPER(II) COMPLEXES AND MWCNT

Because of its lower electrical resistivity, metallic Cu has started to be used for interconnect-lines in electronics. However, the electron theory of metals predicts that the electrical resistivity of metals will rise as the film thickness or line width approaches the conduction electron mean free path. Hanaoka *et al.* (2002) reported the electron mean free path of Cu to be around 50 nm,

and a rapid increase in resistivity of thinner films, particularly ones thinner than 100 nm is suggested. On the other hand, multiwalled carbon nanotubes (MWCNTs) are being considered for application in nanoelectronics. With a typical diameter and length of 5–100 nm and 1–20 μm, respectively, MWCNT have a high current carrying capacity (> 10^9 A cm^{-2}). Currently, the combination of carbon nanotubes and Cu to form CNT/Cu composite materials is under active research and such composite materials are promising candidates to replace pure Cu in nanoelectronics. In this thesis, the fabrication of the MWCNT/Cu composite thin films is discussed in **Chapter 5**. Composite thin films of MWCNTs and Cu on non-crystalline quartz glass substrates were fabricated by the heat-treatment of precursor films spray-coated with an aqueous ammonia solution of Cu(II) complexes (used for the fabrication of the highly-conductive copper thin film in Chapter 3) combined with an MWCNTs dispersion. Precursor solutions with MWCNTs' volume fractions of 10, 20, 30 and 50%, could be easily prepared and could be successfully spray-coated onto a quartz glass substrate preheated to 180°C, without clogging the nozzle tip. Each precursor film formed onto the substrate at 180°C in the air was heat-treated at 350°C and post-annealed at 400°C by placing an identical-sized glass on top, under Ar gas flow in a tubular furnace. The crystal structures of the resultant composite thin films were successfully analyzed by XRD and, the co-presence of MWCNTs and Cu grains was confirmed from the FE-SEM images. From the coating solution with an MWCNT volume fraction of 10%, the resultant film of 110 nm thickness has an adhesion strength and electrical resistivity of 21(7) MPa and 4.8(1) × 10^{-5} Ω cm, respectively. This composite thin film has a reflectance of more than 70% in the far-infrared region.

CHAPTER 6: CONCLUDING REMARKS AND RECOMMENDATIONS

In conclusion, the study conducted in this thesis successfully used the spray-coating method to obtain precursor films which could be heat-treated and result in thin films with acceptable functionalities. Specifically, the highly conductive and well-adhered thin film of copper could

be easily fabricated by carefully varying the ratios of the Cu(II) complexes in the aqueous precursor solution. Therefore, I believe that this method has the potential to be fine-tuned at the industrial level for the simple and cost-effective fabrication of high-quality copper thin films. The fabrication of a thin film of layered-rock-salt LCO on a non-crystalline quartz glass substrate by a liquid phase deposition method was achieved for the first time in this study. The formation of a coordination complex between the ammonia molecules and the Co^{2+} ion allowed for the preparation of a stable precursor solution which could be easily spray-coated and deposit LCO precursors, without any reaction between the Li^{+} ions and the non-crystalline quartz glass substrate. With these results, I believe that the fabrication of functional thin films of LCO can be achieved not only by heat-treating at temperatures as low as 500°C for short periods of time but also on non-crystalline quartz glass substrates. Finally, the use of the aqueous-based solution is of great advantage in terms of improved handling safety at the industrial level. A brief summary of conclusions from these major outcomes is given in **chapter 6**. In addition, recommendations for future investigations related to the fabrication of thin films for copper, LCO and MWCNT/Cu are outlined.

Publications from the major results

1. Philipus N. Hishimone, Hiroki Nagai, Masato Morita, Tetsuo Sakamoto and Mitsunobu Sato, "Highly-Conductive and Well-Adhered Cu Thin Film Fabricated on Quartz Glass by Heat Treatment of a Precursor Film Obtained Via Spray-Coating of an Aqueous Solution Involving Cu(II) Complexes.", *Coatings*, **8(10)**, **352** (**2018**).

2. Philipus N. Hishimone, Kenta Watarai, Hiroki Nagai and Mitsunobu Sato, "Thin Film Fabrication and Characterization of a Layered-rock-salt $LiCoO_2$ on a Quartz Glass Spray-coated with an Aqueous Ammonia Solution Involving Metal Acetates.", Manuscript submitted to *Coatings*, **9(2)**, **97** (**2018**).

分子プレカーサー水溶液を用いたスプレー法による機能性薄膜形成

Applied Chemistry and Chemical Engineering Program

PHILIPUS NGHILUKUNANYE HISHIMONE

本研究は，金属錯体を設計したプレカーサー水溶液をスプレー法で石英ガラス基板上へ塗布し，金属銅（Cu）とコバルト酸リチウム（LCO）薄膜の形成を達成した。薄膜は，マイクロメートル以下の厚さからなり，電気的，磁気的，光学的機能などの多様な機能を材料表面に付与できる。要するに，バルクの機能をナノレベルで置き換えることが可能である。このような機能性薄膜は，現代的なニーズを満たしつつ，未来世代のニーズをも満足させられる開発（持続可能な開発）にとって，省資源，省エネルギーなど環境の観点からも非常に重要な点である。機能性薄膜の形成法は，気相の原料と基板を反応させる気相法と，液相の原料と基板を反応させる液相法に大別できる。これまで半導体産業での成膜は，主に前者が担ってきた。一般に，原料が溶解した溶液を用いる液相法は，原料自体を気相状態にする気相法に比べて，エネルギー効率がより高い。このような観点から，気相法に匹敵する機能性薄膜形成法とその応用が望まれている。

私たちの研究室で開発した分子プレカーサー法（MPM）は，金属錯体が溶解したプレカーサー溶液を塗布，熱処理して金属や金属酸化物，リン酸化合物の薄膜を形成する方法である。プレカーサー溶液は，優れた安定性，均一性，塗布性，混和性等のような多くの実用的な利点をもつ。耐熱性の基板にプレカーサー溶液を塗布，乾燥したプレカーサー膜を熱処理で機能性薄膜を形成する。MPMは，プレカーサー溶液中の金属錯体の設計を基盤としており，安定性，均一性，混和性，塗布性の高さなどにおいて実用的な利点をもつ。エチレンジアミン四酢酸（EDTA）やニトリロ三酢酸（NTA）などの汎用的配位子を用いた安定な金属錯体と，適切なアルキルアミンを酸塩基反応によって反応させると，多種類の溶媒に溶解する組成物が得られる。さらに質の高いプレカーサー膜が，多様な塗布方法でプレカーサー溶液から形成できる。金属錯体を含むプレカーサー膜は，ゾルゲル法における有機無機ポリマーと同様に，非晶質（アモルファス）の必要がある。さもなければ，熱処理後に基板上で均一な目的膜は生成しない。このように，用いるアルキルアミン中のアルキル基は，多様な溶媒への可溶化のみならず，プレカーサー膜成分のアモルファス化にも重要な役割を果たしている。これまでにスピンコート法でプレカーサー溶液を塗布し，様々な金属酸化物，リン酸化合物，金属薄膜の形成を報告してきた。もちろん，本研究で対象としている LCO 薄膜や Cu 薄膜の形成も報告した。しかし，これまでに分子プレカーサー水溶液を調製して，スプレー法によるリン酸化合物の報告はあるが，金属酸化物と金属薄膜を形成した例が無い。また，スピンコート法で塗布する場合は，一般的に揮発性有機化合物（VOCs）を溶媒とするのが塗布性の観点から適当である。しかし，工業的には，引火の危険性や人間の健康と生態系に悪影響を与えることから，VOCs フリーの溶媒が望まれる。

現在，スプレー噴霧技術は，工業的な塗装で多く用いられる。これはシンプルなプロセスであり，スピンコート法といった塗布方法と比較してロールツーロールやハイスループットプロセスなど膜の大量形成が可

能な点や材料損失が少ないという長所があげられる。

これらの背景から，本研究では，金属錯体を設計した新たなプレカーサー水溶液を調製し，その水溶液をスプレー法で石英ガラス基板に塗布し機能性薄膜を形成することを目的とした。具体的には，金属錯体を設計し，石英ガラス基板に良く密着した Cu 薄膜の形成やスピンコート法では形成できなかった石英ガラス基板上への LCO 薄膜の形成をスプレー法で試みた。

第 1 章　背景

第 1 章では，薄膜についての背景を述べた。特に，銅薄膜と層状構造の LCO 薄膜について記載した。この章では，様々な薄膜形成法についても述べ，それらの原理を詳細に解説した。また，スプレー法の理論と実用性について記載した。最後に，研究の目的を述べた。

第 2 章　実験方法

本実験で用いた方法に関して記載した。本研究で使用した試薬リスト，プレカーサー水溶液の調製方法や形成した薄膜測定方法，また測定装置の測定原理についても述べた。

第 3 章　銅プレカーサー水溶液の調製と銅薄膜形成

新たに調製した銅プレカーサー水溶液をスプレー法で塗布してプレカーサー膜を形成した。具体的には，先に [Cu(H_2edta)]錯体を含む水溶液（S_{edta}）を調製し，スプレー法で塗布した。形成したプレカーサー膜は，アモルファスだった。その膜を熱処理したところ，銅に結晶化した。その膜の電気抵抗率は，10^6 Ω cm 以上だった。電界放出型走査電子顕微鏡（FE–SEM）と原子間力顕微鏡（AFM）から，形成した薄膜は，不連続膜だった。プレカーサー水溶液中の錯体を設計し，新たにギ酸銅とアンモニアを反応させた水溶液（S_{form}）を調製した。S_{edta} に対して S_{form} の物質量を変えて混合水溶液を調製した。S_{form} の物質量を増やした水溶液をスプレー法で塗布したプレカーサー膜は，酸化銅(I)に結晶化した。S_{edta} : S_{form} の比が 1：4 となるプレカーサー水溶液（S_{mix}）を用いて形成した場合，最も薄膜形成の再現性が高かった。この水溶液をスプレー法で塗布したプレカーサー膜を 180°C の石英ガラス基板に空気中で塗布してプレカーサー膜を形成した。形成したプレカーサー膜を Ar 雰囲気中 350°C で熱処理後，膜表面をガラスでカバーして Ar 雰囲気中 400°C でさらに熱処理した。得られた薄膜の XRD パターンは，Cu のピークに帰属できた。膜厚は 100 nm で，ガラス基板に対する密着性と電気抵抗率は，それぞれ 37(7) MPa と $3.8(6) \times 10^{-5}$ Ω cm だった。AFM と FE–SEM 像から，形成した膜の平均表面粗さが 11 nm で，粒子がよく結合した連続膜だった。得られた薄膜の反射率は，遠赤外域で 90%以上を示した。オージェ電子分光法（AES）から，得られた薄膜は，中性炭素原子が均一に膜全体に分布していた。

第４章　$LiCoO_2$ プレカーサー水溶液の調製と石英ガラス基板上への層状構造 $LiCoO_2$ 薄膜の形成

スプレー法で形成した層状構造 LCO 薄膜について詳細に述べる。アンモニア水に酢酸リチウムと酢酸コバルトを加えた LCO プレカーサー水溶液を調製した。LCO プレカーサー水溶液及び LCO プレカーサーエタノール溶液の紫外可視分光法（UV-Vis）から，溶液中で Co^{2+} の錯体を形成したと考えられた。そ

の水溶液を 180°C の石英ガラス基板上へスプレー法で塗布して，プレカーサー膜を形成した。形成したプレカーサー膜を 500°C の空気中で 0.5 時間熱処理した。また，形成した膜上に酢酸リチウムと酢酸コバルトを含んでいるエタノール溶液をスピンコート法で塗布し，500°C の空気中で 0.5 時間熱処理した。得られた薄膜の XRD パターンは，層状構造の $LiCoO_2$ のピークを示した。ラマン分光測定より，形成した薄膜は，スピネル構造の Co_3O_4 を 5 mol%含む $LiCoO_2$ だった。FE–SEM より，形成した薄膜の膜厚は，0.21 μm だった。形成した薄膜のホール効果測定から，電気抵抗率，キャリア濃度とキャリア移動度は，35(2) Ω cm，$8(2) \times 10^{16}$ cm^{-3}，2(1) cm^{-2} V^{-1} s^{-1} だった。また，石英ガラス基板上へスピンコート法で塗布・形成した薄膜の XRD パターンは，酸化コバルト（Co_3O_4）の単一相を示した。これらの結果から，石英ガラス基板への LCO 薄膜の形成は，スピンコート法とスプレー法で明確だった。これらは，スプレー法による成膜メカニズムに起因していると考えられる。

第５章　MWCNT/Cu プレカーサー水溶液の調製と MWCNT/Cu 複合薄膜の形成

MWCNT/Cu 複合薄膜の形成についてまとめた。市販の水分散多層カーボンナノチューブ（MWCNT）とギ酸銅四水和物と EDTA を配位子とする銅（II）錯体を混合したアンモニア水溶液を調製した。その水溶液を 180°C の石英ガラス基板へスプレー法で塗布して，プレカーサー膜を形成した。形成したプレカーサー膜を Ar 雰囲気中 350°C で熱処理後，膜表面をガラスでカバーして Ar 雰囲気中 400°C でさらに熱処理した。

得られた薄膜の結晶構造は，銅だった。MWCNT と Cu の混合状態を FE–SEM 像で確認した。MWCNT を 10 vol%含む銅プレカーサー水溶液をスプレー法で塗布，熱処理した膜の膜厚は 110 nm だった。この膜の密着強度と電気抵抗率は，それぞれ 21(7) MPa と $4.8(1) \times 10^{-5}$ Ω cm だった。この複合薄膜は，遠赤外域で 70%以上の反射率を示した。

第６章　まとめ

本研究は，スプレー法を用いて形成したプレカーサー膜を熱処理し，機能性薄膜を形成した。先に，プレカーサー水溶液中の銅錯体の設計で高導電性かつ高密着な薄膜を容易に形成できた。この方法は，高品質の銅薄膜を簡便かつ費用対効果が高い薄膜形成法で，工業的にも有用であると考えられる。液相法による石英ガラス基板への層状構造 LCO の薄膜の形成は，この研究で初めて成し遂げられた。Li^+イオン，Co^{2+}イオンとアンモニアとの反応で形成した錯体を含むプレカーサー水溶液は，スプレー法による塗布が可能だった。層状構造の LCO 薄膜を 500°C という熱処理温度で形成できるだけでなく，石英ガラス基板上にも形成できた。水溶液は，工業において安全性の高さで大きな利点がある。これらの主要な結果からの結論の要約は，**第 6 章**で述べる。さらに銅，LCO および MWCNT / Cu 薄膜形成の今後の研究に関して提言する。

Publications from the major results

1. Philipus N. Hishimone, Hiroki Nagai, Masato Morita, Tetsuo Sakamoto and

Mitsunobu Sato, “Highly-Conductive and Well-Adhered Cu Thin Film Fabricated on Quartz Glass by Heat Treatment of a Precursor Film Obtained Via Spray-Coating of an Aqueous Solution Involving Cu(II) Complexes.”, *Coatings*, **8(10)**, **352** (**2018**).

2. Philipus N. Hishimone, Kenta Watarai, Hiroki Nagai and Mitsunobu Sato, “Thin Film Fabrication and Characterization of a Layered-rock-salt $LiCoO_2$ on a Quartz Glass Spray-coated with an Aqueous Ammonia Solution Involving Metal Acetates.”, Manuscript submitted to *Coatings*, **9(2)**, **97** (**2019**).

Ph.D. THESIS

THE SPRAY METHOD FOR FABRICATION OF FUNCTIONAL THIN FILMS BY DESIGNED MOLECULAR PRECURSORS IN AQUEOUS SOLUTIONS

Applied Chemistry and Chemical Engineering Program

PHILIPUS NGHILUKUNANYE HISHIMONE

OUTLINE OF THESIS

CHAPTER 1: INTRODUCTION AND BACKGROUND

CHAPTER 1: INTRODUCTION AND BACKGROUND

Functional materials can be defined as "the materials fabricated for the purpose of generating their desirable properties and functionalities" with a focus on enhancing the electronic, electrochemical properties and so on. At the present, pertinent issues such as energy shortage, the exploitation of the non-renewable sources and the negative environmental impacts arising from the burning of fossil fuels are challenges facing the global community and, the effect is expected to extend to the future generations. Therefore, the main goal of thousands of scientific research groups around the world has been to find scientific breakthroughs that can improve the quality of life *via* the fabrication of efficient and tailor-designed materials. To counter the energy crisis, the research in the field of energy materials and devices has been relentless. Specifically, in the search for various materials capable of being used in devices that can utilize the energy with much-improved efficiency, and materials capable of effectively converting and storing renewable energy.

Various functional materials have been investigated under the many different disciplines of material science and engineering. In the field of electrical conductors, the research is focused on replacing materials that are expensive and in short supply and, copper (Cu) has emerged as an ideal candidate for applications in microelectronic devices. In the field of energy materials, secondary lithium-ion batteries (LIBs) have emerged as the ideal power sources for most of the portable electronics and power tools and, have been identified to be capable of fulfilling the demand of high energy-to-weight and energy-to-volume ratios which are essential for future energy devices [1, 2]. Lithium cobaltite ($LiCoO_2$, LCO) has been extensively studied and successfully applied as a Li intercalation compound in the LIBs due to its high specific energy and structural stability that promotes extended battery cycle-ability [3–8]. Due to the above-mentioned benefits of Cu and LCO, this thesis focused on the fabrication of functional thin film of these materials as discussed in the following sections.

1.1. Thin films of functional materials

A thin film can be defined as a material measuring less than 1 μm in thickness, fabricated on a supporting substrate by intensifying, one-by-one, and ionic/molecular/atomic species of matter [9]. Since the observation of the first generation of a thin film layer on the surface of glass by Fraunhofe over 195 years ago, thin films have been used for manufacturing optical coatings, electronic devices, decorative parts, and instrument hard coatings [10]. At the present, the thin film has been transformed into a conventional well-established material technology and, the improvement of novel materials at the nanometer scale is still being developed on a daily basis [9, 10]. In addition to saving natural resources, the application of thin films to achieve the fabrication of thin coatings of various functional materials is an important and active field owing to the enhanced functional properties of materials at the nano-scale level.

1.1.1. Established methods for fabricating thin films of functional materials

Owing to the above-mentioned benefits of the functional thin films, a considerable number of techniques have been established for the fabrication of these thin films. In the context of this thesis, the thin film fabrication methods have been divided into two categories representing (1) gas phase deposition and (2) liquid phase deposition methods, according to the reaction phase of the chemical precursors involved. In the gas phase fabrication methods, the atomic level reactions between the chemical precursor and the surface of the substrate, involve chemical precursors in the gaseous phase. On the other hand, the liquid phase fabrication methods involve reactions at both atomic and molecular level, in which the chemical precursors are in the liquid phase.

Table 1. Classification of some of the common thin film fabrication methods.

Phase of reaction	**Fabrication method**	
Gas	Physical	Magnetron sputtering
		Pulsed laser deposition (PLD)
	Chemical	Atomic layer deposition (ALD)
		Chemical vapor deposition CVD
Liquid	Electrospray deposition (ESD)	
	Electrochemical deposition (ECD)	
	Sol-gel method	
	Molecular precursor method (MPM)	

1.1.1.1. Gas phase fabrication methods

1.1.1.1.1. Magnetron sputtering

This is one of the most well-established techniques that is widely used in the industries to fabricate coatings of many different materials, including metals, semiconductors, alloys, and insulators, etc. [11, 12]. Thin films fabricated *via* magnetron sputtering prove to be of superior quality in comparison to those fabricated using other gas phase fabrication methods [11, 13], and thin films of Cu [14], $LiCoO_2$ [15, 16], TiO_2 [17–19], etc. have been successfully fabricated. The schematic representation of the magnetron sputtering set-up is shown in Figure 1.

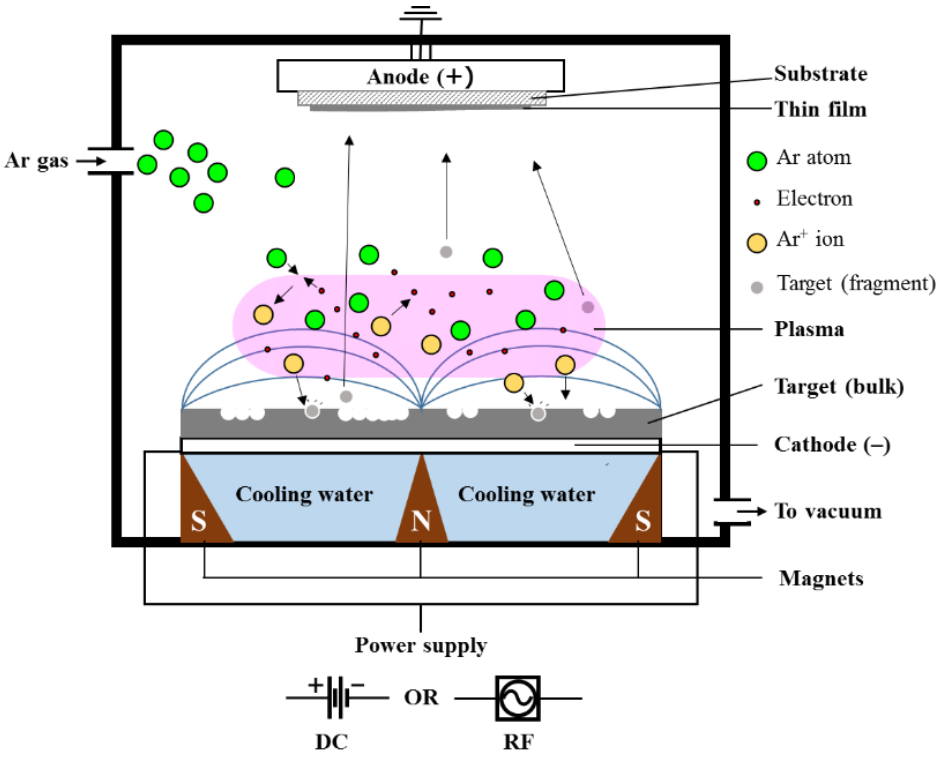

Figure 1. Schematic representation of a magnetron sputtering equipment and deposition process.

Before deposition, the chamber is evacuated to ca. 10^{-4} kPa and then refilled with Ar gas which is used as the sputter gas. Using strong electrical and magnetic field, magnetron sputtering employs the bombardment of the selected target's surface by Ar^+ ions which are formed as a result of the collision between Ar gas atoms and electrons trapped within the magnetic field. The Ar^+ ions are attracted toward the negatively charged target (cathode) and the bombardment leads to the ejection of the targets particles which are then redeposited as a thin film on the substrate placed on the anode, opposite to the target. Depending on the type of power source utilized, magnetron sputtering can be divided into two types namely, (1) direct current (dc) magnetron sputtering and (2) radio frequency (rf) sputtering. While dc magnetron sputtering is relatively cheaper in comparison to rf, only electrically conductive targets like metals or doped semiconductors are used [20]. Additionally, reactive gases such as oxygen or nitrogen gas are used to react with the sputtered materials, in the fabrication of thin films for

metal oxides or nitrides, respectively. The technique is referred to as “reactive magnetron sputtering”.

1.1.1.1.2. Pulsed laser deposition (PLD)

The PLD technique employs the ablation of a target material with a strong, pulsed laser beam to produce a plume of vaporized materials which is then re-condensed and deposited onto a substrate, placed opposite the target, under a reduced pressure atmosphere of ca. 10^{-1} – 10^{-5} kPa [21–23]. Depending on the target material, its morphology, and the laser pulse wavelength and duration, there is a specific threshold power density that is required to cause ablation [24]. Therefore, a good understanding of the various parameters is required for a successful plume generation and subsequent thin film deposition. The stoichiometric transfer of materials from the target to the substrate earned PLD a reputation as fabrication of choice for thin films with complicated stoichiometry or sandwich structures [25], in comparison to other gas phase fabrication methods. Figure 2 shows the schematic representation of a PLD setup.

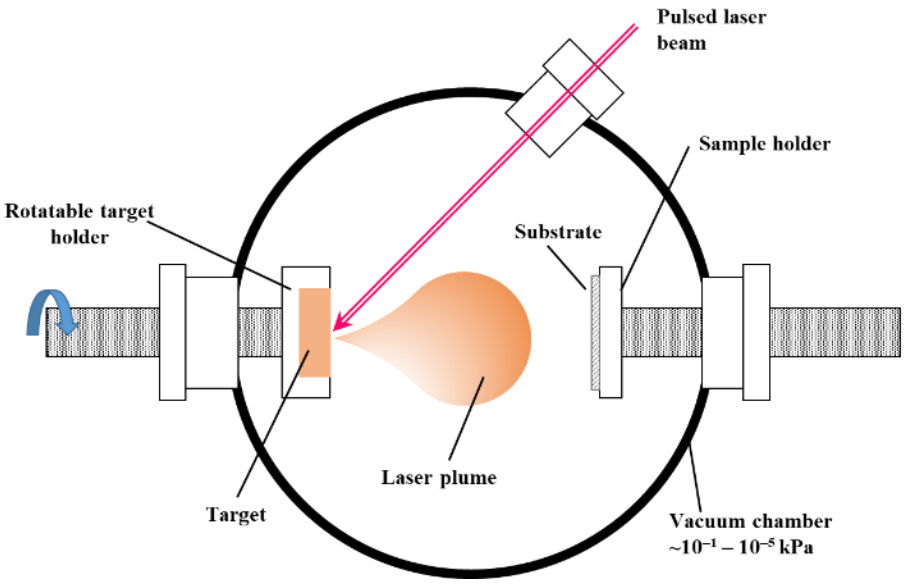

Figure 2. Schematic representation of PLD setup.

Although the fabrication of thin films with identical stoichiometry as the target materials is one of the superior characteristics of PLD, the stoichiometry can be compromised when multi-

component materials with volatile constituents are used [24–26]. As a remedy, a background gas such as oxygen or nitrogen is introduced in the reaction chamber to compensate for the lack of stoichiometry, during the fabrication of metal oxides or nitrides' thin films, respectively.

1.1.1.1.3. Atomic layer deposition (ALD)

The ALD technique is based on sequential and self-limiting reactions of a chemical precursor in vapor form, with an activated or functionalized surface of the substrate [27, 28]. The self-limiting property of this technique is realized in a sense that, if all functional sites on the substrate have reacted, no further reaction between the chemical precursor and the substrate will take place [27, 29].

The superiority of ALD over other gas phase fabrication methods for the deposition of thin films is realized through its exceptional conformity, the ability to control thickness at the atomic level and tunable film composition [28, 30, 31]. Through this route, the deposition of thin films on substrates with highly-structured geometries can be easily achieved, and ALD has been considered as the ideal method for fabricating highly conformal seed layers [32, 33]. This is also of great importance for applications in the concept of integrated batteries [2], that aims at maintaining the storage capacity of miniaturized LIBs. Figure 3 illustrates the concept of ALD in the fabrication of a TiO_2 thin film.

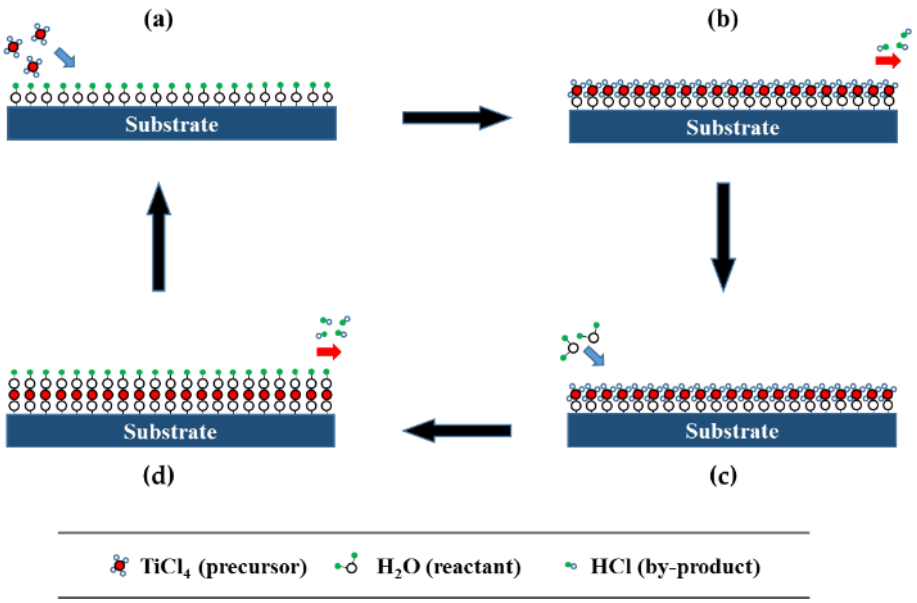

Figure 3. Schematic representation of 1 cycle of an ALD process for the deposition of a TiO_2 thin film from titanium tetrachloride and water. The steps are defined as follows: (a) precursor exposure, (b) purge, (c) reactant exposure, and (d) purge. By repetition of step (a) to (d), layers of TiO_2 can be easily formed and the thickness can be controlled at the atomic level.

Under a vacuum pressure of ca. 10 kPa or less, the chemical precursors are maintained in a vapor phase by adjusting a specific temperature referred to as the "ALD temperature window" [34], to achieve optimum reaction kinetics and avoiding condensation or thermal decomposition of the precursor. Although the fabrication of metallic copper thin films has been achieved [33–37], the deposition of metallic thin films is generally limited due to the lack of precursors suitable for ALD processes. The vaporization of chemical precursors, difficulty in controlling their thermal decomposition and lack of efficient self-limited reactivity with surfaces are some of the challenging aspects in ALD [31]. In addition, during the designing stages of certain chemical precursors, the by-products associated with the proposed chemical reaction need to be carefully considered as toxic or corrosive chemicals are likely to be those by-products.

1.1.1.1.4. Chemical vapor deposition (CVD)

Defined as the deposition of solids onto heated substrates from chemical reactions in vapour phase [38,39], CVD represents a versatile deposition technique of thin films for a wide range of materials, under vacuumed atmospheres and temperatures over 600°C, and it is an established technique for the deposition of thin film for microelectronics, ohmic and Schottky diode contacts, diffusion barriers, wear-resistant coatings, etc. [38–41]. In a typical CVD experiment, a combination of chemical precursors showing stable vaporization behavior is carefully selected. Using an inert carrier gas, usually Ar or N_2 gas, the vaporized precursors are carried into an evacuated furnace (reaction chamber) and mixed with an additional reactive gas or two. In the fabrication of thin films for $LiCoO_2$, oxygen gas is used as the additional carrier gas [42]. On the other hand, if the desired thin film is metallic, such as Cu, a reducing atmosphere is created by using H_2 gas [43, 44]. The schematic representation of a CVD setup is shown in Figure 4.

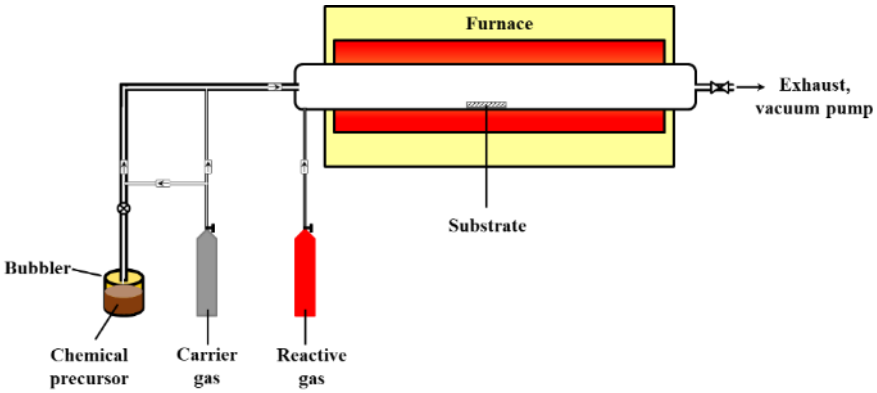

Figure 4. Schematic representation of a CVD setup.

The CVD technique benefits from the fact that it does not require ultrahigh vacuum systems like in the magnetron sputtering and PLD techniques [38, 45]. In addition, CVD is a kinetically driven process, associated with minimized agglomeration and also benefiting from faster deposition rates, in comparison to ALD [45, 46]. Because different precursors have different evaporation rates, it is generally difficult to deposit multicomponent thin films by CVD. Other

drawbacks of CVD include possible chemical and safety hazards of toxic, corrosive and flammable precursors or exhaust gases, and poor thin film adhesion-strength [39, 40].

1.1.1.2. Liquid phase deposition methods

1.1.1.2.1. Electrospray deposition (ESD)

ESD involves the deposition of charged particles formed as a result of liquid atomization by an electrical force. The atomization of the liquid by electrical force allows for the generation of small particles, of narrow size distribution which can be uniformly dispersed over the substrate and, ESD has been considered as a promising technique for the formation of high-quality layers and films [47]. ESP refers to an ESD process employed at elevated temperatures, leading to the deposition of materials obtained from the thermal decomposition of the precursor solution [48]. The schematic representation of the ESD setup is shown in Figure 5.

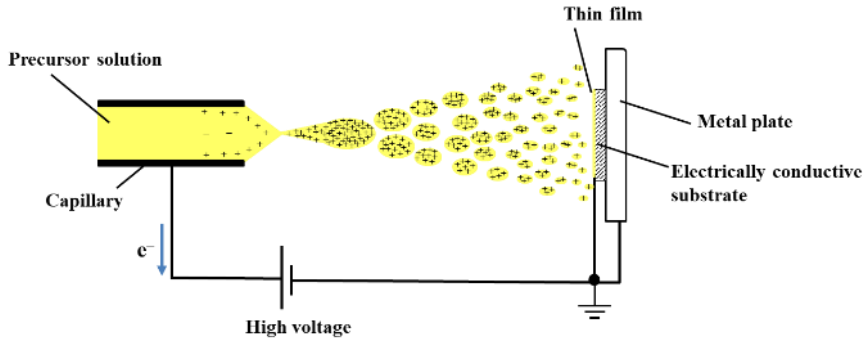

Figure 5. Schematic representation of an ESD setup.

As shown in Figure 5, the ESD method is based on supplying a precursor solution through a metallic capillary which is maintained at the high electrical potential. Ideally, the solution forms a Taylor cone at the tip of the capillary and emitted as a solution jet composed of many highly charged droplets that are homogeneously dispersed in the space between the nozzle and the counter metallic plate (substrate holder) by Coulomb repulsion forces [47]. The quality of the resultant thin films can be easily controlled by adjusting variables such as the applied

voltage, distance between the atomizing nozzle and, the flow rate, concentration and amount of the precursor solution.

In addition to a very low throughput associated with the ESD technique, thin film deposition on insulating substrates is generally not possible due to charge accumulation on the substrate, which leads to the repulsion of more incoming charged particles [47]. Modifications such as the use of alternating current (ac) [49] and extractor electrodes [47] have been employed to solve the charge repulsion issue and ensure the thin film deposition on insulating substrates *via* ESD. However, this complicates an initially simple experimental setup.

1.1.1.2.2. Electrochemical deposition (ECD)

Considered as one of the cheapest methods for the deposition of thin films, ECD represents a major technology for mass production of large area metallic protective coatings in the industry [50]. The deposition technique employs a combination of reduction and oxidation reactions of chemical precursors in electrolytes of aqueous solutions, organic solutions or fused salts [51, 52]. in addition to cost, other advantages of the ECD include low fabrication temperature, high purity and, the ease of controlling thin film thickness, uniformity and rate of deposition by adjusting the deposition parameters [53–55]. The electrochemical technique can be divided into two groups, namely, (1) electrolysis plating which uses external power source to drive the electrochemical reaction that leads to the deposition of a thin film onto an electrically conductive substrate and, (2) electroless plating which does not require external power supply but requires the use of catalysts to activate the surface of the specimen. The schematic representations of the electrochemical techniques for the fabrication of metallic copper thin films are given in Figure 6.

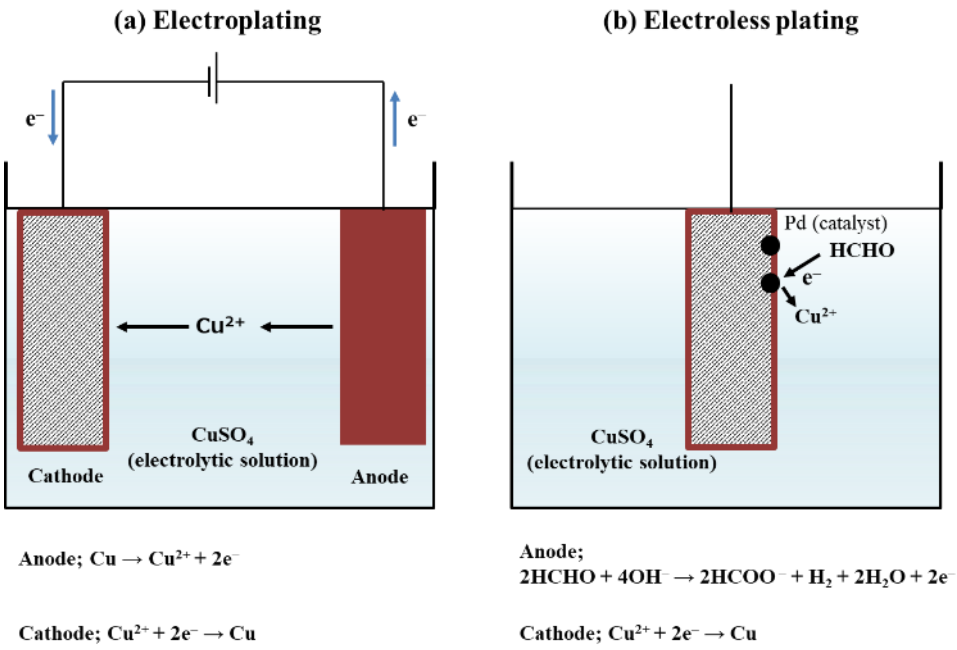

Figure 6. Schematic representation of the electrochemical deposition techniques.

As illustrated in Figure 6, for electrolysis deposition, the external power source causes the dissolution of the metal from the anode (usually a copper rod or plate). The dissolved Cu^{2+} ions are then reduced and redeposited on the surface of the electrically conductive substrate (Cathode). An electrolytic solution involving a salt of copper such as $CuSO_4$ is used for the electrochemical bath to maintain the balance of Cu^{2+} ions. In electroless plating, the electrolytic solution is also the source of the Cu^{2+} ions and a reducing agent such as formaldehyde (HCOH) is added to the plating bath. The introduction of a substrate with an activated surface (by $PdCl_2$ or $SnCl_2$) initiates the reduction of Cu^{2+} to metallic copper, subsequently forming a film on the surface of the substrate. In both the electrolytic and electroless plating, various alkaline or acidic electrolytic solutions are used and are important for maintaining the pH and stabilities of the plating baths [56].

Unlike in the field of metal plating, the deposition of thin films with semiconducting properties is challenging due to complications in controlling the reaction kinetics of multiple compounds in the solutions, at ppm level [50]. However, the major breakthrough came with

the preparation of CdTe layers for solar cells and modules and, since then films of semiconducting materials such as CIGS [50] and $LiMn_2O_4$ [57] have been successfully fabricated. Although electroless plating is considered as a promising technique for the deposition of thin films especially on insulating substrates, the use of $PdCl_2$ or $SnCl_2$ compromises the quality of the thin films [58]. In addition, the selection of the chemical components for the electrolytic solution is important for ensuring that the reduction reaction occurs only on the surface of the activated substrate [56].

1.1.1.2.3. Sol-gel method

The sol-gel method has emerged as a method of choice for the fabrication of ceramics and glasses and, it is considered as the cost-effective alternative to the well-established gas phase fabrication methods. The sol-gel method is a two-chemical processes technique based on the hydrolysis and condensation of molecular precursors and has since been considered to be capable of offering new routes for the low-temperature fabrication of oxide materials [59]. Because all gel products may contain nanoparticles or are nano-composites, the sol-gel method has been deemed as typical nanotechnology [60] and the fabrication of thin films can be easily achieved after integration with spin-coating or dip-coating. In a typical sol-gel process, metal precursors (of the desired metal oxide) derived from metal salts in aqueous solutions, metal alkoxides in organic solvents, or a combination of the two is used. During the hydrolysis step, metal-hydroxide groups are formed by changing the pH of the aqueous solution or adding water to the metal alkoxides. The subsequent condensation reaction results in the formation of metal-oxygen-metal bonds, with different polymerization and poly-condensation processes leading to the gradual formation of the solid phase network [61]. A typical sol-gel process for the formation of SiO_2 from silicone alkoxides is given in Figure 7 [62].

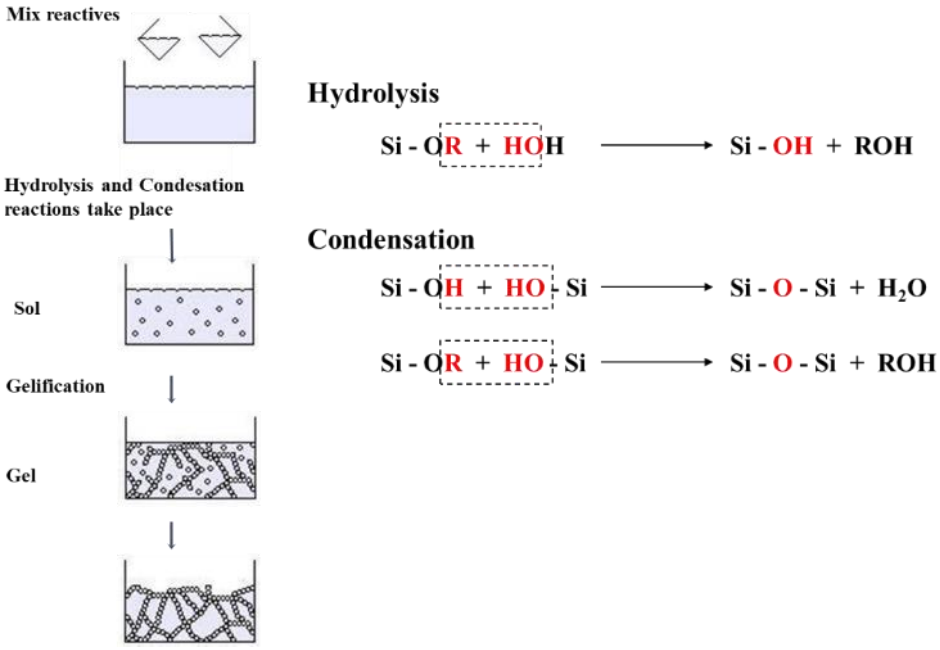

Figure 7. Typical sol-gel process for SiO_2 formation from silicon alkoxides [62].

Although the sol-gel method has become an indispensable technique in the fabrication of thin films for different metal oxides, principally, the fabrication of metallic thin films is not viable. In addition, a good understanding is required for the selection of appropriate precursors and the sophisticated chemical processes leading to the hydrolysis and condensation. The stabilization of the transition metals against hydrolysis, condensation, and other nucleophilic attacks is generally challenging. It is also important to make sure that the transition metal is sufficiently saturated in solution, to avoid different reaction mechanism. Finally, proper control of the moisture and hydrolysis conditions are required to avoid precipitation of the transition metal alkoxides [61]. Therefore, all these aspects make the preparation of suitable coating precursors for the sol-gel method quite complicated.

1.1.1.2.4. Molecular precursor method (MPM)

The molecular precursor method is an effective, wet chemical process that was developed by the current authors, for fabricating nano-crystalline thin films of metals and, various metal oxides and phosphates [62–67]. In the fabrication of these thin films by the MPM, metal

complexes are dissolved in ethanol by combining them with appropriate alkylamines and this yields good coating solutions, with many practical advantages and are ideal for various coating procedures such as spin-coating, dip-coating, and flow-coating. Additionally, the development of aqueous precursor solutions have been successfully achieved [68] and, these solutions can be easily applied for the fabrication of thin films *via* spray-coating at ambient conditions.

To date, over 40 different kinds of thin films for metal oxides or phosphates have been easily fabricated by using the MPM. The procedure employed by the MPM is represented by the example of fabricating the titanium dioxide thin film [69] illustrated in Figure 8. The procedure starts with the preparation of a coating solution by reacting an isolated Ti(IV) complex of ethylenediamine-*N,N,N',N'*-tetraacetic acid with dipropylamine in ethanol. The precursor solution which shows stability against up to 10% water [70], is suitable for spin-coating onto a glass substrate and dried at 70°C to yield an amorphous film. In order to obtain a thin film of metal oxide spread homogeneously on the substrate after the subsequent heat-treatment, it is important that the precursor film is amorphous. Just as the case with the metal/organic polymers in the sol-gel method. The precursor film is then heat-treated at 450°C in air, to eliminate the organic components involved and a transparent thin film of titania is obtained.

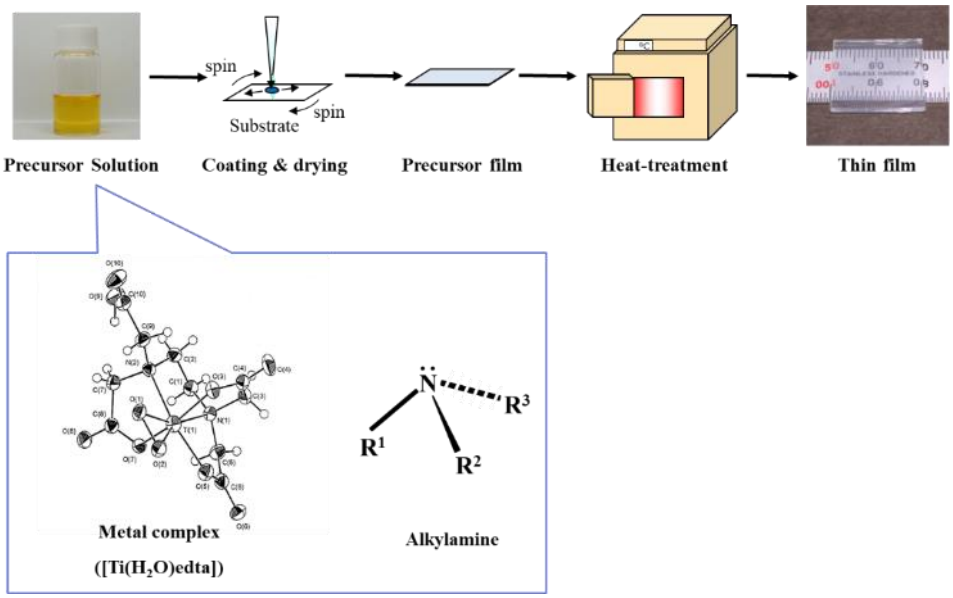

Figure 8. Procedure for fabricating a titanium dioxide thin film via the MPM.

In comparison to the sol-gel method, the MPM produces precursor solutions that are stable and can be stored for longer periods without being hydrolyzed. It is considered that thin films with much smaller crystallite sizes can be fabricated by the MPM due to the ease of metal oxides' nucleation. This is a result of a large number of crystallites instantly formed during the removal of organic ligands *via* the heat-treatment step of the MPM, in comparison to the rearrangement of polymer chains during the same stage in the sol-gel method [62]. Consequently, thin films of metal oxides can be easily fabricated at relatively low annealing temperatures *via* the MPM in comparison to the sol-gel method.

By following the procedure outlined in Figure 8, the fabrication of thin films for a novel thin-film lithium-ion battery (LIB) which can be charged by light irradiation, and thus functioning as a photovoltaic-LIB was recently achieved [71]. The device uses thin films of TiO_2 and $LiCoO_2$ deposited on fluorinated tin oxide (FTO) pre-coated glass substrates, as the anodic and cathodic active materials, respectively, and an electrolytic solution containing $LiPF_6$. In another study employing the MPM, the fabrication of the first *p*-type Cu_2O transparent thin film with properties identical to those of thin films fabricated by using gas phase fabrication methods was also achieved [72]. A dry-type solar cell utilizing this Cu_2O transparent thin film combined with a Vis-responsive anatase thin film also fabricated by the MPM could be successfully constructed and evaluated [62].

The fabrication of thin films for metallic copper has also been facilely achieved by using the MPM. A conductive and semi-transparent Cu thin film was obtained after heat-treating a precursor film containing Cu(II) complexes, spin-coated onto a Na-free glass [73]. In a subsequent study, metallic copper was completely embedded in trenches of a Si substrate after heat-treating a mixed precursor film obtained by dip-coating [74]. The plausible scheme for the formation of Cu thin film form the precursor film is shown in Scheme 1 [73].

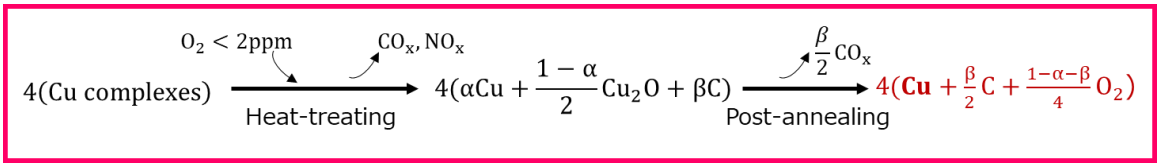

Scheme 1. Plausible scheme for the formation of Cu thin film from the precursor film.

Established just over 22 years ago, the MPM is a relatively new method in comparison to other thin film fabrication methods described earlier in this chapter. However, it is emerging as an effective chemical method for the fabrication of various transparent thin films of metal oxides and highly conductive thin films of metallic Cu.

1.1.2. Summary of the techniques for fabricating functional thin films

Although there are other additional fabrication techniques, subsection 1.3.1. provided an insight into some of the well-established and promising techniques for the fabrication of future energy materials and devices, taking into consideration the costs in terms of the required instrumentation and thin film deposition conditions. Gas phase fabrication methods such as magnetron sputtering and PLD have been identified to be capable of fabricating thin films of high quality and are well-established in the coating industry. However, expensive and complicated instruments are required. The ALD and CVD techniques are suitable for the fabrication of thin films onto substrates with complicated 3-D structures. However, potentially toxic and corrosive chemical precursors are used. Additionally, the fabrication of thin film with different chemical components is challenging due to the different properties of chemical species in the vapor phase.

The liquid phase fabrication methods are cost-effective alternatives to their gas phase counterparts. The ESD benefits from the ability to control the surface morphology of the deposited thin film but suffers from low throughput and difficulties to deposit films onto insulating substrates. ECD is well-established for the fabrication of thin films for metallic coatings such as copper, on a large area. However, the resultant thin films suffer from weak

adhesion and poor surface morphology. The sol-gel method has been extensively developed for the fabrication of thin films for metal oxides at relatively low-costs in comparison to the gas phase fabrication methods. The poor stability of the chemical precursors against hydrolysis and deviating reaction mechanisms are some of the challenges encountered.

The MPM is an emerging wet process capable of fabricating thin films of metal oxides such as TiO_2, $LiCoO_2$, and *p*-type Cu_2O, etc. and the functionalities of these thin films in energy devices have been evaluated in a PV-LIB [67] and a dry-type solar cell [62]. Thin films of metallic copper have also been successfully fabricated by the MPM. This shows that the MPM is earning its place among affordable and effective techniques for the fabrication of thin films for future energy materials and devices.

1.1.3. Coating methods compatible with the MPM

As discussed under subsection 1.3.1.2.4, the fabrication of functional thin films by the MPM is achieved through the heat-treatment of the respective precursor films formed on the various substrates. To obtained these precursor films, coating techniques such as spin-coating, dip-coating, flow-coating, and spray-coating are employed. These coating techniques are discussed in details under the following subsections.

1.1.3.1. Spin-coating

The spin-coating method is a well-established for the formation of thin films of precursor solutions on flat substrates. In the industry, the spin-coating method is used during the fabrication of polymeric photoresists to the silicon wafers and it is involved in crucial steps during the production of digital versatile discs (DVDs) and compact disc (CDs) [75, 76]. The concept of the method is based on: (1) the application of a liquid solution onto a substrate and (2) acceleration of the substrate to a chosen rotational speed [75–77]. Due to the angular velocity of the substrate, most of the solution is ejected leaving only a thin film of the solution

on the substrate. The process for the formation of a precursor film *via* the spin-coating method is shown in Figure 9.

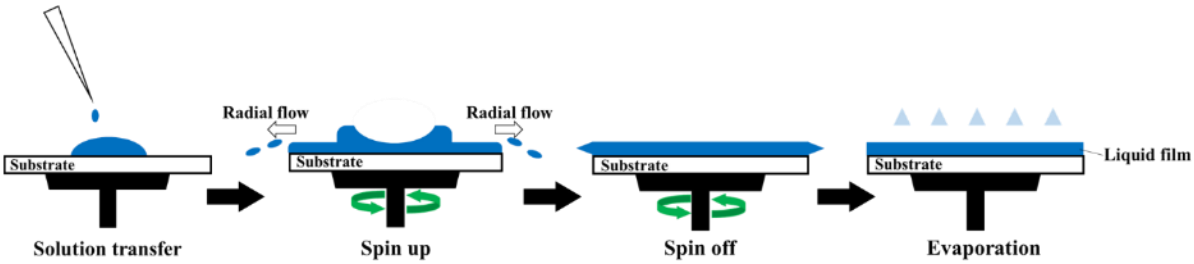

Figure 9. Schematic representation of a spin-coating process.

One of the benefits of the spin-coating method is that, properties such as the thickness, morphology and surface topography of the final film obtained from a particular solution are highly reproducible and strongly dependent on the (1) rotational speed of the substrate, (2) volatility, (3) viscosity, (4) diffusivity and, (5) the molecular weight and concentration of the solutes. In order to find conditions that adequately separate thinning by a spin-off from later thinning and solidification by drying, volatile organic compounds (VOCs) are commonly used as solvents. This is a great setback especially due to the safety concerns associated with the handling of VOCs. Additionally, the spin-coating method is limited to batch processes and/ or thin films with small effective surface areas, making them unsuitable for real-world applications [78]. It is also impossible to achieve the formation of films on substrates of different shapes other than flat, by using the spin-coating method. The thickness control of spin-coated film is highly depended on the concentration of the solute and the rotational speed. When a thicker film is required, process repetition is often required to obtain the desired thickness.

1.1.3.2. Spray-coating

The spray-coating method is being used as a viable method for low cost-fabrication of functional films for various materials, based on fluid-atomization to produce nanodrops which

are then transported onto the surface of a substrate and form a thin layer of coating. It is worth noting that, because the surface to volume ratio of the nanodrops is very large, the surface coatings obtained *via* the spray-coating method are highly receptive to heat-treating [79]. The spray-coating method offers higher suitability and flexibility with respect to large-area application processes, ensures ideal coatings for a variety of surfaces with different morphologies and is used for inline production [80–82]. Additional merits of the spray-coating methods are based on the fact that material waste is minimized, the thickness of the spray-coated layer can be controlled over a wide range by changing the amount of solution used, coatings can be easily patterned by simple shadow masking and, a broad range of solutions with different rheologies which include aqueous solutions can be used to obtain any kind of thin film [68, 81, 83].

Specifically, the minimized loss of materials stems from the fact that the coverage of the spray-stream can be easily adjusted to ensure maximum transfer of the atomized precursors onto the substrate. From the point of facile patterning, if a mask with the desired masking is placed on the substrate, the covered parts of the substrates will be shielded from the incoming nanodrops. Therefore, easily creating a patterned coating. Because of the ability to use aqueous-based solutions in the spray-coating method, environmental consequences caused by the use of VOCs are eliminated. In addition, in the industries, the use of VOC-based solutions is discouraged due to the concerns over fire hazards as a result of the static electric charge. Therefore, methods that use aqueous-based solutions are highly preferred over their VOC-based counterparts. The general setup for a spray-coating procedure is given in figure 10 below.

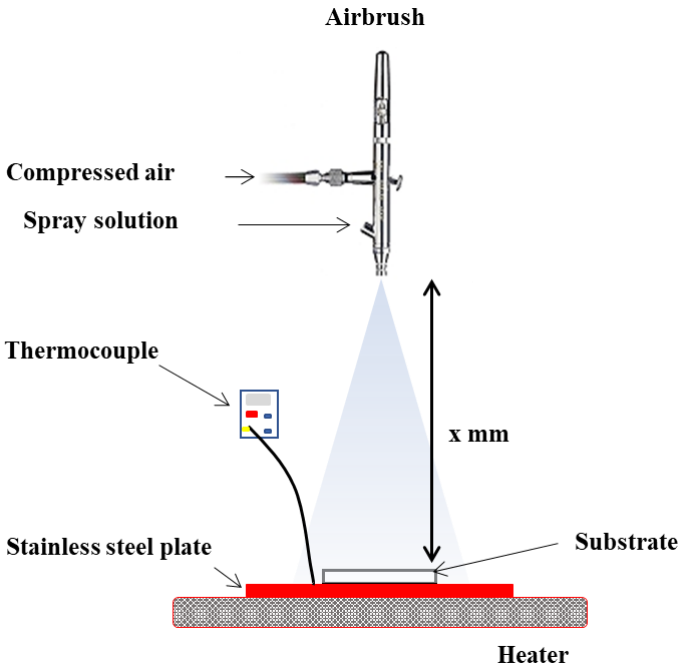

Figure 10. Schematic representation of the spray-coating setup

Prior to the development of the spray-coating method, other spray-on methods such as the electrostatic spraying and spray pyrolysis have been developed for the fabrication of different kinds of coatings. Although operating at higher temperatures to facilitate simultaneous deposition and thermal decomposition of chemical precursors under controlled atmospheres (Such as under vacuum or hydrogen gas), the processes involved in spray pyrolysis, from atomization to droplet spreading and drying are identical to those of spray-coating. Therefore, because the models of these processes have been clearly constructed in the literature of spray pyrolysis, their concept will be used in this thesis. Consequently, the principle of obtaining coatings *via* the spray-coating is based on the following processes, which have to be well-understood and controlled in order to obtain a high-quality and acceptable spray-coated layer [80–85].

(1) Pressurized atomization of the solution through the nozzle

(2) Coalesce and flight of the nanodrops in the vertical direction

(3) Solvent evaporation

(4) Droplet spreading and drying

(5) Adhesion of solid parts attached on the substrates to form the thin film layer.

Solution atomization is the first step in the whole spray-coating process that aims at the generation of droplets from the spray solutions by using pressurized air and, direct these droplets towards the surface of the substrate with some initial velocity and with the aim of depositing as many droplets as possible [86]. The initial velocity of the droplet is an important parameter as it determines the rate at which the droplet reaches the surface of the substrate, the heating rate of the droplet and the amount of time the droplet remains in transport. The resulting droplet size, rate of atomization and initial velocity of the droplets mainly depend on the type of the atomizer used. As expected, an increase in the atomizing air pressure causes a decrease in the generated mean droplet diameter. In the spray pyrosis process, it has been established that the size of the generated droplet is not related to any fluid property of the precursor solution and depends solely on the fluid charge density level [86, 87].

To ensure sufficient solvent evaporation and appropriate droplet drying that leads to a well-formed coating the deposition of the atomized solution on the surface of the substrate is usually categorized into three regimes as follows [83]: (1) the wet regime – when the droplets are transported onto the substrate in intact form, resulting in the formation of a wet layer on top of the substrate, hence producing inhomogeneous layers with poor adhesion and no real thickness control. (2) the dry regime – whereby the entire solvent is evaporated before reaching the substrate and powder of the precursor solution is deposited instead, leading to poor adhesion and failed deposition. Finally, (3) the intermediate regime has been considered as a suitable regime for the formation of homogenous layers of coatings. In this region, the is just sufficiently removed to form fine droplets that immediately dry after hitting the substrate. The occurrence of the above-mentioned regimes depends on various parameters involved in the spray-coating process such as the distance between the atomizer and the substrate, the initial

size of the droplet and the temperature of the substrate. As the droplets travel through the ambient, they experience physical and chemical changes that determine the deposition regime. These changes a depicted in figure 11 below, showing conditions of constant droplet size vs increasing temperature and constant temperature vs decreasing droplet size [83,86,88,89].

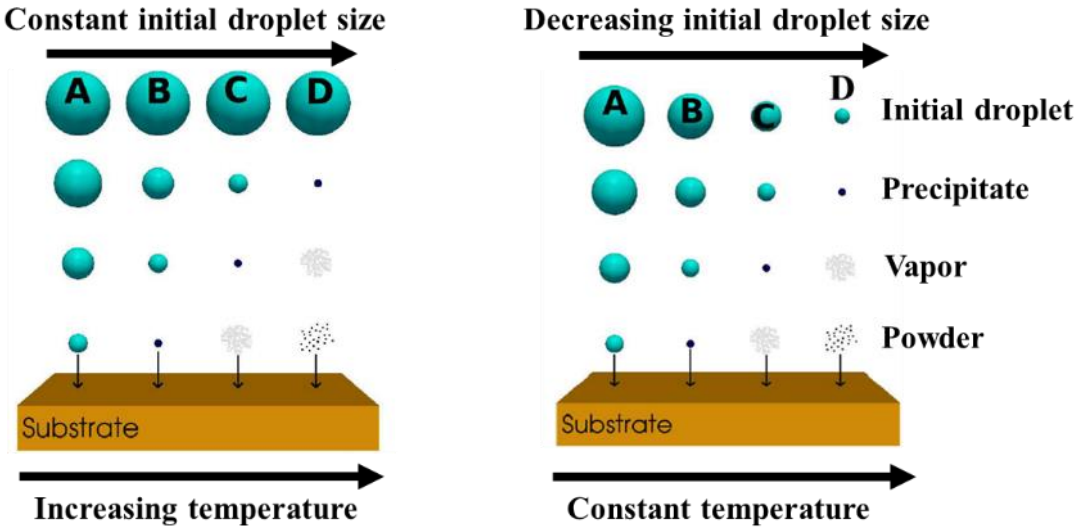

Figure 11. Potential changes experienced by the sprayed droplet during a flight from the atomizer to the substrate [86].

In a typical spray-coating process, the droplets cannot the droplets travel through the air as a flux which makes it impossible to view the droplets individually and model the interaction between the droplet and the surface of the substrate. In the case of ESD however, the acceleration of the droplets towards the substrate by electric field allows for the observation of individual droplets and a model of droplet/substrate interaction has been proposed [86]. This is illustrated in Figure 12.

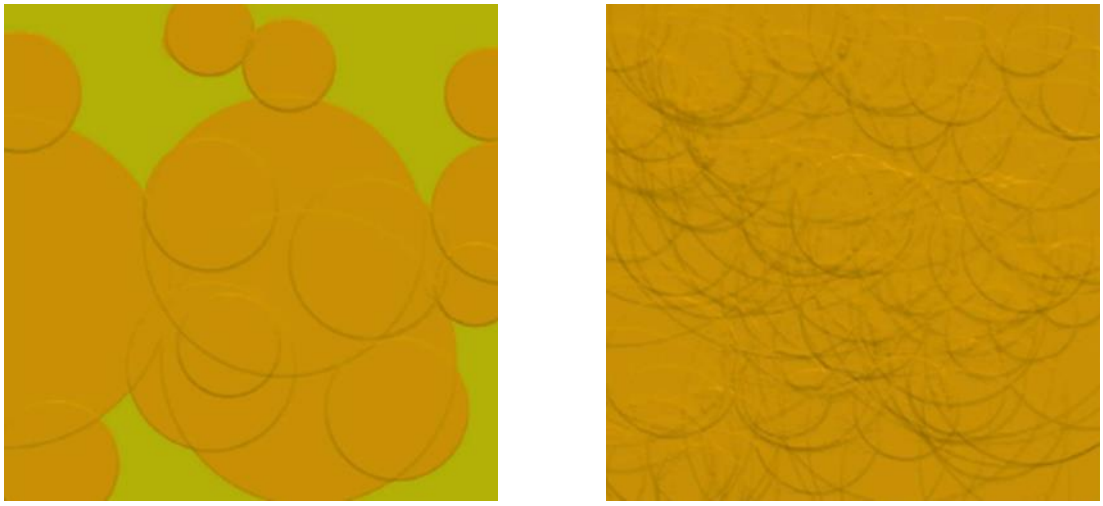

(**a**) (**b**)

Figure 12. Spray pyrolysis simulation on a 250 μm × 250 μm geometry using: (a) 15 droplets and (b) 100 droplets. The lighter surface is the substrate while the darker discs are the deposited droplets [86].

From the figures above, it is clearly indicated that the droplets are deposited in the disc-like phenomenon and the surface coverage increases with an increasing amount of the spray solution. It has been established that the coatings obtained *via* the spray-coating method are characterized by high surface roughness in comparison to the coatings obtained by using methods such as spin-coating and, a substantial number of droplets is required to obtain total surface coverage. The surface roughness is attributable to the interaction of the droplets with the surface of the substrate and the subsequent striking of the earlier formed layers by the incoming droplets. Several factors have been identified to be contributing to the overall morphology of the resultant coating and they include Spraying time, the volume of sprayed solution, air pressure, the distance between the atomizer and the substrate and the temperature of the substrate.

1.2. Aims and Objectives

In this study, we have realized the importance of thin films for metallic copper and LCO in applications related to energy materials and devices. We have also identified the advantages of using precursor solutions involving metal complexes in the fabrication of nanocrystalline thin films of metals and metal oxides according to the principle of the MPM. The benefits associated with the spray-coating technique due to its ability to be scaled up for mass production, reduced material losses, and simple experimental set-up are motivating. Additionally, the spray-coating technique is suitable for solutions which are free of the VOCs which are technically difficult to coat onto substrates by employing techniques such as spin-coating or dip-coating.

Although, a broad range of solutions which includes the aqueous-based solutions has been successfully used to obtain various kinds of thin films, scientific reports on the formation of the precursor films necessary for the fabrication of thin films of metallic Cu and thin films of metal oxides such as LCO on non-crystalline substrates such as the amorphous quartz glass are lacking.

Copper and cobalt are among the mining products of Namibia. Unfortunately, most of these resources are exported out of the country in raw form. It's, therefore, a challenge to realize the industrialization of Namibia if there is no value addition is made to the mined resources. Therefore, the main aim of this study was to successfully fabricate the copper and LCO thin films by heat-treating the corresponding precursor films obtained via spray-coating. Spray-coating is a simple procedure and we believe that it can be facilely used for the fabrication of functional thin films in Namibia, without requiring complicated and expensive instruments.

The objectives of the study will be divided into the following parts.

1. To prepare stable aqueous solutions involving the respective metal complexes.
2. Use spray-coating to obtain precursor films of the respective thin films.
3. Heat-treat the precursor films in order to obtain the desired functional thin films.

References

1. Tarascon, J.-M.; Armand, M. Issues and challenges facing rechargeable lithium batteries. *Nature* **2001**, *414*, 359.
2. Donders, M.E.; Arnoldbik, W.M.; Knoops, H.C.M.; Kessels, W.M.M.; Notten, P.H.L. Atomic Layer Deposition of $LiCoO_2$ Thin-Film Electrodes for All-Solid-State Li-Ion Micro-Batteries. *J. Electrochem. Soc.* **2013**, *160*, A3066–A3071, doi:10.1149/2.011305jes.
3. Mizushima, K.; Jones, P.C.; Wiseman, P.J.; Goodenough, J.B. A new cathode material for batteries of high energy density. *Mater. Res. Bull.* **1980**, *15*, 783–789, doi:10.1016/0025-5408(80)90012-4.
4. Nitta, N.; Wu, F.; Lee, J.T.; Yushin, G. Li-ion battery materials: Present and future. *Mater. Today* **2015**, *18*, 252–264, doi:10.1016/j.mattod.2014.10.040.
5. Porthault, H.; Baddour-Hadjean, R.; Le Cras, F.; Bourbon, C.; Franger, S. Raman study of the spinel-to-layered phase transformation in sol-gel $LiCoO_2$ cathode powders as a function of the post-annealing temperature. *Vib. Spectrosc.* **2012**, *62*, 152–158, doi:10.1016/j.vibspec.2012.05.004.
6. Mendiboure, A.; Delmas, C.; Hagenmuller, P. New layered structure obtained by electrochemical deintercalation of the metastable $LiCoO_2$ (O_2) variety. *Mater. Res. Bull.* **1984**, *19*, 1383–1392, doi:10.1016/0025-5408(84)90204-6.
7. Reimers, J.N.; Dahn, J.R. Electrochemical and In Situ X-Ray Diffraction Studies of Lithium Intercalation in Li_xCoO_2. *J. Electrochem. Soc.* **1992**, *139*, 2091, doi:10.1149/1.2221184.
8. Bak, T.; Nowotny, J.; Rekas, M.; Sorrell, C.C.; Sugihara, S. Properties of the electrode material Li_xCoO_2. *Ionics (Kiel).* **2000**, *6*, 92–106.
9. Wasa, K.; Kitabatake, M.; Adachi, H. *Thin Film Materials Technology: Sputtering of*

Compound Materials; Elsevier Science, 2004; ISBN 9780815519317.

10. Jameel, D.A. Thin film deposition processes. *Int. J. Mod. Phys. Appl.* **2015**, *1*, 193–199.
11. Kelly, P.. J.; Arnell, R.. D. Magnetron sputtering: a review of recent developments and applications. *Vacuum* **2000**, *56*, 159–172, doi:10.1016/S0042-207X(99)00189-X.
12. Swann, S. Magnetron sputtering. *Phys. Technol.* **1988**, *19*, 67–75, doi:10.1088/0305-4624/19/2/304.
13. Bräuer, G.; Szyszka, B.; Vergöhl, M.; Bandorf, R. Magnetron sputtering - Milestones of 30 years. *Vacuum* **2010**, *84*, 1354–1359, doi:10.1016/j.vacuum.2009.12.014.
14. Ogwu, A. A. Electrical resistivity of copper oxide thin films prepared by reactive magnetron sputtering. *J. Achiev. Mater. Manuf. Eng.* **2007**, *24*, 172–177.
15. Tintignac, S.; Baddour-Hadjean, R.; Pereira-Ramos, J.P.; Salot, R. High performance sputtered LiCoO2thin films obtained at a moderate annealing treatment combined to a bias effect. *Electrochim. Acta* **2012**, *60*, 121–129, doi:10.1016/j.electacta.2011.11.033.
16. Rao Kosuri, Y.; Rao Penki, T.; Nookala, M.; Morgen, P.; Rao Gowravaram, M. Investigations On Sputter Deposited $LiCoO_2$ Thin Films From Powder Target. *Adv. Mater. Lett.* **2013**, *4*, 615–620, doi:10.5185/amlett.2012.12479.
17. Takeda, S.; Suzuki, S.; Odaka, H.; Hosono, H. Photocatalytic TiO_2 thin film deposited onto glass by DC magnetron sputtering. *Thin Solid Films* **2001**, *392*, 338–344, doi:10.1016/S0040-6090(01)01054-9.
18. Senthilkumar, V.; Jayachandran, M.; Sanjeeviraja, C. Preparation of anatase TiO_2 thin films for dye-sensitized solar cells by DC reactive magnetron sputtering technique. *Thin Solid Films* **2010**, *519*, 991–994, doi:10.1016/j.tsf.2010.08.027.
19. Nezar, S.; Saoula, N.; Sali, S.; Faiz, M.; Mekki, M.; Laoufi, N.A.; Tabet, N. Properties of TiO_2 thin films deposited by rf reactive magnetron sputtering on biased substrates. *Appl. Surf. Sci.* **2017**, *395*, 172–179, doi:10.1016/j.apsusc.2016.08.125.

20. Hahn, H.; Averback, R.S. The production of nanocrystalline powders by magnetron sputtering. *J. Appl. Phys.* **1990**, *67*, 1113–1115, doi:10.1063/1.345798.

21. Lowndes, D.H.; Geohegan, D.B.; Puretzky, A.A.; Norton, D.P.; Rouleau, C.M. Synthesis of novel thin-film materials by pulsed laser deposition. *Science (80-.).* **1996**, *273*, 898–903, doi:10.1126/science.273.5277.898.

22. Smith, H.M.; Turner, A.F. Vacuum deposited thin films using a ruby laser. *Appl. Opt.* **1965**, *4*, 147, doi:10.1364/AO.4.000147.

23. Singh, R.K.; Narayan, J. Pulsed-laser evaporation technique for deposition of thin films: Physics and theoretical model. *Phys. Rev. B* **1990**, *41*, 8843–8859, doi:10.1103/PhysRevB.41.8843.

24. Willmott, P.R.; Huber, J.R. Pulsed laser vaporization and deposition. *Rev. Mod. Phys.* **2000**, *72*, 315–328, doi:10.1103/RevModPhys.72.315.

25. Schou, J. Physical aspects of the pulsed laser deposition technique: The stoichiometric transfer of material from target to film. *Appl. Surf. Sci.* **2009**, *255*, 5191–5198, doi:10.1016/j.apsusc.2008.10.101.

26. Ashfold, M.N.R.; Claeyssens, F.; Fuge, G.M.; Henley, S.J. Pulsed laser ablation and deposition of thin films. *Chem. Soc. Rev.* **2004**, *33*, 23–31, doi:10.1039/b207644f.

27. Lu, J.; Elam, J.W.; Stair, P.C. Atomic layer deposition - Sequential self-limiting surface reactions for advanced catalyst "bottom-up" synthesis. *Surf. Sci. Rep.* **2016**, *71*, 410–472, doi:10.1016/j.surfrep.2016.03.003.

28. Johnson, R.W.; Hultqvist, A.; Bent, S.F. A brief review of atomic layer deposition: From fundamentals to applications. *Mater. Today* **2014**, *17*, 236–246, doi:10.1016/j.mattod.2014.04.026.

29. George, S.M. Atomic layer deposition: An overview. *Chem. Rev.* **2010**, *110*, 111–131, doi:10.1021/cr900056b.

30. Leskelä, M.; Ritala, M. Atomic layer deposition chemistry: Recent developments and future challenges. *Angew. Chemie - Int. Ed.* **2003**, *42*, 5548–5554, doi:10.1002/anie.200301652.

31. Bernal Ramos, K.; Saly, M.J.; Chabal, Y.J. Precursor design and reaction mechanisms for the atomic layer deposition of metal films. *Coord. Chem. Rev.* **2013**, *257*, 3271–3281, doi:10.1016/j.ccr.2013.03.028.

32. Suntola, T. Atomic layer epitaxy. *Mater. Sci. Reports* **1989**, *4*, 261–312, doi:10.1016/S0920-2307(89)80006-4.

33. Li, Z.; Gordon, R.G. Thin, continuous, and conformal copper films by reduction of atomic layer deposited copper nitride. *Chem. Vap. Depos.* **2006**, *12*, 435–441, doi:10.1002/cvde.200606485.

34. Knisley, T.J.; Kalutarage, L.C.; Winter, C.H. Precursors and chemistry for the atomic layer deposition of metallic first row transition metal films. *Coord. Chem. Rev.* **2013**, *257*, 3222–3231, doi:10.1016/j.ccr.2013.03.019.

35. Mane, A.U.; Shivashankar, S.A. Atomic layer chemical vapour deposition of copper. *Mater. Sci. Semicond. Process.* **2004**, *7*, 343–347, doi:10.1016/j.mssp.2004.09.094.

36. Li, Z.; Rahtu, A.; Gordon, R.G. Atomic layer deposition of ultrathin copper metal films from a liquid copper(I) amidinate precursor. *J. Electrochem. Soc.* **2006**, *153*, C787, doi:10.1149/1.2338632.

37. Moon, D.Y.; Han, D.S.; Shin, S.Y.; Park, J.W.; Kim, B.M.; Kim, J.H. Effects of the substrate temperature on the Cu seed layer formed using atomic layer deposition. *Thin Solid Films* **2011**, *519*, 3636–3640, doi:10.1016/j.tsf.2011.01.346.

38. Hugh Pierson. Handbook of chemical vapor deposition (cvd). *Library of Congress Cataloging-in-Publication Data*; ISBN 0-8155-1432-8.

39. Choy, K.L. Chemical vapour deposition of coatings. *Prog. Mater. Sci.* **2003**, *48*, 57–170,

doi:10.1016/S0079-6425(01)00009-3.

40. Thurier, C.; Doppelt, P. Platinum OMCVD processes and precursor chemistry. *Coord. Chem. Rev.* **2008**, *252*, 155–169, doi:10.1016/j.ccr.2007.04.005.

41. Kafizas, A.; Carmalt, C.J.; Parkin, I.P. CVD and precursor chemistry of transition metal nitrides. *Coord. Chem. Rev.* **2013**, *257*, 2073–2119, doi:10.1016/j.ccr.2012.12.004.

42. Katsui, H.; Goto, T. Epitaxial growth of (104)- and (018)-oriented $LiCoO_2$ films on MgO single crystals prepared by chemical vapor deposition. *Surf. Coatings Technol.* **2013**, *218*, 57–61.

43. Kim, H.; Bhandari, H.B.; Xu, S.; Gordon, R.G. Ultrathin CVD Cu Seed Layer Formation Using Copper Oxynitride Deposition and Room Temperature Remote Hydrogen Plasma Reduction. *J. Electrochem. Soc.* **2008**, *155*, H496, doi:10.1149/1.2912326.

44. Maruyama, T.; Ikuta, Y. Copper thin films prepared by chemical vapour deposition from copper dipivalylmethanate. *J. Mater. Sci.* **1993**, *28*, 5540–5542, doi:10.1007/BF00367827.

45. Creighton, J.R.; Ho, P. Chapter 1 Introduction to Chemical Vapor Deposition (CVD). *Springer* **2001**, 11–13, doi:10.1162/ARTL_a_00098.

46. Bhandari, H.B.; Yang, J.; Kim, H.; Lin, Y.; Gordon, R.G.; Wang, Q.M.; Lehn, J.-S.M.; Li, H.; Shenai, D. Chemical vapor deposition of cobalt nitride and its application as an adhesion-enhancing layer for advanced copper interconnects. *ECS J. Solid State Sci. Technol.* **2012**, *1*, N79–N84, doi:10.1149/2.005205jss.

47. Gaskell, S.J. Electrospray: Principles and Practice. *J. Mass Spectrom.* **1997**, *32*, 677–688, doi:10.1002/(SICI)1096-9888(199707)32:7<677::AID-JMS536>3.0.CO;2-G.

48. Chen, C.H.; Buysman, A.A.J.; Kelder, E.M.; Schoonman, J. Fabrication of LiCoO2thin film cathodes for rechargeable lithium battery by electrostatic spray pyrolysis. *Solid State Ionics* **1995**, *80*, 1–4, doi:10.1016/0167-2738(95)00140-2.

49. Kessick, R.; Fenn, J.; Tepper, G. The use of AC potentials in electrospraying and electrospinning processes. *Polymer (Guildf).* **2004**, *45*, 2981–2984, doi:10.1016/j.polymer.2004.02.056.

50. Lincot, D.; Guillemoles, J.F.; Taunier, S.; Guimard, D.; Sicx-Kurdi, J.; Chaumont, A.; Roussel, O.; Ramdani, O.; Hubert, C.; Fauvarque, J.P.; et al. Chalcopyrite thin film solar cells by electrodeposition. *Sol. Energy* **2004**, *77*, 725–737, doi:10.1016/j.solener.2004.05.024.

51. Yadav, A.A.; Chavan, U.J. Electrochemical supercapacitive performance of spray deposited Co3O4thin film nanostructures. *Electrochim. Acta* **2017**, *232*, 370–376, doi:10.1016/j.electacta.2017.02.157.

52. Mallik, A.; Ray, B.C. Evolution of Principle and Practice of Electrodeposited Thin Film: A Review on Effect of Temperature and Sonication. *Int. J. Electrochem.* **2011**, *2011*, 1–16, doi:10.4061/2011/568023.

53. Zhen, Q. Synthesis and Electrochemical Properties of Advanced Nanostructured Electrode for Lithium Secondary Batteries Starting from Layered Compounds.

54. Morales, J.; Sánchez, L.; Bijani, S.; Martínez, L.; Gabás, M.; Ramos-Barrado, J.R. Electrodeposition of Cu_2O: An excellent method for obtaining films of controlled morphology and good performance in Li-ion batteries. *Electrochem. Solid-State Lett.* **2005**, *8*, A159, doi:10.1149/1.1854126.

55. Bacsa, R.; Ravindranathan, P.; Dougherty, J.P. Electrochemical-hydrothermal synthesis of barium titanate thin films on titanium substrates. **1996**, *7*.

56. *Copper and Copper Alloys*; Davis, J.R., Ed.; ASM international: Ohio, USA, 2001; ISBN 0-87170-726-8.

57. Quan, Z.; Ohguchi, S.; Kawase, M.; Tanimura, H.; Sonoyama, N. Preparation of nanocrystalline LiMn2O4thin film by electrodeposition method and its electrochemical

performance for lithium battery. *J. Power Sources* **2013**, *244*, 375–381, doi:10.1016/j.jpowsour.2012.12.087.

58. Han, S.; Lee, T.L.; Yang, C.J.; Shih, H.C. Trench gap-filling copper by ion beam sputter deposition. *Mater. Chem. Phys.* **2006**, *97*, 19–22, doi:10.1016/j.matchemphys.2005.05.042.

59. Livage, J. Sol-gel chemistry and electrochemical properties of vanadium oxide gels. *Solid State Ionics* **1996**, *86–88*, 935–942, doi:10.1016/0167-2738(96)00336-0.

60. Dimitriev, Y.; Ivanova, Y.; Iordanova, R. History of sol–gel science and technology. *J. Univ. Chem. Technol. Metall.* **2008**, *34*, 181–192.

61. Chen, D. Anti-reflection (AR) coatings made by sol–gel processes: A review. *Sol. Energy Mater. Sol. Cells* **2001**, *68*, 313–336, doi:10.1016/S0927-0248(00)00365-2.

62. Nagai, H.; Sato, M. Heat treatment in molecular precursor method for fabricating metal oxide thin films. In *Heat Treatment—Conventional and Novel Applications*; Czerwinski, F., Ed.; InTech: Rijeka, Croatia, 2012; pp. 297–322.

63. Takano, I.; Nagai, H.; Mochizuki, C.; Aoyama, S.; Hara, H.; Sato, M.; Honda, T. Photoluminescence and photoreactivity affected by oxygen defects in crystal-oriented rutile thin film fabricated by molecular precursor method. *J. Mater. Sci.* **2010**, *45*, 5704–5710, doi:10.1007/s10853-010-4640-z.

64. Nagai, H.; Sato, M. Molecular Precursor Method for Fabricating p -Type Cu_2O and Metallic Cu Thin Films. *Mod. Technol. Creat. Thin-film Syst. Coatings* **2017**, 3–20, doi:10.5772/66476.

65. Nagai, H.; Mochizuki, C.; Hara, H.; Takano, I.; Sato, M. Enhanced UV-sensitivity of vis-responsive anatase thin films fabricated by using precursor solutions involving Ti complexes. *Sol. Energy Mater. Sol. Cells* **2008**, *92*, 1136–1144, doi:10.1016/j.solmat.2008.04.005.

66. Likius, D.S.; Nagai, H.; Aoyama, S.; Mochizuki, C.; Hara, H.; Baba, N.; Sato, M. Percolation threshold for electrical resistivity of Ag-nanoparticle/titania composite thin films fabricated using molecular precursor method. *J. Mater. Sci.* **2012**, *47*, 3890–3899, doi:10.1007/s10853-011-6245-6.

67. Nagai, H.; Suzuki, T.; Takahashi, Y.; Sato, M. Photovoltaic lithium-ion battery fabricated by molecular precursor method. *Funct. Mater. Lett.* **2016**, *9*, 1650046-1–4, doi:10.1142/S1793604716500466.

68. Mochizuki, C.; Hara, H.; Takano, I.; Hayakawa, T.; Sato, M. Application of carbonated apatite coating on a Ti substrate by aqueous spray method. *Mater. Sci. Eng. C* **2013**, *33*, 951–958, doi:10.1016/j.msec.2012.11.027.

69. Nagai, H.; Sato, M. Molecular precursor method for fabricating *p*-Type Cu_2O and metallic Cu thin films. In *Mod. Technol. Creat. Thin-film Syst. Coatings*; Nikitenkov, N., Ed.; InTech: Rijeka, Croatia, 2017; pp. 3–20, doi:10.5772/66476.

70. Sato, M.; Hara, H.; Nishide, T.; Sawada, Y. A water-resistant precursor in a wet process for TiO2 thin film formation. *J. Mater. Chem.* **1996**, *6*, 1767, doi:10.1039/jm9960601767.

71. Nagai, H.; Sato, M. Highly functionalized lithium-ion battery. In *Alkali-ion Batteries*; InTech, 2016.

72. Nagai, H.; Suzuki, T.; Mochizuki, C.; Takano, I.; Honda, T.; Sato, M. Formation Mechanism of *p*-Type Cu_2O Thin Films via Intermediate Cu^0 Species Derived from Cu(II) Complex of Ethylenediamine-*N*,*N*,*N*′,*N*′-Tetraacetic Acid. *Sci. Adv. Mater.* **2014**, *6*, 603–611, doi:10.1166/sam.2014.1788.

73. Nagai, H.; Mita, S.; Takano, I.; Honda, T.; Sato, M. Conductive and semi-transparent Cu thin film fabricated using molecular precursor solutions. *Mater. Lett.* **2015**, *141*, 235–237, doi:10.1016/j.matlet.2014.11.056.

74. Nagai, H.; Suzuki, T.; Nakano, T.; Sato, M. Embedding of copper into submicrometer trenches in a silicon substrate using the molecular precursor solutions with copper. *Mater. Lett.* **2016**, *182*, 206–209, doi:10.1016/j.matlet.2016.06.123.

75. Scriven, L.E. Physics and applications of dip coating and spin coating. *MRS Proc.* **1988**, *121*, 717, doi:10.1557/PROC-121-717.

76. Norrman, K.; Ghanbari-Siahkali, A.; Larsen, N.B. Studies of spin-coated polymer films. *Annu. Reports Prog. Chem. - Sect. C* **2005**, *101*, 174–201, doi:10.1039/b408857n.

77. Jilani, A.; Abdel-wahab, M.S.; Hammad, A.H. Advance deposition techniques for thin film and coating. In *Modern Technologies for Creating the Thin-film Systems and Coatings*; InTech, 2017; Vol. 7, pp. 137–149.

78. Habibi, M.; Rahimzadeh, A.; Bennouna, I.; Eslamian, M. Defect-free large-area (25 cm^2) light absorbing perovskite thin films made by spray coating. *Coatings* **2017**, *7*, 42, doi:10.3390/coatings7030042.

79. Singh, I.; Bedi, R.K. Studies and correlation among the structural, electrical and gas response properties of aerosol spray deposited self assembled nanocrystalline CuO. *Appl. Surf. Sci.* **2011**, *257*, 7592–7599, doi:10.1016/j.apsusc.2011.03.133.

80. Eslamian, M. Spray-on Thin Film PV Solar Cells: Advances, Potentials and Challenges. *Coatings* **2014**, *4*, 60–84, doi:10.3390/coatings4010060.

81. Girotto, C.; Rand, B.P.; Genoe, J.; Heremans, P. Exploring spray coating as a deposition technique for the fabrication of solution-processed solar cells. *Sol. Energy Mater. Sol. Cells* **2009**, *93*, 454–458, doi:10.1016/j.solmat.2008.11.052.

82. Vak, D.; Kim, S.S.; Jo, J.; Oh, S.H.; Na, S.I.; Kim, J.; Kim, D.Y. Fabrication of organic bulk heterojunction solar cells by a spray deposition method for low-cost power generation. *Appl. Phys. Lett.* **2007**, *91*, 1–4, doi:10.1063/1.2772766.

83. Abdellah, A.; Baierl, D.; Fabel, B.; Lugli, P.; Scarpa, G.; München, T.U. Spray-coating

deposition for large area organic thin-film devices. *NSTI-Nanotech* **2009**, *2*, 447–450.

84. Hsu, H.-W.; Liu, C.-L. Spray-coating semiconducting conjugated polymers for organic thin film transistor applications. *RSC Adv.* **2014**, *4*, 30145–30149, doi:10.1039/c4ra03726j.

85. Zabihi, F.; Eslamian, M. Characteristics of thin films fabricated by spray coating on rough and permeable paper substrates. *J. Coatings Technol. Res.* **2015**, *12*, 489–503, doi:10.1007/s11998-015-9656-5.

86. Filipovic, L.; Selberherr, S.; Mutinati, G.C.; Brunet, E.; Steinhauer, S.; Anton, K.; Teva, J.; Kraft, J.; Schrank, F. Modeling spray pyrolysis deposition. *Proc. World Congr. Eng.* **2013**, *II*, 6–11, doi:10.1021/ja411509g.

87. Kelly, A.J. Charge injection electrostatic atomizer modeling. *Aerosol Sci. Technol.* **1990**, *12*, 526–537, doi:10.1080/02786829008959367.

88. Viguié, J.C. Chemical vapor deposition at low temperatures. *J. Electrochem. Soc.* **1975**, *122*, 585–588, doi:10.1149/1.2134266.

89. Choy, K.L.; Su, B. Growth behavior and microstructure of CdS thin films deposited by an electrostatic spray assisted vapor deposition (ESAVD) process. *Thin Solid Films* **2001**, *388*, 9–14, doi:10.1016/S0040-6090(00)01894-0.

CHAPTER 2: METHODOLOGY

CHAPTER 2: METHODOLOGY

In this chapter, the materials and methods used in the present study are given. The chapter starts with the presentation of all chemical reagents and other consumables, followed by the procedures for the preparation of the substrates to be coated. Because of the differences in the contents of the coating solution for each type of thin films fabricated in this study, the procedures for the preparation of precursor solutions are given in chapter 3–5. The procedures used to carry-out the spray-coating a described, followed by the heat-treating procedures. Finally, all measurements employed to achieve full characterization of the prepared precursor solutions and the resultant films are described. In addition, results from the characterization of materials that were mainly used as starting reagents are also given in this chapter.

2.1. Materials

The chemical reagents and other consumables used in this study are listed in Table 1 below. Unless specified, all chemicals were used without further purification.

Table 1. List of chemical reagents and consumables used in this study.

Chemical/ Consumable	Formula/ Abbreviation[*1]	Fw	Supplier[*3]
2-propanol	IPA	60.10	KC
2mass% multiwalled carbon nanotubes ink	2mass% MWCNT	-	MNC
Ammonium hydroxide	NH_4OH	17.03	TC
Ar gas	Ar	39.95	
Butylamine	$BuNH_2$	73.14	WPC
Cobalt(II) acetate tetrahydrate	$Co(OAc)_2 \cdot 4H_2O$		WPC
Copper(II) acetate monohydrate	$Cu(OAc)_2 \cdot H_2O$	199.65	KC

Copper(II) formate tetrahydrate	$Cu(HCOO)_2 \cdot 4H_2O$	225.64	WPC
Cobalt(II, III) oxide (99.995%)	Co_3O_4	240.80	SA
Deionized water	H_2O	18.02	KP
Ethanol[*2]	EtOH	46.07	UCI
Ethylenediamine-*N,N,N′,N′*-tetraacetic acid	EDTA	292.25	KC
Lithium acetate dihydrate	$LiCH_3COO \cdot 2H_2O$	102.01	KC
Layered-rock-salt lithium cobalt(III) oxide (99.8%)	LCO	97.87	SA
Molecular sieves 4A	-	-	WPC
Quartz glass (100 × 100 × 1.6 mm^3)	-	-	AG

[*1] The abbreviations used a recognized in the chemical industry.

[*2] The purchased solvent was dried over molecule sieves 4A.

[*3] The codes for the suppliers are as follows: KC - Kanto Chemical Co., Inc.; MNC - Meijo Nano Carbon Co. Ltd; TC - Taisei Chemical Co., Ltd.; WPC - Wako Pure Chemical Industries, Ltd.; SA - Sigma-Aldrich Co.; KP - Kyoei Pharmaceuticals Co., Ltd.; UCI - Ueno Chemical Industries, Ltd.; AG - Akishima Glass Co., Ltd.

2.2. Cleaning of the substrates

The properties of any product are highly dependent on the fabrication conditions. In the case of the thin films, the condition of the substrate onto which the thin film is to be deposited is very important. This implies that the prior to the deposition process, the surface of the substrate need to be free of any contaminations as they are able to compromise the quality of the deposited film, leading to poor characteristics such as weak adhesion strength or unwanted different reactions. In our laboratory, the task of proper substrate-cleaning has been effectively incorporated in the experimental procedures and a cleaning process has been proposed.

This cleaning process was employed in this thesis to clean the used quartz glass substrates after they have been cut into small pieces measuring 20 × 20 cm^2 in size. The steps involved are described as follows: first, to remove any organic materials or metallic impurities from the surface of the substrates, the cut pieces were ultrasonicated for 30 minutes in a detergent/water mixture prepared by mixing 100 mL of Clean Ace with 200 mL of water. After ultrasonication, the substrates were then cleaned using a sponge and rinsed with DI H_2O. The cleaned substrates were further ultrasonicated in water for 30 minutes and the procedure was repeated one more time. To remove any remaining organic molecules physisorbed onto substrates, the substrates were ultrasonicated in IPA for 30 minutes. Finally, after the ultrasonication in IPA, the substrates were rinsed in fresh IPA and stored in a container filled with IPA. Prior to the spray-coating procedures, the substrates are dried in the drying oven at 70°C.

2.3. Coating procedures

2.3.1. Spray-coating

The spray-coating onto pre-heated quartz glass substrates of 20 × 20 mm^2 size were separately performed using the corresponding precursor solutions for the desired thin films. In each case, the quartz glass was placed on a steel plate on top of a hot-plate. The temperature of the steel plate was kept at 180°C and continuously monitored with a thermocouple (chromel-alumel type, surface probe A3-K-1-Q). Each coating solution was sprayed onto the pre-heated substrate from the airbrush (HP-SAR; ANEST IWATA Co., Japan) using compressed air (0.2 MPa) as a carrier gas, spraying for 5 s at 20 s intervals and at a spray rate of 1.67 mL min^{-1}. The vertical distance between the tip of the airbrush and the substrate was 300 mm. the schematic representation of the spray-coating setup used in this thesis is given below.

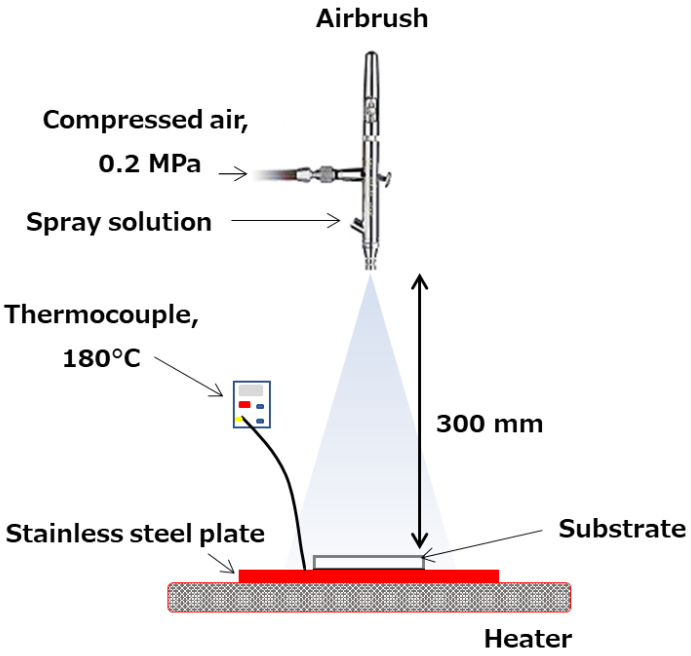

Figure 1. Schematic representation of the spray-coating setup used in this thesis.

2.3.2. Spin-coating

In this thesis, the spin-coating was done at ambient temperature and pressure, using a spin-coater (KYOWARIKEN, K-359S1) in double-step mode. The first step was carried out at 500 rpm for 5 s, and the second step at 2000 rpm for 30 s.

2.4. Heat-treatment

As described in chapter 1(on the protocol of the MPM), heat-treatment of the precursor films is an important aspect. In this thesis, two different heat-treating conditions were employed and have been divided into two categories. The first category is for the heat-treatment conditions involved in the fabrication of Cu and MWCNT/Cu thin films. The second category is on the heat-treatment conditions involved in the fabrication of LCO thin films.

2.4.1. Cu and MWCNT/Cu thin films

The precursor films were heat-treated at 350°C for 50 min under Ar gas with a flow rate of 1.5 L min^{-1} in a tubular furnace (EPKRO-12K, Isuzu, Tokyo, Japan) with a quartz glass tube (40 mm diameter and 650 mm length). The tube was filled with Ar gas by purging air for 10

min at a flow rate of 1.5 L min^{-1}. The furnace was heated to 350°C from 25°C at a constant temperature raising rate of 14°C min^{-1}, kept at 350°C for 50 min, and then cooled to room temperature.

On the basis of our previous experiments, as outlined in the plausible scheme for the formation of Cu thin film from the precursor film by the MPM (in chapter 1), the heat-treated films were post-annealed by placing clean identical-sized quartz glasses on top and heat-treating at 400°C for 50 min under an Ar gas at a flow rate of 1.5 L min^{-1}, in the same tubular furnace. The post-annealing procedure is very important for the fabrication of single-phase Cu thin films by removing the Cu_2O phase that is formed as a result of heat-treating the precursor film in an Ar gas atmosphere that contains less than 10 ppm of air as its impurity.

2.4.2. LCO thin films

The precursor films were heat-treated at 500°C for 30 min in the air using a separation muffle furnace (Asahi, Japan).

2.5. Measurements

A combination of various analytical techniques was used for the successful characterization of the prepared materials. In this section, all techniques that were helpful for characterization of the prepared solutions and the fabricated films are briefly summarized along with the instruments used.

2.5.1. Functional groups characterization by FTIR

Fourier transform infrared (FTIR) spectroscopy has been identified as the most useful tool for the identification of organic or inorganic chemicals. The technique is based on the interaction between matter and electromagnetic field in the IR region. Practically, all compounds show characteristic absorption/ emission in the IR spectral region. Depending on the elements and type of bonds, molecular bonds vibrate at various frequencies upon absorbing

light energy. Therefore, fingerprint information on the chemical composition of any sample can be obtained. Substantial advantages of FTIR include improved signal-to-noise ratio, resolution, speed, and detection limit.

From the previous studies conducted in our laboratory, the fabrication of Cu thin films required the use of a Cu(II) complex of EDTA as a starting material. Therefore, the Cu(II) complex of EDTA was prepared according to the procedures previously reported [1], with the aim of preparing a complex with the $[Cu(H_2edta)]\ H_2O$ formula. The molecular structure of the prepared complex was determined by Fourier-transform infrared (FT-IR) spectroscopy, using an FT-IR 620 spectrophotometer (JASCO). The measurements were performed by using the KBr pellet method. Before measurements, the dried powders of the prepared complex and an unreacted EDTA, each mixed with KBr were vacuum-dried at room temperature for 1 h. Figure 2 shows the FT-IR spectra of the EDTA and the prepared blue powder.

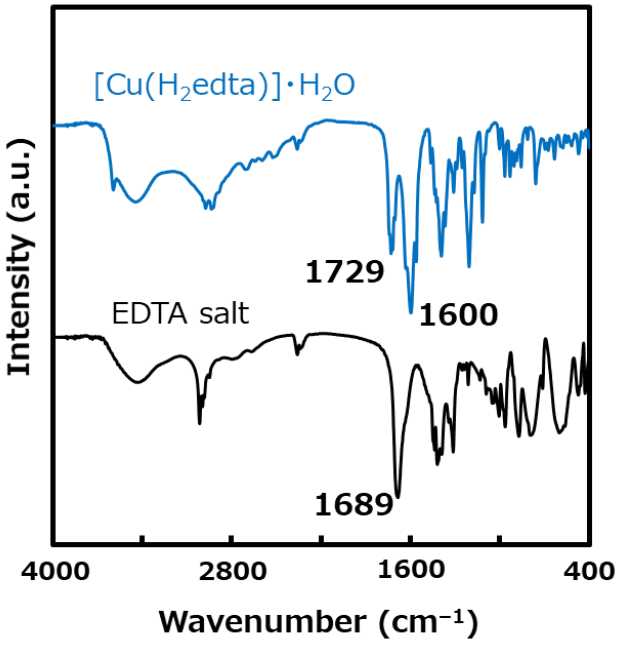

Figure 2. FT-IR spectra of the EDTA and prepared Cu(II)-edta complex.

The main characteristic peaks of interest could be observed at 1680 cm^{-1} in the spectrum of the EDTA and, at 1600 and 1729 cm^{-1} for the prepared powder. According to Nakamoto [2],

we can use infrared to distinguish the coordination properties of metal chelate compounds of EDTA based on the position of the peak(s) assignable to the COO stretching bands. It has been reported that the un-ionized and uncoordinated COO stretching band occurs at 1750–1700 cm^{-1}, whereas the ionized and coordinated COO stretching band, is at 1650–1590 cm^{-1} [2]. Form Figure 2, the spectrum of an un-complexed EDTA salt shows a peak at 1689 cm^{-1} assignable to the stretching band of an un-ionized and uncoordinated COO group. However, when a Cu(II) complex of EDTA is successfully coordinated, two of the oxygen atoms of the carboxyl groups for EDTA will be deprotonated and form bonds with the Cu^{2+} ion. This was therefore confirmed by the observed two peaks at 1600 and 1729 cm^{-1} for the prepared powder. In this case, the peak at 1600 cm^{-1} is assignable to the COO^- stretching band whereas the peak at 1729 cm^{-1} is assignable to the remaining un-deprotonated COO stretching band.

2.5.2. Thermal characterization by TG-DTA

TG-DTA is a simultaneous thermal analysis combining thermogravimetric (TG) analysis and differential thermal analysis (DTA), to obtain the thermal properties of a sample in a single experiment. TG measures temperatures where changes in physical and chemical properties of materials occur as a function of increasing temperature (with constant heating rate). Simultaneously, it also measures the mass changes associated with decomposition, oxidation, and any other physical or chemical change associated with mass loss or gain. The DTA component shows whether the decomposition processes are endothermic or exothermic, and also measures temperature corresponding to the phase changes where no mass loss occur, as the sample is subjected to higher temperatures. These changes include melting, crystallization and glass transition. In this thesis, the TG-DTA analysis was done to confirm the preparation of the Cu(II) complex of EDTA and characterize the purchased MWCNT inks. TG-DTA curves of the samples were measured on a TG-2010s instrument (Bruker AXS).

Exactly 5.10 mg of the dried powder for the Cu(II) complex of EDTA was placed into the pre-weighed platinum pan. The platinum sample holder with the powder was then heated from room temperature (25°C) to 1000°C at a rate of 10°C min^{-1} in the air at a flow rate of 0.1 L min^{-1} and using α-Al_2O_3 powder as the reference material. The TG-DTA curves of the are shown in figure 3. The DTA curve shows an endothermic peak at 178°C associated with a 5% mass decrease on the TG curve. This mass decrease corresponds to the removal of one molecule of crystalline water. There are other two exothermic peaks on the DTA curve of the powder at 243°C and 431°C assignable to the thermal decomposition of the organic components of the ligand, with a final weight loss of 79% leaving behind a residue of ca. 21% which can be assigned to CuO. Therefore, the TG-DTA results confirm the formation of the desired complex.

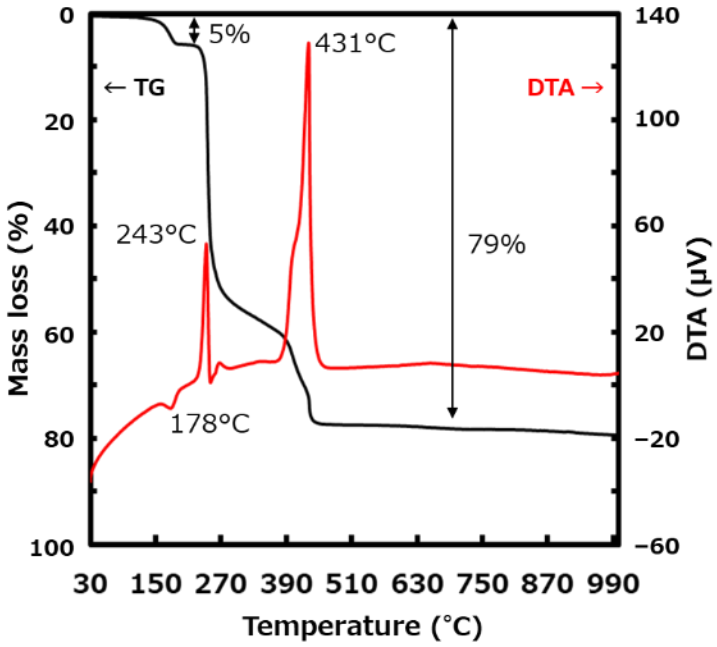

Figure 3. TG-DTA curves of the [Cu(H_2edta)] H_2O complex

In the case of MWCNT, 100.8 mg of the ink was transferred into a pre-weighed platinum sample holder and the solvent was removed by heating at 70°C for ten minutes. This was done repeatedly until the weight of the dried ink is constant, at a final mass of 6.00 mg. At 2 mass%, the total mass of the MWCNT in the used ink was 2.02 mg, equivalent to 34% of the final 6.00

mg. The platinum sample holder with the dried MWCNT ink was then heated from 25°C to 1000°C at a rate of 20°C min^{-1} in the air at a flow rate of 0.1 L min^{-1} and using α-Al_2O_3 powder as the reference material. The TG-DTA curves of the MWCNT ink are given in figure 4.

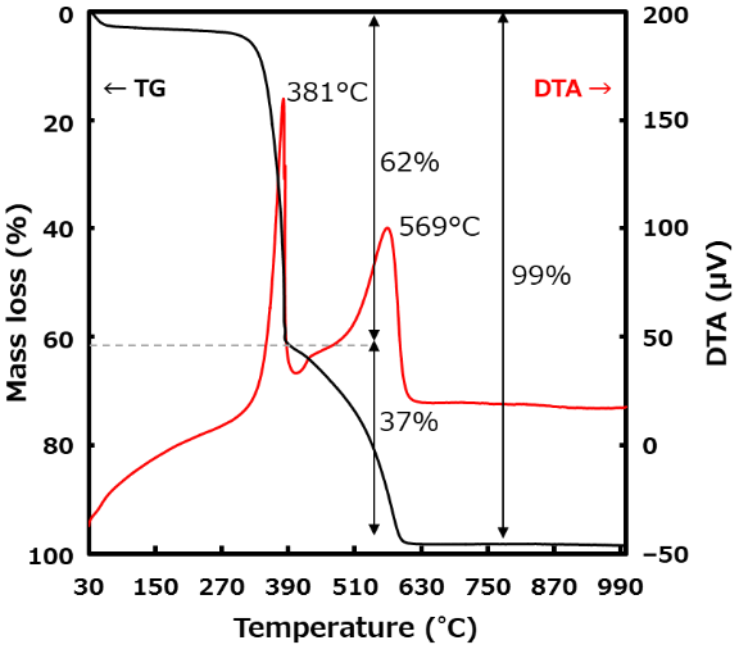

Figure 4. TG-DTA curves of the purchased 2 mass% MWCNT ink.

The two DTA peaks in the figure indicate the presence of two different components in the purchased ink. The exothermic peak at 381°C is accompanied by a weight loss of 62% and it is attributable to the combustion of the organic materials derived from the dispersant, and amorphous carbon in the ink. The final exothermic peak at 569°C is attributable to the combustion of the MWCNT, and it is accompanied by an extra 37% which includes the 34% of MWCNT in the sample. The total weight loss attained in this analysis was 99% implying that the ink contained about 1% of unspecified contaminations. From these results, I could confirm that the purchased MWCNT ink contains 2 mass% MWCNT and that, the MWCNT is thermally stable up to over 500°C in the air. This is important because heat-treatment is a required procedure for the fabrication of copper thin films in the MPM.

2.5.3. Structural characterization

X-ray diffraction (XRD)

XRD is a non-destructive method which has become an indispensable tool in modern industry and routine investigation, employed to determine the structure of materials based on the diffraction of x-rays. In the crystal lattice of any material, the atoms are orderly arranged in various phases, forming diffraction planes. Because the distance between the reflecting planes in a crystal is very small, it is impossible to obtain constructive interference with visible light. Therefore, rays of much smaller wavelength have to be used, such as x-rays. Additionally, in order to obtain constructive interference, three factors, distance between the reflecting planes (***d***), wavelength of the x-ray (***λ***) and the incidence angle theta (***θ***) bear a certain relation to each other and have been correlated together in the equation by Sir Lawrence Bragg which constitutes the concept of x-ray diffraction, and is referred to as the Bragg's Law. In order to obtain reflection with a certain distance, only one angle theta at a fixed wavelength can apply. The relation between these three factors is given by equation (1). The "n" in the equation is a positive integer.

$$2\boldsymbol{d}\sin\boldsymbol{\theta} = \mathrm{n}\,\boldsymbol{\lambda} \tag{1}$$

The crystal structures of all films were determined by means of XRD using a SmartLab X-ray diffractometer (Rigaku, Japan) with Cu *K*α radiation-source at a power of 45 kV and 200 mA. Parallel beam optics at an incidence angle 0.3° was used in the 2θ range of 10–80°, scanning at 0.05° step width and a speed of 5° min^{-1}.

Raman spectroscopy

Raman spectroscopy is based on the scattering of monochromatic radiation by the vibrating bonds in a molecule. The Raman technique is often superior to FTIR for the spectroscopy investigation of inorganic systems. In addition, the vibrational energies of metal-ligand bonds

are generally in the range of 100–700 cm^{-1}, a region of the IR that is experimentally difficult to study. However, interpreting the Raman spectra of compounds or materials in the solid state requires the knowledge of concepts and mathematical treatments other than those of molecular spectroscopy. For example, the Raman spectra of crystalline and amorphous solids of the same chemical composition can be significantly different, primary because of the presence or absence of spatial order and long-range translational symmetry, respectively [3]. In order to produce Raman scattering, high intensity is necessary. Therefore, lasers are preferably used as sources of monochromatic radiation. The laser line is used as a reference and the peaks arising from the Raman scattering are measured as the shift from the laser line.

In this thesis, the Raman spectra of the films were measured at room temperature under dark condition, using the Raman micro-spectrometer LaBRAM HR800 (Horiba, Kyoto, Japan) having a CCD detector. The Nd:YAG laser (532 nm) was used as the excitation source with the intensity of 10 mW and exposure times of 180 s. The spectra were measured in back-scattering geometry. The resolution was ca. 1 cm^{-1} and the spot size of the laser light was 100 μm^2.

The content of Co_3O_4 in the fabricated LCO films was determined using a calibration curve obtained from the peak area of the Raman spectrum of pure layered LCO and Co_3O_4 crystal powders [4]. In addition, mixtures of pure layered-structure LCO and CO_3O_4 crystal powders were prepared by mixing the two powders so that the mole ratios of Co_3O_4/LCO were 0, 1, 2, 4 and 8%. The Raman spectra were analyzed by using the corrected background fitted with a β-spline curve, and the background-corrected peaks were fitted using the Gaussian function. The peaks were separated by trial and error on the assumption of plural components until the tolerance T converged to 10^{-9}, where T is expressed by equation (2).

$$T = |(\chi')^2 - \chi^2|/|(\chi')^2 + \chi^2| \quad (2)$$

The χ^2 and $(\chi')^2$ values are the residuals in least-square refinement at the present- and previous-iteration calculations, respectively.

The results from the Raman analysis of the pure reference powders are given in figure 5. As expected, the Raman spectrum of pure layered-structure LCO (Figure 5(a)) shows two peaks at 485 and 595 cm^{-1} assignable to the layered-structure LCO [5–7]. In figure 5(b), the Raman spectrum of the pure Co_3O_4 reference sample shows all the expected peaks of the spinel Co_3O_4 at 194, 482, 522, 619 and 690 cm^{-1} [8].

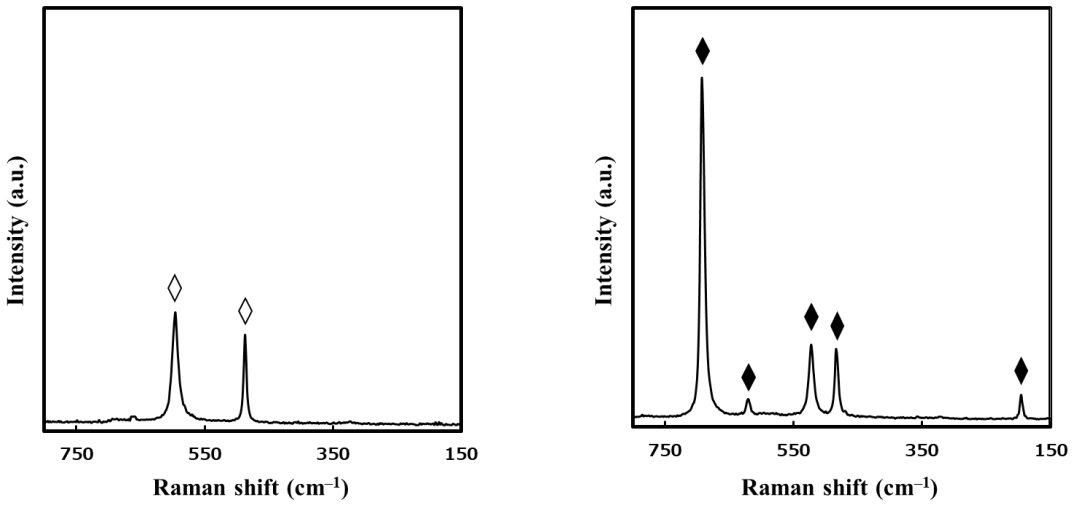

(**a**) (**b**)

Figure 5. Raman spectra of the pure reference powders. (a) Pure layered-structure LCO and (b) pure Co_3O_4.The peaks assignable to the vibration modes for layered-structure LCO and the Co_3O_4 are represented using ◊ and ♦, respectively.

Finally, the Raman spectra of the mixed powders and the calibration curve are presented in Figure 6. The percentage of Co_3O_4 in each mixture was then calculated as the area ratio of the fitted peaks assignable to the F_{2g} and E_g modes of Co_3O_4 and layered-structure LCO, respectively, with reference to the work by Tintignac *et al.*[9].

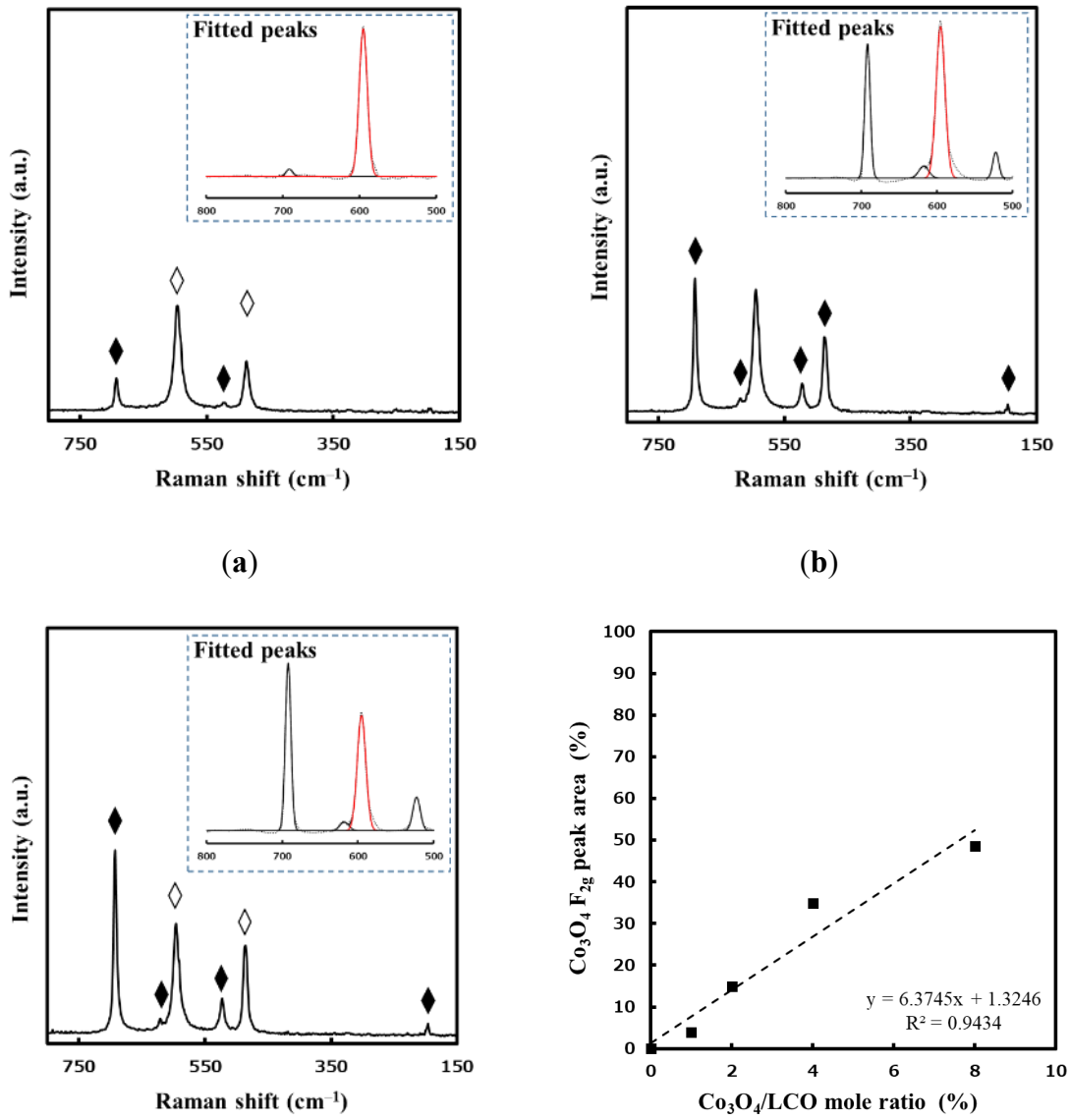

Figure 6. Raman spectra of the mixed reference powders for the (a) 2, (b) 4 and (c) 8 Co_3O_4/LCO mole ratios. The fitted curves are given as insets. (d) the calibration curve of the Co_3O_4 F_{2g} peak area vs the Co_3O_4/LCO mole ratio.

2.5.4. Surface morphology characterization

Field-emission scanning electron microscopy (FE-SEM)

FE-SEM is the ideal tool for obtaining topographical information at magnifications of 10× to 300 000×, with virtually unlimited depth of field. The principle of operation is based on the use of extremely focused high and a low-energy beam of electrons obtained from a field

emission gun (usually tungsten needles) to generate an image of the specimen. The extremely focused beam of electrons greatly improves spatial resolution and enables work to be carried out at very low potentials (0.02–5 kV). This helps to minimize the charging effect on non-conductive specimens and to avoid damage to electron beam sensitive samples.

In this thesis, the surface morphologies were of the films were observed by FE-SEM using a JSM-6701F (JEOL, Japan) at an accelerating voltage of 5 kV. For some samples, the film thicknesses were calculated as averages of ten different points taken from the cross-sectional SEM image. The cross-section images also assisted in establishing if the film is densely deposited on the quartz glass substrates or not.

Atomic force microscopy (AFM)

AFM represents a simple yet highly sensitive tool for obtaining morphological images of specimens. It is based on sensing of the forces between a sharp stylus and the surface of the specimen and uses the interatomic forces to image topography on the nanometer scale. The AFM technique employs an optical scheme identical to the one used in photothermal spectroscopy, capable of detecting displacements on the order of 10^{-4} Å [10]. The displacement of a cantilever is measured by detecting the deflection of a weak laser beam which is reflected off its backside with a position-sensitive-detector (PSD). AFM is considered most useful over other imaging techniques such as SEM because it can be used to image both conducting and non-conducting surfaces.

In this thesis, the surface 3D views of the Cu thin films were obtained by atomic force microscopy (AFM) using a LEXT OLS3500/SFT-3500 (Olympus Inc., Japan) by scanning each 5×5 μm^2 area.

2.5.5. Optical properties characterization by UV-vis spectroscopy

UV-vis spectroscopy is used to analyze the optical properties of the sample as it interacts with light in the visible adjacent ranges of the electromagnetic spectrum. The two main interactions of interest are the absorption and reflectance of light, and the perceived color of any material directly depends on these two interactions. Molecules containing π-electrons or non-bonding electrons (n-electrons) absorb energy in the form of ultraviolet or visible light to excite these electrons to higher antibonding molecular orbitals. This phenomenon is therefore used for the determination of different analytes such as transition metal ions, highly conjugated organic compounds, and biological macromolecules. In this thesis, the absorption spectra of precursor solutions were measured in the range from 300 to 800 with a double beam mode, using a Hitachi U-2800 spectrophotometer (Hitachi, Tokyo, Japan). Water and ethanol were used as references for the aqueous and ethanol-based solutions, respectively.

Generally, the reflectance of visible light is related to the number of free electrons in the reflecting body and the availability of free electrons means excellent electrical conductivity. In this thesis, the reflectance spectra of the Cu and MWCNT/Cu films were measured with a UV-3600 spectrophotometer (SHIMADZU, Japan). The measurements were done in the 220–2600 nm range using a double beam mode and air as the reference.

2.5.6. Physical properties characterization

Thickness measurements by profilometry

The film thicknesses of some films were measured by a stylus profilometer (DEKTAK-3, Sloan, California, USA). Prior to coating, a portion of ca. 3 mm size on the substrate edge was masked to leave an uncoated area. Thus, the thickness of the specific film was then measured as the level differences between the uncoated part of the substrate and the thin film.

Adhesion strength measurements by stud-pull

The adhesion strengths of the Cu and MWCNT/Cu films onto the quartz glass substrates were tested by the stud-pull coating adhesion test. In both cases, a stud-pin, P/N901106 with an internal diameter of 2.7 mm was attached to the film with epoxy glue and set in an oven at 150°C for 1 h. The test was then performed by pulling the stand pin with a load of 0 to 100 kg at a rate of 2.0 kg s^{-1}. Figure 7 shows the schematic representation of the stud-pull adhesion test along with the images of one sample as an example for the peeling results at the interface between the film and the substrate.

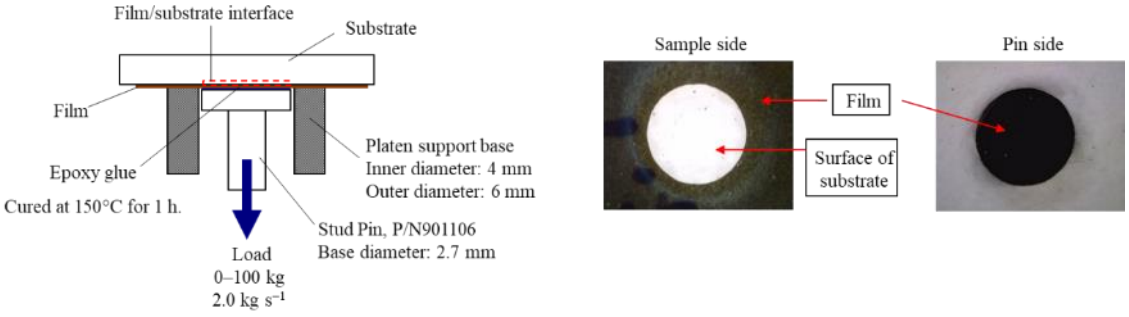

(**a**) (**b**)

Figure 7. (a) Schematic representation of the stud-pull test. (b) Example: sample result

2.5.7. Electrical properties characterization

Four probe measurements

The electrical resistance of each of the Cu and MWCNT/Cu films were evaluated using the four-probe method at 25°C. The four-probe set-up consisted of a regulated DC power supply (Model PAB32-1.2, Kikusui Electronics Corp.), two multimeters (VOAC7512, Iwatsu and Model 2010, Keithley, as a current source and voltmeter, respectively), and four Au-plated tungsten probes placed at intervals of 1 mm (FELL type, K&S) with an added load of 0.1 kg. the schematic representation of the measurements is shown in figure 8.

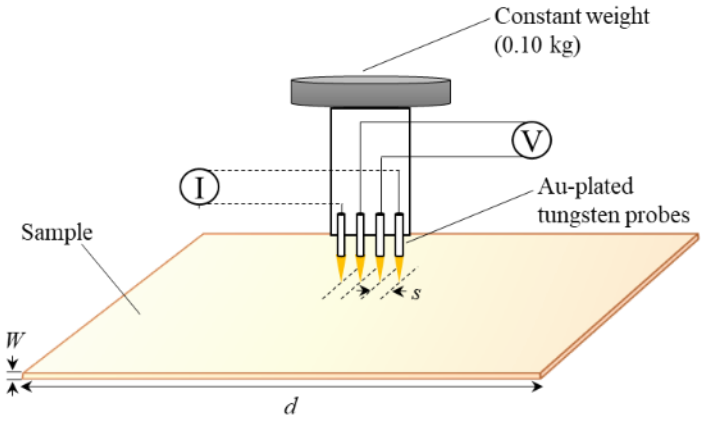

Figure 8. Schematic representation of the setup for Four-probe measurement

The electrical resistivity (ρ) of each sample was then calculated using the formula expressed by equation (3).

$$\rho = (V/I) \times W \times CF \tag{3}$$

where V is the measured voltage, I is the applied current, W is the film thickness and CF is the correction factor. The width of the measured samples, d was at least twenty times greater than the spacing (s) between the Au-plated tungsten probes. Therefore, the value of CF equals to 4.54 [11].

Hall effect measurements

In 1879, Edwin Hall discovered that the combination of a magnetic field and electric current flowing perpendicular to each other through a sample creates a transverse voltage that is perpendicular to both the magnetic field and the current. Since the discovery of this phenomenon, Hall effect measurements have been a valuable tool for the characterization of every material used in producing semiconductors, as well as most compound semiconductor materials [12]. Important parameters such as hall voltage ($\mathbf{V_H}$), carrier mobility ($\boldsymbol{\mu}$), carrier concentration ($\boldsymbol{n}$), electrical resistivity (ρ) and conductivity type (N or P) can be easily determined via Hall effect measurements.

In this thesis, the electrical resistivity, carrier concentration and carrier mobility of the LCO films were measured at ambient temperature using a Hall effect measurement system, HL5500 Hall system (Nanometrics, California, USA), using the magnetic field of 0.517 T.

2.5.8. Chemical characterization

Auger electron spectroscopy (AES)

AES is a surface-sensitive analytical technique that utilizes Auger electrons that are emitted from the surface of a sample, upon bombardment by an incident high-energy electron beam. It collects and measures the kinetic energies of the emitted Auger electrons, which are characteristic of elements present at the surface of a sample with a typical sampling depth of 2–5 nm [13]. Although AES is a destructive analysis technique, the ability to focus the electron beam onto diameters as small as 10 nm and less makes AES an extremely useful tool for elemental analysis of small surface features. It is useful in identifying concentrated areas of contamination and can also be used for quantitative analyses when standards are available for quantification. Samples to be analyzed must be vacuum compatible as the analysis is carried out under ultrahigh vacuum conditions. Additionally, the sample must be electrically conductive to avoid charge up.

In this thesis, the chemical composition of the Cu thin film was analyzed by means of AES using a field emission Auger microprobe, JAMP-9500F (JEOL, Japan) with a probe voltage and current of 10 kV and 10 nA, respectively. The sample was cleaned by slightly etching a 100 μm area with an Ar^+ beam (1000 eV, 10 nA, 30 s). The state of carbon present in the thin film was determined by curve-fitting of the carbon (C_{KLL}) curve of the film being analyzed with those of neutral and tetravalent carbon.

References

1. Nagai, H.; Suzuki, T.; Hara, H.; Mochizuki, C.; Takano, I.; Honda, T.; Sato, M. Chemical fabrication of p-type Cu_2O transparent thin film using molecular precursor method. *Mater. Chem. Phys.* **2012**, *137*, 252–257, doi:10.1016/j.matchemphys.2012.09.016.

2. Nakamoto, K. *Infrared and Raman Spectra of Inorganic and Coordination Compounds*; 4th ed.; John Wiley & Sons, Inc.: New York, 1986; ISBN 0-471-01066-9.

3. Tushcel, D. Why are the raman spectra of crystalline and amorphous solids different? *Spectroscopy* **2017**, *32*, 26–33.

4. Suzuki, T.; Nagai, H.; Lu, L.; Sato, M. Electrical properties of partially nitrided $LiCoO_2$ thin films with an equivalent amount of Li and Co, involving small amounts of amorphous or crystallized Co_3O_4. Manuscript submitted for publication.

5. Porthault, H.; Baddour-Hadjean, R.; Le Cras, F.; Bourbon, C.; Franger, S. Raman study of the spinel-to-layered phase transformation in sol-gel LiCoO2cathode powders as a function of the post-annealing temperature. *Vib. Spectrosc.* **2012**, *62*, 152–158, doi:10.1016/j.vibspec.2012.05.004.

6. Kosuril, Y.R.; Penki, T.R.; Nookala, M.M.; Morgen, P.; Gowravaram, M.R.; Rao Kosuri, Y.; Rao Penki, T.; Nookala, M.M.; Morgen, P.; Rao Gowravaram, M. Investigations on sputter deposited $LiCoO_2$ thin films from powder target. *Adv. Mater. Lett.* **2013**, *4*, 615–620, doi:10.5185/amlett.2012.12479.

7. Inaba, M.; Todzuka, Y.; Yoshida, H.; Grincourt, Y.; Tasaka, A.; Tomida, Y.; Ogumi, Z. Raman spectra of $LiCo_{1-y}Ni_yO_2$. *Chem. Lett.* **1995**, *24*, 889–890,

doi:10.1246/cl.1995.889.

8. Hadjiev, V.G.; Iliev, M.N.; Vergilov, I. V. The Raman spectra of Co_3O_4. *J. Phys. C Solid State Phys.* **1988**, *21*, L199–L201, doi:10.1088/0022-3719/21/7/007.

9. Tintignac, S.; Baddour-Hadjean, R.; Pereira-Ramos, J.P.; Salot, R. High performance sputtered $LiCoO_2$ thin films obtained at a moderate annealing treatment combined to a bias effect. *Electrochim. Acta* **2012**, *60*, 121–129, doi:10.1016/j.electacta.2011.11.033.

10. Meyer, G.; Amer, N.M. Erratum: Novel optical approach to atomic force microscopy. *Appl. Phys. Lett.* **1988**, *53*, 2400–2402, doi:10.1063/1.100425.

11. Sze, S.M. *Semiconductor Devices: Physics and Technology*; 2nd ed.; Wiley, 2002; ISBN 0471333727.

12. Green, R. Hall effect measurements in materials characterization. *Keithley White Pap.* **2011**, *3111*, 1–11, doi:10.1103/PhysRevLett.98.046601.

13. Welker, R.W. Chapter 4 - Size Analysis and Identification of Particles. In *developments in surface contamination and cleaning*; Kohli, R., Mittal, K.L., Eds.; William Andrew Publishing: Oxford, 2012; pp. 179–213 ISBN 978-1-4377-7883-0.

CHAPTER 3: FABRICATION OF COPPER THIN FILM BY SPRAY-COATING USING AQUEOUS SOLUTIONS OF COPPER(II) COMPLEXES

CHAPTER 3: FABRICATION OF HIGHLY CONDUCTIVE AND WELL-ADHERED COPPER THIN FILM ON A QUARTZ GLASS SUBSTRATE BY HEAT-TREATMENT OF A PRECURSOR FILM OBTAINED VIA SPRAY-COATING OF AN AQUEOUS SOLUTION INVOLVING COPPER(II) COMPLEXES

3.1. Introduction on copper

Copper is referred to as the first metal of humankind civilization. This is because it among some of the few metals found in the Earth's crust in its native form and can be easily used for various purposes without extensive processing. For example, due to its bright reddish appearance and ductility, metallic copper has been used for decorative purposes since ancient times and records show that it has been used by man for more than 10 000 years, with discoveries dating back to as far as 8700 B.C [1]. Presently, copper and copper alloys form part of the major groups of commercial metals, ranking third behind iron/steel and aluminum in production and consumption. Since its discovery, the applications of copper have increased significantly, owing to its many useful properties. Figure 1 shows the crystal structure of the unit cell of copper. And, other properties of copper are listed in Table 1.

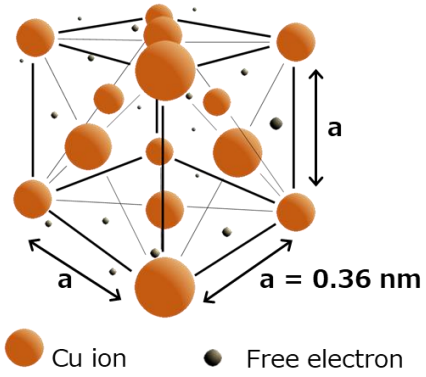

Figure 1. Face Centered Cubic (FCC) crystal structure of Cu.

Table 1. Electronic configuration of the copper atom and properties of metallic copper.

Electronic configuration	$[Ar]3d^{10}4S^{1}$
Electrical conductivity	103.06 %IACS[(a)] (pure silver 106, pure aluminum 65)
Thermal conductivity	398 W m^{-1} K^{-1} (pure silver 428, pure aluminum 247)
Other properties	Corrosion resistance, workability, color for surface finishes

[(a)] International Annealed Copper Standard. The electrical conductivity scale established in 1913 was based on a copper standard. **Definition:** The electrical conductivity of a specific material is expressed as the percent IACS, equal to 100 times the ratio of the volume resistivity of the annealed copper standard at 20°C to the value measured for the material concerned [1].

Based on the electronic structure of the copper atom (shown in table 1), there is a single 4s electron on the outer shell. In metallic copper, this 4s electrons does not remain associated with any particular atom but becomes part of the electron cloud extending throughout the crystal lattice. This is responsible for its many important physical properties of metallic copper, including the high electrical conductivity, chemical stability and the reddish color [1]. With an electrical resistivity of 1.72 μΩ cm, copper is an excellent conductor of electricity, only second to silver but more affordable. Therefore, copper plays an important role in the infrastructure of power transmission and electronics [2, 3], whereby materials from pure copper such as wires and cables, metal plates, strips, foils, and windings are used to conduct electricity and electronic signals especially in the electronics, telecoms, electronic data-processing and construction industries [1, 2]. As an excellent conductor of heat and resistant to corrosion, copper has found applications as components in heat exchangers, water and gas pipes and in the construction of machines, locomotives and vehicles [1, 4].

3.2. Copper thin films

Owing to the exceptional properties of Cu mentioned in the introduction section, thin films of metallic Cu have been identified as promising conductive materials and extensively used in

microelectronics [5]. Leading techniques, such as radio-frequency sputtering [6] and chemical vapor deposition [7], have been found to be capable of depositing Cu thin films of good quality. However, the high cost, complicated experimental setups, and procedures associated with these techniques [8] make it impossible for effective and low-cost fabrication of Cu thin films. Although electroless plating is another promising technology for the deposition of Cu thin films especially on insulating substrates, the use of $PdCl_2$ and $SnCl_2$ to activate the surface of the specimens compromises the quality of the thin films [9]. The use of inks containing Cu nanoparticles is also a promising technique for fabricating Cu films, usually of several microns in thickness and this research area is very active [10–12]. The multiple steps required in preparing the Cu nanoparticles, protecting them against oxidation using capping agents and finding appropriate solvents to obtain suitable inks still remain as some of the challenging aspects.

In this chapter, the fabrication of a highly conductive Cu thin film from aqueous solutions involving Cu(II) complexes, under ambient conditions via the MPM is reported. The experimental procedures discussed in this chapter is the preparation of the precursor solutions only.

3.3. Designing of the Cu(II) complexes in the coating solution

Based on previous experiments by our group, the conductive and semitransparent thin film of copper was fabricated by heat-treating a precursor film obtained after spin-coating a precursor solution involving a mixture of two Cu(II) metal complexes [13]. Before obtaining the final precursor solution, the two Cu(II) complexes were prepared separately. Firstly, an ethanol solution containing a dibutylammonium salt of Cu(II) complex of EDTA ($[Cu(H_2edta)]\cdot H_2O$) was prepared. Secondly, another ethanol solution was obtained by reacting Cu(II) formate with propylamine in ethanol. The two solutions were then mixed in a mole ratio

of 1: 8 [Cu(H_2edta)]·H_2O:Cu(II) formate. The schematic representations of the plausible Cu(II) complexes involved in the separate solutions are given in Figure 2, along with the counter-ions.

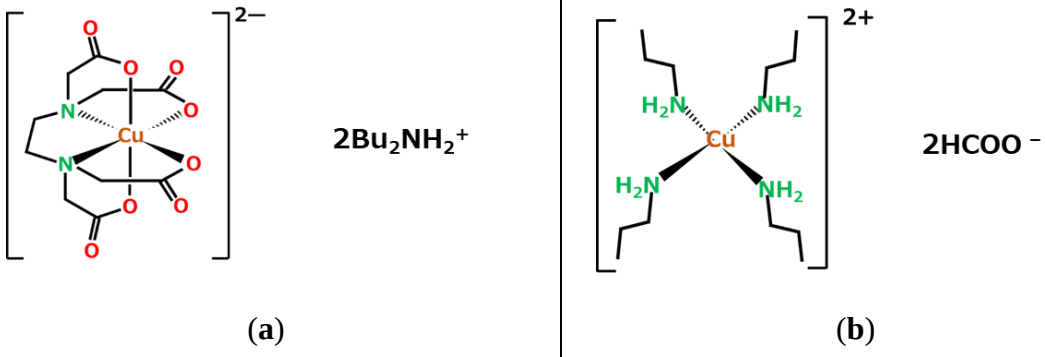

Figure 2. Chemical structures of the plausible Cu(II) complexes in the ethanol-based solution prepared by the previous work in the MPM.

The aim of the present study is to prepare an aqueous solution ideal for spray-coating, and by using the identical starting materials of [Cu(H_2edta)]·H_2O and Cu(II) formate as the sources of copper for the precursor solution. However, the solubility of these salts in water is very poor and, dibutylamine and propylamine cannot be used in aqueous solutions. Therefore, aqueous ammonium hydroxide (NH_4OH) is the ideal candidate to replace dibutylamine and propylamine. Figure 3 shows the plausible Cu(II) complexes in the proposed aqueous precursor solutions.

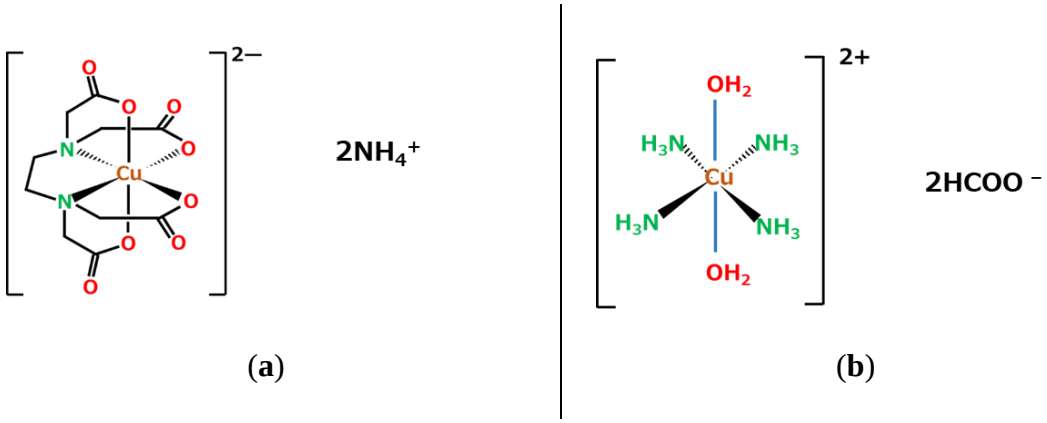

Figure 3. Chemical structures of the plausible Cu(II) complexes in the aqueous precursor solution proposed for the study reported in this thesis.

3.4. Thin film fabrication from a precursor solution involving an identical ratio of Cu(II) complexes identical to previous studies in the laboratory.

3.4.1. Preparations of the aqueous precursor solution.

The $[Cu(H_2edta)]\cdot H_2O$ complex was isolated according to the procedures previously reported [14]. Preparations of an aqueous precursor solution involved obtaining a mixture of a $[Cu(H_2edta)]\cdot H_2O$, $Cu(HCOO)_2\cdot 4H_2O$ and NH_4OH in deionized water, stirring the mixture on a magnetic stirrer for 1 hour at room temperature, and then filtering through a 0.8 µm membrane filter. As introduced in the previous section, Cu(II) complexes were mixed in a 1:8 $[Cu(H_2edta)]$:Cu(II) formate ratio. Therefore, in this study, the aqueous solution with the identical ratio between the two main sources of Cu(II) complexes was prepared, based on equation (1).

$$[Cu(H_2edta)]_{(aq)} + 8Cu(HCOO)_{2(aq)} + 36NH_{3(aq)} \rightarrow [Cu(NH_3)_4][Cu(edta)]_{(aq)} + 7[Cu(NH_3)_4]^{2+}{}_{(aq)} + 16HCOO^{-}{}_{(aq)} + 2NH_4{}^{+}{}_{(aq)} + 2NH_{3(aq)} \quad (1)$$

To prepare the precursor solution, $[Cu(H_2edta)]\cdot H_2O$ (0.218 g, 0.586 mmol) and $Cu(HCOO)_2\cdot 4H_2O$ (1.06 g, 4.70 mmol) were mixed in 25 g of deionized water followed by the addition of 28% NH_4OH (1.30 g, 21.4 mmol NH_3). The solution was used with no further modifications. Hereinafter, this precursor solution is denoted as $\mathbf{S_{mix\text{-}8}}$.

The spray-coating and the heat-treating procedures are explained in the previous chapter under section 2.3 and 2.4, respectively. Using the earlier-mentioned spray-coating and heat-treating procedures, in this chapter, the fabricated films are denoted as follows: $\mathbf{F_{mix\text{-}8}}$, $\mathbf{F'_{mix\text{-}8}}$, and $\mathbf{F''_{mix\text{-}8}}$ refer to the film obtained after spray-coating a quartz glass with the $\mathbf{S_{mix\text{-}8}}$ solution, the film obtained by heat-treating $\mathbf{F_{mix\text{-}8}}$ at 350°C for 50 min under Ar gas with a flow rate of 1.5 L min^{-1}, and the final resultant thin film obtained by post-annealing $\mathbf{F'_{mix\text{-}8}}$ at 400°C for 50 min under Ar gas with a flow rate of 1.5 L min^{-1}, respectively.

3.4.2. XRD results and a brief discussion on the resultant thin films obtained from $S_{mix\text{-}8}$.

The XRD patterns of the films obtained from **$S_{mix\text{-}8}$** are given in Figure 4. Figure 4(a) shows the XRD patterns of the **$F_{mix\text{-}8}$**, **$F'_{mix\text{-}8}$**, and **$F''_{mix\text{-}8}$** films that were fabricated during the initial trials of this study. The XRD patterns of the **$F_{mix\text{-}8}$** and **$F'_{mix\text{-}8}$** exhibit peaks assignable to the (111), (200) and (220) crystal phase of metallic copper at 2θ values of 43.5, 50.7 and 74.2°, respectively (ICDD card no. 00-004-0836). In addition, peaks assignable to the (111) and (220) crystal phase of Cu_2O can be observed at 36.6 and 61.6°, respectively (ICDD card no. 00-041-0254). For **$F''_{mix\text{-}8}$**, only peaks assignable to the crystal phase of metallic copper are present.

The XRD patterns of the films identical to **$F_{mix\text{-}8}$**, **$F'_{mix\text{-}8}$**, and **$F''_{mix\text{-}8}$**, fabricated in the subsequent trials during the course of the study are shown in Figure 4(b). Although the XRD pattern of the film right after spray-coating was identical to that of the **$F_{mix\text{-}8}$** from initial trials, the XRD patterns of the heat-treated and post-annealed films (**$F'_{mix\text{-}8}$** and **$F''_{mix\text{-}8}$**, respectively) showed a significantly high level of oxidation as observed from the increased height of the peaks assignable to the (111) and (220) crystal phase of Cu_2O, observed at 36.6 and 61.6°, respectively, and the appearance of three additional peaks assignable to the (111), (111), and (220) crystal phase of Cu_2O can be observed at 36.6, 36.6, and 61.6°, respectively.

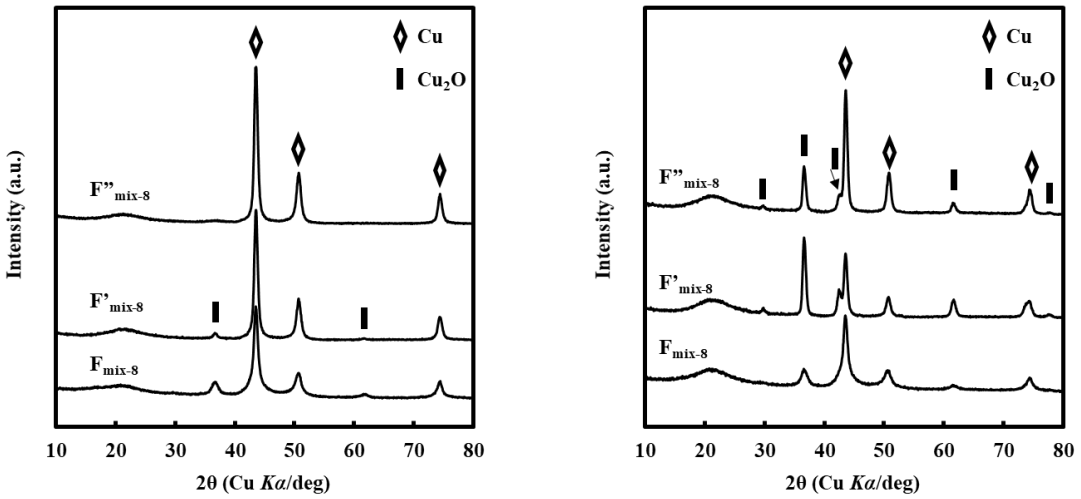

(**a**) (**b**)

Figure 4. XRD patterns of the films fabricated using the aqueous precursor solution **S_{mix-8}**. (a) Films fabricated during the first trials (b) Films fabricated during the subsequent trials.

In summary, although an aqueous precursor solution involving the Cu(II) complexes in mole ratios identical to previous studies in the laboratory was successfully prepared and used for spray-coating, the thin film reproducibility was difficult as observed from the XRD patterns of the films fabricated in the subsequent trials during the study (Figure 4(b)).

3.5. Preparation of coating solutions with different mole ratios of the Cu(II) complexes

As observed from the previous section, the reproducibility of a single-phase copper thin film was poor. Therefore, a precursor solution with a different [Cu(H_2edta)]:Cu(II) formate ratio is necessary to achieve excellent reproducibility. In addition, to observe the influence of each of the two Cu(II) complexes used in this research, two separate solutions one containing [Cu(H_2edta)] only and another containing Cu(HCOO)$_2$ only, were prepared as references.

3.5.1. Preparations of the aqueous precursor solutions with individual Cu(II) complexes.

The precursor solution **S_{edta}** was prepared by mixing [Cu(H_2edta)]·H_2O (0.980 g, 2.63 mmol) with 28% NH_4OH (0.360 g, 5.90 mmol NH_3) in 25 g of deionized water. **S_{form}** was prepared by mixing Cu(HCOO)$_2$·4H_2O (0.600 g, 2.66 mmol) with 28% NH_4OH (0.99 g, 16.3 mmol NH_3) in 25 g of deionized water. The proposed Cu(II) complexes in the solutions were prepared according to equation (2) and (3).

$$[Cu(H_2edta)]_{(aq)} + 2NH_{3(aq)} \rightarrow [Cu(edta)]^{2+}_{(aq)} + 2NH_4^{+}{}_{(aq)} \quad (2)$$

$$Cu(HCOO)_{2(aq)} + 4NH_{3(aq)} \rightarrow [Cu(NH_3)_4]^{2+}_{(aq)} + 2HCOO^{-}{}_{(aq)} \quad (3)$$

Using the earlier-mentioned spray-coating and heat-treating procedures, in this chapter, the fabricated films are denoted as follows: **F_{edta}** and **F_{form}** refer to the precursor films obtained after spray-coating a quartz glass with the **S_{edta}** and **S_{form}** solutions, respectively. The resultant

films obtained by heat-treating $\mathbf{F_{edta}}$ and $\mathbf{F_{form}}$ at 350°C for 50 min under Ar gas with a flow rate of 1.5 L min^{-1} are denoted as $\mathbf{F'_{edta}}$ and $\mathbf{F'_{form}}$, respectively. Finally, the films obtained from the post-annealing of $\mathbf{F'_{edta}}$ and $\mathbf{F'_{form}}$ at 400°C for 50 min under Ar gas with a flow rate of 1.5 L min^{-1} are denoted as $\mathbf{F''_{edta}}$ and $\mathbf{F''_{form}}$, respectively.

3.5.2. XRD results and a brief discussion on the resultant films obtained from S_{edta} and S_{form}.

Figure 5a presents the XRD patterns of $\mathbf{F_{edta}}$, $\mathbf{F'_{edta}}$, and $\mathbf{F''_{edta}}$. It was clarified that the film $\mathbf{F_{edta}}$ is amorphous because no peak was observed in its pattern. The three peaks at 43.4°, 50.5° and 74.2° for both $\mathbf{F'_{edta}}$ and $\mathbf{F''_{edta}}$ are assignable to the (111), (200) and (220) crystal phase of metallic Cu, respectively (ICDD card no. 00-004-0836). Figure 5(b) shows the XRD patterns of films fabricated using $\mathbf{S_{form}}$ only. For $\mathbf{F_{form}}$, the diffraction pattern shows peaks assignable to the (110), (111), (200), (220), (311) and (222) crystal phase of Cu_2O at 29.8, 36.7, 42.6, 61.7, 73.9 and 77.6°, respectively (ICDD card no. 00-041-0254). In addition to the Cu_2O peaks, a peak corresponding to the (111) crystal phase of CuO is observed at 38.7 (ICDD card no. 01-071-3645). The diffraction patterns of $\mathbf{F'_{form}}$ and $\mathbf{F''_{form}}$ show that the resultant films are composed of a combination of the two oxides for copper. For these two films, peaks assignable to the (110), (111), (200), (220), (311) and (222) crystal phase of Cu_2O can be observed at 29.8, 36.7, 42.6, 61.7, 73.9 and 77.6°, respectively. In addition, peaks assignable to the (110), (002), (111), (11–2), (20–2), (020), (202), (022), (113), (311), and (004) crystal phase of CuO can be observed at 32.6, 35.7, 38.8, 46.6, 49.1, 53.5, 58.3, 66.4, 68.1, 72.5, and 75.1°, respectively.

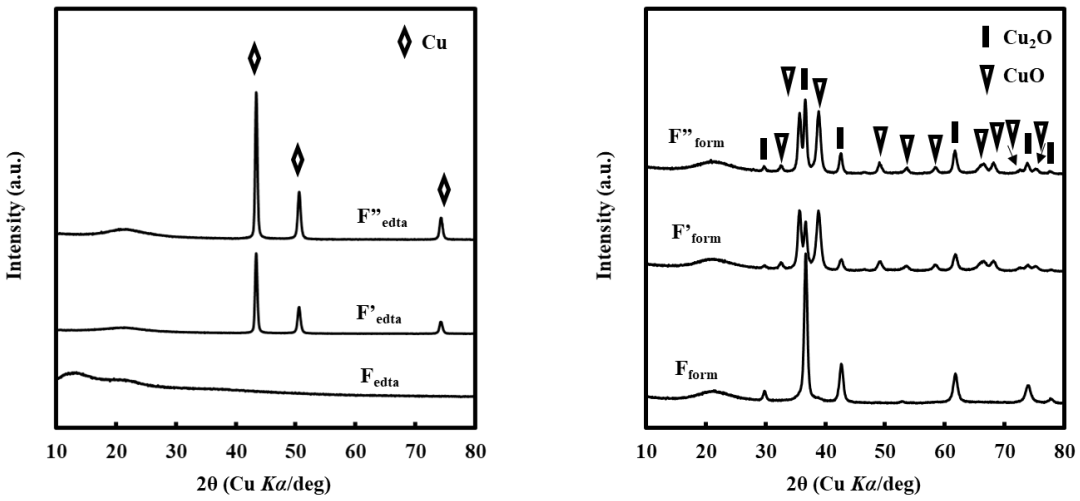

(**a**) (**b**)

Figure 5. XRD patterns of the films fabricated using (a) **S$_{edta}$** and (b) **S$_{form}$**

It has been proposed that the formation of a copper lattice in the MPM is a result of a redox reaction achieved through the thermal decomposition of organic materials present in the precursor film. It is therefore important to note that the **F$_{edta}$** film is amorphous because the pre-heating temperature of 180°C is not sufficient for thermal decomposition of the EDTA components and induce the crystallization of metallic copper. After heat-treating and post-annealing at elevated temperatures of 350°C and 400°C under Ar gas, respectively, the formation of the metallic copper phase could be observed. However, although the XRD patterns of **F'$_{edta}$** and **F''$_{edta}$** showed only peaks assignable to the metallic copper phase, these two films had no metallic appearance and they were not electrically conductive.

On the other hand, the formation of the Cu_2O phase in **F$_{form}$** implies that the employed pre-heating temperature of 180°C is sufficient for the decomposition of the formate anion and leading to the reduction of Cu^{2+} to Cu^{+}, in the air. This was confirmed by the XRD patterns of **F'$_{form}$** and **F"$_{form}$** which indicate that heat-treating and post-annealing procedures do not lead to the formation of a metallic copper phase due to the absence of carbon within the film. Specifically, the XRD pattern of **F'$_{form}$** confirms that: (1) the formation of metallic copper is

only achievable if the precursor/ as-sprayed film contains carbon materials from the precursor solution, and (2) the Ar gas is effective for creating the oxygen-free environment and does not introduce any material necessary for the formation of metallic copper.

From the above results, a clear picture of the influence of each Cu(II) complex on the identity of the resultant film was obtained. The reproducibility problem encountered with the precursor solution involving Cu(II) complexes in a 1:8 [Cu(H_2edta)]:Cu(II) formate ratio was due to the high level of oxidation. It was elucidated that the precursor solution $\mathbf{S_{form}}$ is ideal for the formation of the Cu_2O phase. Therefore, in order to fabricate a thin film of metallic copper with a minimized undesirable oxidation, preparation of a precursor solution involving a reduced amount of Cu(II) formate is proposed.

3.5.3. Preparations of the aqueous precursor solution involving Cu(II) complexes in a 1:4 [Cu(H_2edta)]:Cu(II) formate ratio, and thin film fabrication.

The mixed solution $\mathbf{S_{mix\text{-}4}}$ was prepared by mixing [Cu(H_2edta)]·H_2O (0.20 g, 0.53 mmol) with $Cu(HCOO)_2{\cdot}4H_2O$ (0.48 g, 2.11 mmol) in 25 g of deionized water, followed by the addition of 28% NH_4OH (0.64 g, 10.5 mmol NH_3). The mixture was stirred on a magnetic stirrer for 1 h at room temperature, filtered through a 0.8 μm membrane filter and used with no further modifications.

Using the previously-mentioned spray-coating and heat-treating procedures, the fabricated films are denoted as follows: $\mathbf{F_{mix\text{-}4}}$ refers to the precursor film obtained after spray-coating a quartz glass with the $\mathbf{S_{mix\text{-}4}}$ solution. The resultant film obtained by heat-treating $\mathbf{F_{mix\text{-}4}}$ at 350°C for 50 min under Ar gas with a flow rate of 1.5 L min^{-1} is denoted as $\mathbf{F'_{mix\text{-}4}}$. Finally, the film obtained by post-annealing $\mathbf{F'_{mix\text{-}4}}$ at 400°C for 50 min under Ar gas with a flow rate of 1.5 L min^{-1} is denoted as $\mathbf{F''_{mix\text{-}4}}$.

3.6. Results and discussions

3.6.1. Crystal structures of the resultant thin films

Figure 6 presents the XRD patterns of **F_{mix-4}**, **F'_{mix-4}**, and **F''_{mix-4}**. In all patterns, the three peaks at 43.5°, 50.6°, and 74.3° are assignable to the (111), (200) and (220) crystal phase of metallic Cu, respectively (ICDD card no. 00-004-0836). In the XRD pattern of **F'_{mix}**, two additional peaks assignable to the (111) and (220) crystal phase of Cu_2O can be observed at 36.6° and 61.6°, respectively (ICDD card no. 01-071-3645).

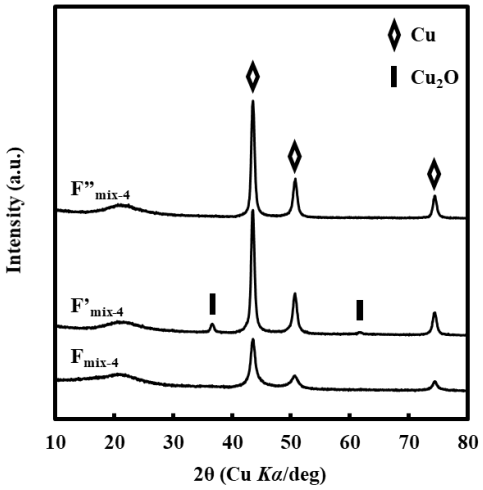

Figure 6. XRD patterns of **F_{mix-4}**, **F'_{mix-4}** and **F''_{mix-4}**.

Influence of the Cu(II) complexes in the coating solution on the crystal structure of the resultant films

From the above results of XRD, it was established that spray-coating an aqueous solution of the Cu(II) complex of EDTA only, onto a quartz glass substrate preheated to 180 °C gives an amorphous film, **F_{edta}** (Figure 5a). However, under identical conditions as abovementioned, **F_{mix-4}** with crystallized Cu^0 phase (Figure 6) could be fabricated using a mixed solution of [$Cu(H_2edta)$] and Cu(II) formate. These results suggest the importance of the used Cu(II) complexes involved in the coating solution. When the solution is made up of the large and stable complex only, such as in the case of **S_{edta}**, the preheating temperature of the substrate at

180 °C does not induce the nucleation of Cu^0 grains on the substrate and the amorphous product is deposited instead. In this case, the nucleation and aggregation of Cu^0 grains occur simultaneously during the heat-treating procedure at higher temperatures. This reaction process could be modified by using a mixed solution whereby the smaller Cu(II) complexes, for example $[Cu(NH_3)_4]^{2+}$, derived from Cu(II) formate and ammonia in the solution promote nucleation of Cu^0 grains during the spray-coating procedure. Because a network of Cu^0 grains has been already formed in the sprayed film $\mathbf{F_{mix\text{-}4}}$, the thermal decomposition of complexes during the heat-treating procedure leads to the densification of these grains resulting in a conductive thin film of well-connected Cu^0 grains.

3.6.2. Surface morphologies, electrical and optical properties of the resultant thin films

The FE-SEM images of the $\mathbf{F''_{edta}}$ and $\mathbf{F''_{mix\text{-}4}}$ films are given in Figure 7a and b, respectively. The morphologies of $\mathbf{F''_{edta}}$ were only observable after sputtering the samples with a thin layer of gold. From the top view of $\mathbf{F''_{edta}}$, isolated agglomerates can be observed. These agglomerates can also be observed in the cross-sectional image. In Figure 5b, a crack-free surface with well-connected and closely packed Cu grains can be observed from the top view of $\mathbf{F''_{mix\text{-}4}}$. The cross-sectional image reveals that the thin film is homogeneously and densely deposited on the quartz glass substrate. The thin film $\mathbf{F''_{mix\text{-}4}}$ has an electrical resistivity of $3.8(6) \times 10^{-5}$ **Ω** cm, which was calculated by using the film thickness of 100 nm.

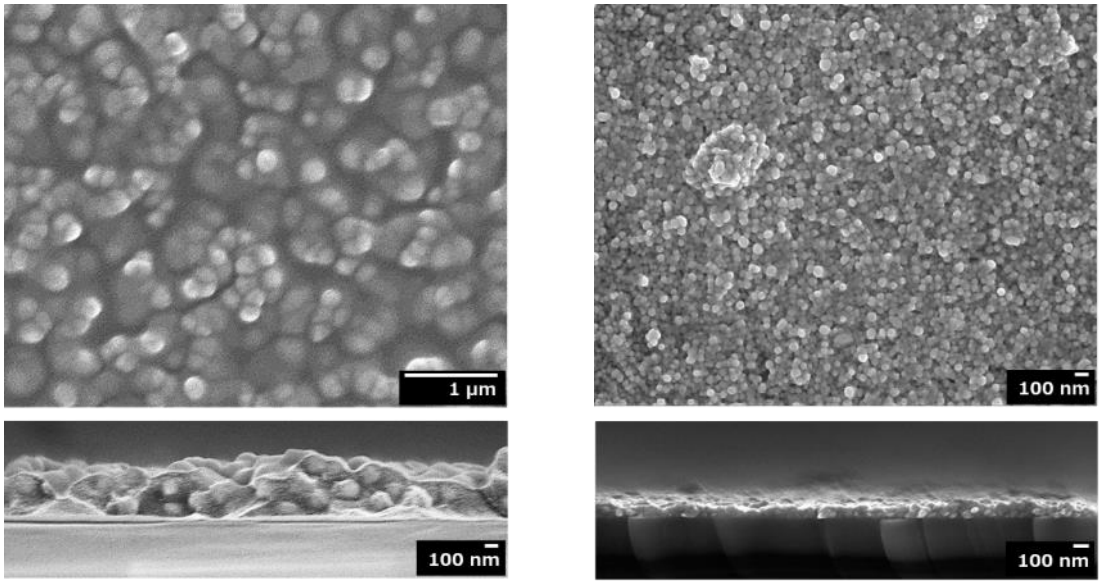

(**a**) (**b**)

Figure 7. Field emission scanning electron microscopy (FE-SEM) images showing the top and cross-section views of the **F''$_{edta}$** (**a**) and **F''$_{mix-4}$** (**b**) films on quartz glass substrates.

The 3D AFM images of **F''$_{edta}$** and **F''$_{mix-4}$** are presented in Figure 8. The 3D image of **F''$_{edta}$** (Figure 8a) shows few, large and isolated grains. On the other hand, many, small and connected grains can be observed on the 3D image of **F''$_{mix-4}$** (Figure 8b). The average surface roughness was determined to be 15 nm and 11 nm for **F''$_{edta}$** and **F''$_{mix-4}$**, respectively.

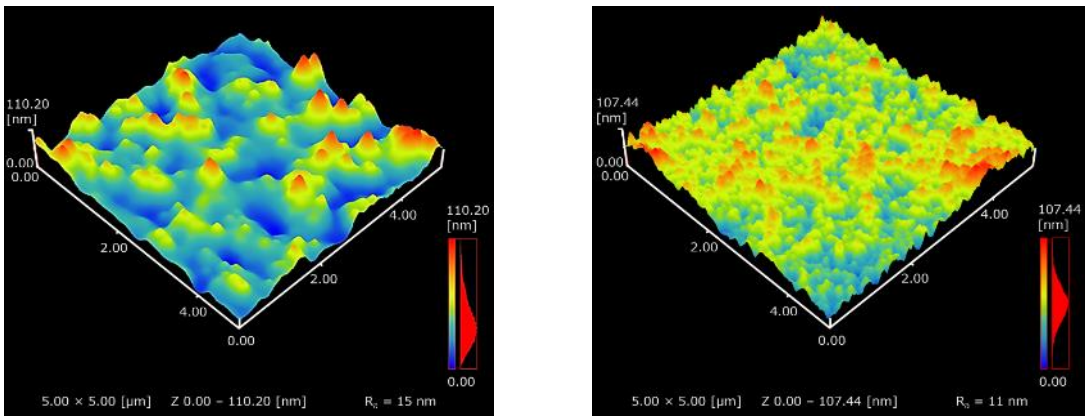

(**a**) (**b**)

Figure 8. 3D atomic force microscopy (AFM) images of (a) **F''$_{edta}$** and (b) **F''$_{mix-4}$**.

Figure 9 shows the reflectance spectra of the resultant films. The reflectance of **F''$_{mix-4}$** approaches over 90% in the far infrared region while that of **F''$_{edta}$** approaches a maximum of 50% in the identical region.

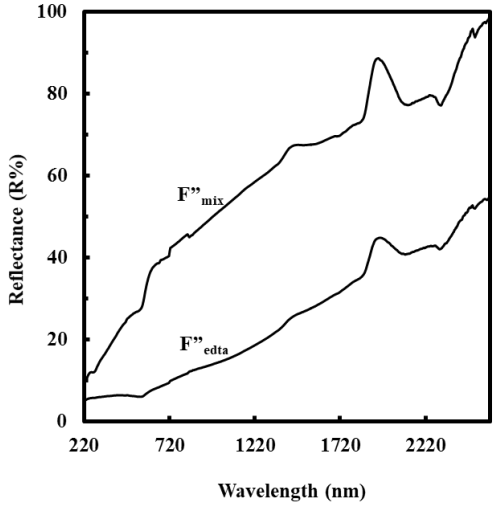

Figure 9. Reflectance spectra of **F''$_{edta}$** and **F''$_{mix-4}$.**

Influence of the Cu(II) complexes in the coating solution on the surface morphologies, electrical conductivities, and reflectance of the resultant films

The reflectance and electrical resistivity are quite different between **F''$_{edta}$** and **F''$_{mix-4}$.** It is known that the formation of island shapes in metal films causes a decrease in the reflectance and electrical conductivity [15]. The insulating thin film **F''$_{edta}$** has island-shape features on the surface, whereas grains in **F''$_{mix-4}$** are well-connected as shown by their corresponding top view FE-SEM and 3D AFM images (Figures 7 and 8, respectively). It is easily accepted that the high degree of connectivity between the Cu^0 grains promoted the very low electrical resistivity of **F''$_{mix-4}$,** whose value is $3.8(6) \times 10^{-5}$ **Ω** cm. The bulk electrical resistivity of Cu is 1.67×10^{-6} **Ω** cm. However, the fabrication of Cu thin films with electrical resistivity values in the order of 10^{-5} **Ω** cm, via radio-frequency sputtering or atomic layer deposition have been reported [6, 16, 17]. Although it is not appropriate to directly compare these values due to different fabrication conditions, the electrical resistivity of the thin film fabricated in the

present study is acceptable. It is, however, important to note that contaminants at grain boundaries, which could not be determined by XRD, SEM, and AES, may cause a decrease in the conductivity of the thin film formed by stacking of pure Cu grains.

It is notable that the reflectance of **F''$_{mix-4}$** approaches over 90% in the far-infrared region (Figure 9). In our previous work [13], we reported the fabrication of a Cu thin film, whose reflectance approaching nearly 100% in the identical region, with a thickness of 100 nm and an electrical resistivity of 1.8×10^{-5} Ω cm. The thin film was fabricated by a spin coating of an ethanol solution and two-step heat treatment. This present thin film **F''$_{mix-4}$** fabricated via spray-coating of the aqueous solution can also be useful as an excellent reflector in the far-infrared region.

3.6.3. Chemical composition and adhesion strength of the **F''$_{mix-4}$** thin film

The AES spectrum of **F''$_{mix-4}$** is presented in Figure 10a. The surface scan indicated that the thin film is composed of C and Cu, as has been confirmed by one peak at 265 eV assignable to electrons of carbon atom and three peaks (LVV) at 764 eV, 835 eV and 914 eV assignable to electrons of Cu ones, respectively. The curve-fitting result (Figure 10b) revealed that all carbon atom present in the thin film is neutral.

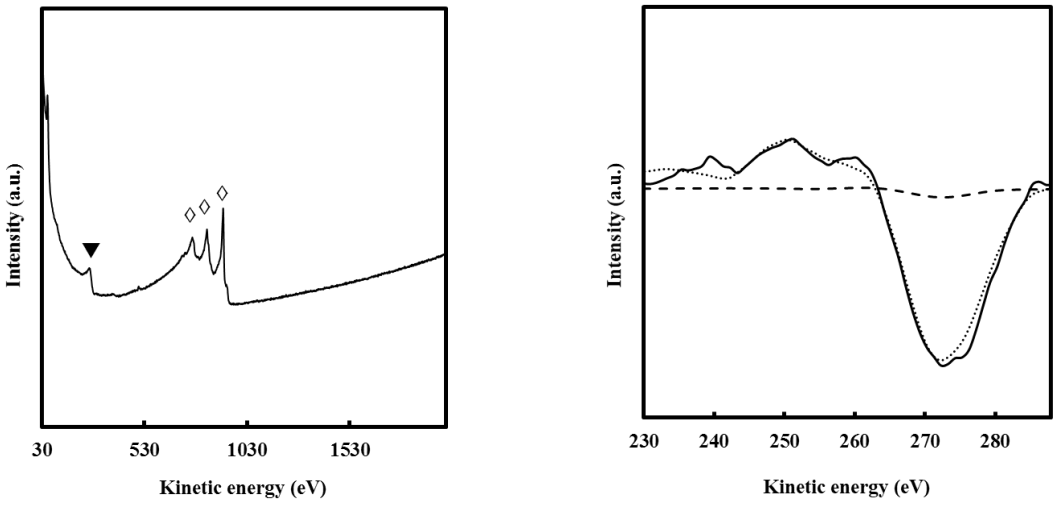

(**a**) (**b**)

Figure 10. (**a**) Auger spectrum of **F''$_{mix-4}$**. Peaks are denoted as follows: ◊ Cu and ▼ C. (**b**) Curve-fitting results for the carbon state in **F''$_{mix-4}$**. The solid, dotted, and dashed lines represent **F''$_{mix-4}$**, C (neutral) and C (tetravalent), respectively.

The AES results revealed that in addition to Cu, the thin film **F''$_{mix-4}$** contains a certain amount of neutral carbon atoms, uniformly distributed within the film. Consequently, these carbon atoms caused no disruption in the electrical conductivity and reflectance of the thin film. In our report on embedding Cu into submicrometer trenches in a silicon substrate [18], relative concentrations indicated that the trenches had a Cu:O:C ratio of 84:4:12 and this higher carbon content in comparison to oxygen might be useful in protecting the Cu from oxidation. Therefore, the thin film **F''$_{mix-4}$** is also likely to be resistant to oxidation. In fact, even though spray-coating was performed in air, the Cu^0 phase in **F$_{mix-4}$** was effectively protected against oxidation as indicated by the XRD pattern (Figure 6). A certain amount of Cu_2O appeared as a by-product during heat-treatment at 350 °C carried out under Ar gas containing less than 10 ppm of air as its impurity, in our previous study [19]. The ratio of Cu_2O:Cu peaks assignable to the (111) phase in that film right after the heat treatment was 57:43. In the present study, a Cu_2O phase was also detected at the corresponding stage (**F'$_{mix-4}$**, Figure 6) and the corresponding ratio was 4:96, indicating a significant difference. It can be concluded that this must be owing to the different ratios of the number of used ligands. On the basis of our previous procedures, the post-annealing step by placing an identical-sized quartz glass on top of the thin film was vital for the removal of the Cu_2O phase by utilizing the carbons remaining within the film and preventing the introduction of oxygen from less than 10 ppm air contained as an impurity in the industrially available Ar gas. This is evident from the XRD patterns of **F'$_{mix-4}$** and **F''$_{mix-4}$** (Figure 6). The effectiveness of carbon atoms derived from the ligands in protecting the film against oxidation is also shown in this present study.

The adhesion strength of the film **F''$_{mix-4}$** onto the quartz glass substrate was found to be 37(7) MPa, with the peeling occurring at the interface between the film and the quartz glass substrate.

The applicability of conductive thin films across various fields depends strongly on their mechanical properties such as the adhesion strength onto the substrate [20]. It is important to note that the thin film **F''$_{mix-4}$** has a strong adhesion strength up to 37 MPa onto the quartz glass substrate. In our previous work, the thin film prepared from the precursor solution had an adhesion strength of 36 MPa whereas another film prepared using ion-beam assisted deposition attained an adhesion strength of 1.7 MPa [13] There are various techniques utilized to modify the surface of substrates in order to promote excellent adhesion strength of thin films and a thin film of copper with an adhesion strength of 34 MPa onto an alumina substrate was fabricated via magnetron sputtering but only after pre-treatment of the substrate with an Ar gas plasma [21]. However, in techniques such as physical vapor deposition (PVD), it has been established that good adhesion can be obtained as a result of the formation of a transition layer between the substrate and thin film [22]. Therefore, the strong adhesion of **F''$_{mix-4}$** onto the quartz substrate is expected to be a result of the interface having bonds between Cu and the O^{2-} belonging to the quartz glass substrate, without any chemical or physical modification of the substrates' surface.

3.7. Attempt to fabricate copper thin films using different copper salts as the starting materials.

To confirm the importance of the Cu(II) complexes in the precursor solution to ensure the fabrication of a conductive copper thin film, a comparison of the starting materials involved in the coating solutions was done. In addition to **S$_{edta}$** and **S$_{mix}$**, additional solutions were prepared according to the identical procedures with a total concentration of the Cu^{2+} ions in the solution at 0.1 mmol g^{-1}. The coating solutions were prepared using Cu(II) acetate only to give film

denoted as **F_{OAc}**, a mixture of [Cu(H_2edta)] and 8 mol of Cu(II) acetate to give film denoted as **$F_{edta\text{-}OAc}$**, and a mixture of Cu(II) formate with Cu(II) acetate to give film denoted as **$F_{form\text{-}OAc}$**.

The above-mentioned solutions were spray-coated onto preheated quartz glass substrates using the procedures identical to the abovementioned ones, in the case of fabricating **F_{edta}** and **F_{mix}**. The XRD patterns of the resultant films are given in Figure 9. From the XRD pattern of **F_{OAc}** (Figure 11(a)), the film is composed of the CuO crystal phase only, with the appearance of the two broad peaks at 35.4 and 38.5°, assignable to the (002) and (111) phase, respectively (ICDD card no. 00-041-0254). A plurality of other peaks assignable to the CuO phase can be observed in the 2-theta range of 49–75°. From the results, the difference between the reducing powers of the acetate ion and the formate ion could be identified. Unlike in the case of Cu(II) formate as the starting material, the film **F_{OAc}** does not contain the reduced phase of copper.

Figure 11(b) shows the XRD patterns of the **$F_{edta\text{-}OAc}$** and **$F_{form\text{-}OAc}$** films. Although, the solution used to fabricate **$F_{edta\text{-}OAc}$** involved the [Cu(H_2edta)] complex with Cu(II) acetate in a 1:8 ratio, the resultant film was amorphous. This result confirmed the inability of the acetate ion to reduce Cu^{2+} and, the fact that the [Cu(H_2edta)] complex is thermally stable at the substrate pre-heating temperature of 180°C. On the other hand, the XRD pattern of **$F_{form\text{-}OAc}$** shows peaks assignable to the (111), (200), (220), and (311) crystal phases of Cu_2O at 36.7, 42.6, 61.7 and 73.9°, respectively (ICDD card no. 01-071-3645), It is therefore accepted that the fabrication of a conductive film of copper using the above-mentioned solutions is not viable. In addition, by comparing the XRD patterns of **F_{OAc}** and **$F_{form\text{-}OAc}$**, it is acceptable that, because formate is a reducing agent, it was possible to reduce the Cu^{2+} in the precursor solution to Cu^{+} in Cu_2O as indicated by the XRD pattern of the **$F_{form\text{-}OAc}$** film, right after spray-coating.

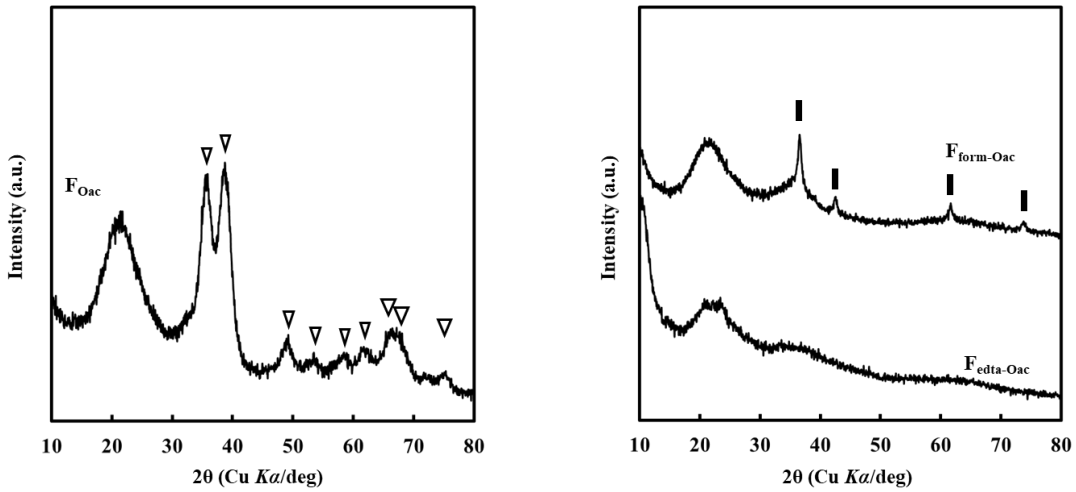

(**a**) (**b**)

Figure 11. (**a**) XRD pattern of **F**$_{OAc}$. (**b**) XRD patterns of **F**$_{edta\text{-}OAc}$ and **F**$_{form\text{-}OAc}$. The peaks are denoted as follows: ∇ CuO and ▌ Cu_2O.

3.8. Formation of Cu^0 from Cu(II) complexes involved in the precursor solution.

The plausible scheme for the formation of metallic copper using the M.P.M. has been proposed by Nagai *et. al.* as shown in Scheme 1. The transformation between the various phases has been represented by redox reactions during the thermal decomposition of the Cu(II) complexes involved in the precursor film.

$$4(\text{Cu complexes}) \xrightarrow[\text{Heat-treating}]{O_2 < 2\text{ppm},\ CO_x, NO_x} 4\left(\alpha Cu + \frac{1-\alpha}{2}Cu_2O + \beta C\right) \xrightarrow[\text{Post-annealing}]{\frac{\beta}{2}CO_x} 4\left(\mathbf{Cu} + \frac{\beta}{2}C + \frac{1-\alpha-\beta}{4}O_2\right)$$

Scheme 1. plausible scheme for the formation of metallic copper using the M.P.M [13].

In the present study, the transformation of Cu^{2+} from Cu(II) complexes in the aqueous precursor solution to Cu^0 can be divided into two sections comprising of (1) the spray-coating step and, (2) the heat-treating of the as-sprayed film. This is because the spray-coating step is carried out at a substrate preheating temperature of 180°C thus, simultaneously inducing thermal decomposition of some components involved in the coating solution. The plausible

scheme representing the transformation of Cu^{2+} into Cu^0 during the spray-coating step is given in Scheme 2.

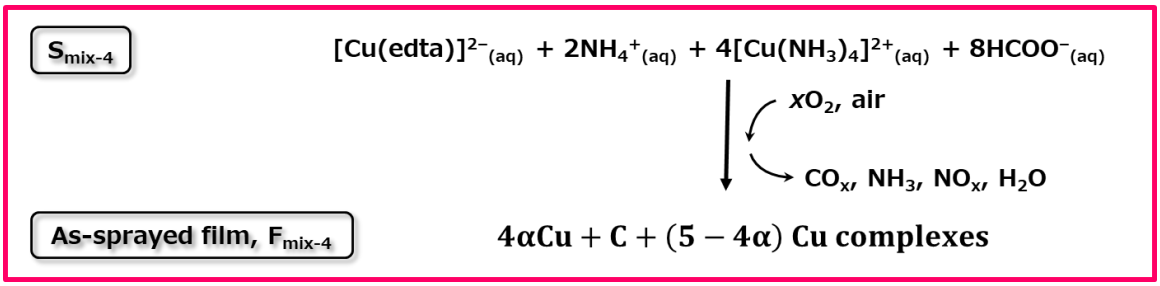

Scheme 2. plausible scheme representing the transformation of Cu^{2+} into Cu^0 during the spray-coating.

During spray-coating, the preheating temperature is sufficient for the solvent evaporation and removal of excess NH_3 of the precursor solution. Simultaneously, the ammine complex of Cu(II) is expected to be thermally decomposed, whereby the formate anion is decomposed into CO and H_2O. Because CO is a reducing agent, Cu^{2+} is consequently reduced to Cu^0. Under the spray-coating conditions employed in the present study, the carbon atoms derived from the Cu-edta complex inhibit oxidation of the formed Cu^0 phase.

During the heat-treating and post-annealing procedures, the plausible reaction equation is identical to that proposed by Nagai *et. al*. However, it is important to note that the identity of the as-sprayed film is different from that of the precursor film. Scheme 3 shows the plausible scheme for this step.

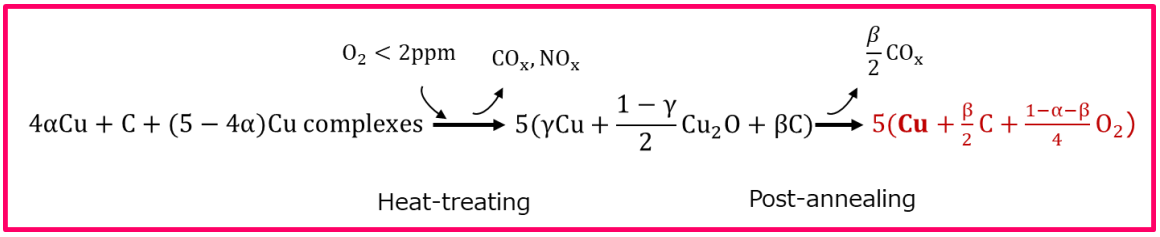

Scheme 3. Plausible scheme for the formation of copper by heat-treating the spray-coated film.

3.9. The effectiveness of the carbon content in inhibiting the oxidation of Cu^0 in the fabricated films.

The established phase diagram of the copper-oxygen system and the *P-T* phase stability diagram of the Cu-Cu_2O-CuO system are shown in Figure 12(a) and (b), respectively.

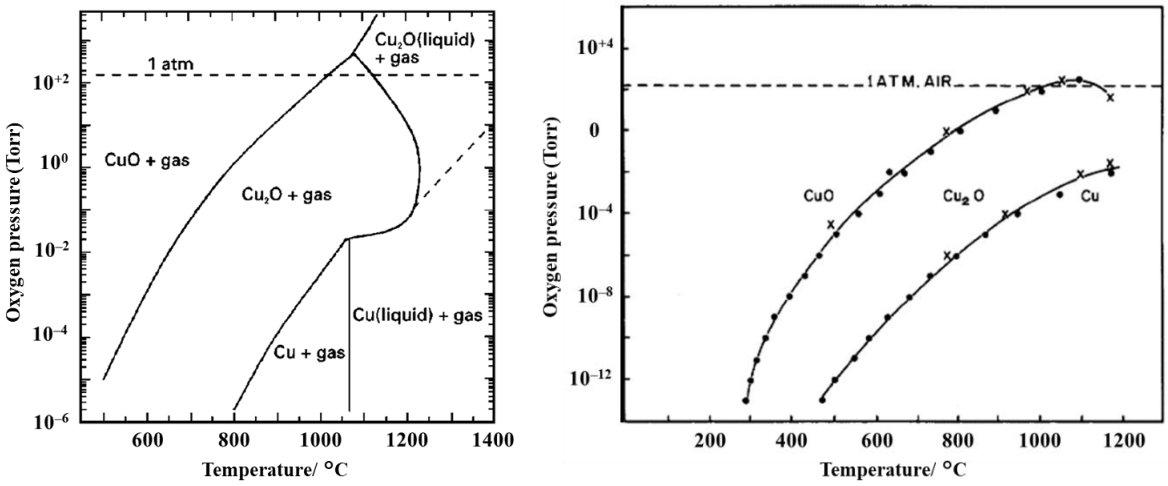

(**a**) (**b**)

Figure 12. (**a**) Phase diagram of the copper-oxygen system (extracted from [23]). (**b**) *P-T* phase stability diagram of the Cu-Cu_2O-CuO system (extracted from [24]).

From these two figures, it is evident that of all the three phases of copper, the CuO phase is the most stable under ambient conditions. The Cu_2O phase is stable only at lower oxygen-pressure and in a limited temperature region. However, with decreasing oxygen pressure, the stability region of Cu_2O shifts to lower temperature as clearly indicated in Figure 12(b). In the copper-oxygen system, the Cu^0 phase appears at the temperature range of 800–1000°C and an oxygen pressure of about 10^{-4} Torr or less. The stability of metallic copper extends to low temperatures as low as 500°C however, under significantly low oxygen content [25].

It is therefore notable that *via* the MPM, the formation of a stable Cu^0 phase can be achieved through the thermal decomposition of the precursor solution at spray-coating, as revealed by the XRD pattern of the $\mathbf{F_{mix\text{-}4}}$ in Figure 6. In this case, the present results indicate that the carbon content in the film is vital in protecting the formed Cu^0 from being oxidized into its oxide

phases. To confirm the effectiveness of the present neutral carbon atoms in protecting the Cu^0 from oxidation was evaluated by heating the thin film **F"$_{mix-4}$** at 200°C in air, for 30 min. Another thin film of pure metallic copper, **F$_{sputter}$**, fabricated by using the sputtering method was also used for this experiment as a reference. Figures 13(a) and (b) show the XRD patterns of the as-fabricated thin films and after heating in air at 200°C for 30 min, respectively.

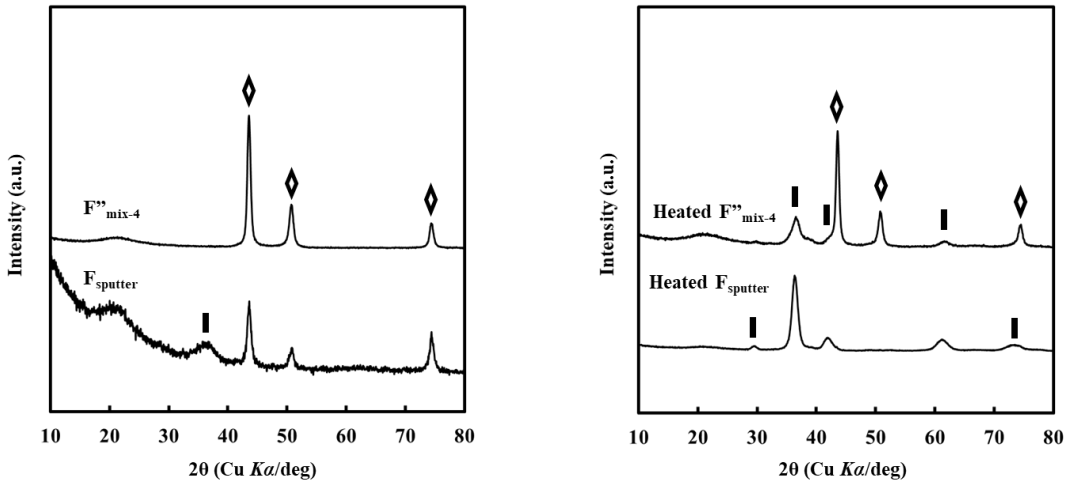

(**a**) (**b**)

Figure 13. (**a**) XRD patterns of the **F"$_{mix-4}$** and **F$_{sputter}$** films, as fabricated. (**b**) XRD patterns of the **F"$_{mix-4}$** and **F$_{sputter}$** films after heating in air at 200°C for 30 min.

Before the heating procedure, the diffraction patterns of both thin films show peaks at 43.5, 50.6 and 74.3° assignable to the (111), (200) and (220) crystal phase of metallic copper, respectively. However, for **F$_{sputter}$**, an additional peak assignable to the (111) crystal phase of Cu_2O can be observed at 36.5° It has been established that under ambient conditions, metallic copper is spontaneously oxidized to it's oxide phases [23–25]. Therefore, a 100nm thick film of sputtered copper is expected to be readily oxidized upon exposure to atmospheric conditions and the appearance of the peak assignable to Cu_2O in the XRD pattern of **F$_{sputter}$** is acceptable. Additionally, the absence of the peak assignable to Cu_2O in the XRD pattern of **F"$_{mix-4}$** implies that the thin film is not easily susceptible to oxidation under identical conditions.

Form Figure 13(b), it is clear that after heating the thin films in the air at 200°C for 30 min, the $\mathbf{F_{sputter}}$ film was heavily oxidized as the XRD pattern of the hated film consisted mainly of peaks assignable to the Cu_2O crystal phase. On the other hand, the XRD pattern of the $\mathbf{F''_{mix\text{-}4}}$ film heated in air at 200°C for 30 min shows a combination of peaks assignable to both Cu^0 and Cu_2O crystal phases, with the Cu^0 being the dominant phase. Because the only difference between these two thin films of identical thicknesses is only the carbon content of $\mathbf{F''_{mix\text{-}4}}$, the low oxidation of $\mathbf{F''_{mix\text{-}4}}$ can be attributed to the neutral carbon atoms.

3.10. Summary

The stable and VOC-free solution S_{mix}, which can be stored for a period of over three months, for fabricating the precursor film of metallic Cu was successfully developed by mixing [Cu(H_2edta)] and Cu(II) formate with ammonia, in water. The aqueous solution was adequate for spraying onto a quartz glass substrate pre-heated to 180 °C, without forming the clogging solid in the nozzle tip. The abovementioned two-step heat-treatment of the sprayed film obtained in a short time produced a crack-free and densified film $\mathbf{F''_{mix\text{-}4}}$ of 100 nm thickness (Figures 7 and 8b) with very low electrical resistivity and strong adhesion onto the substrate. It is important to point out that the precursor solution with a 1:4 of [Cu(edta)]:Cu(II) formate ratio reported here gave the best results with good reproducibility, among several attempts with varying the ratios.

In spray pyrolysis works, the fabrication of Cu_2O thin films onto alkali-free borosilicate, silicon and quartz glass substrates from aqueous solutions involving Cu(II) acetate requires the addition of glucose to act as reducing agent [26,27]. In their study, Kosugi and Kaneko outlined that the Cu^{2+} derived from Cu(II) acetate is reduced by glucose to form Cu^0 which is subsequently oxidized to form Cu_2O. It is also important to note that the properties of the film with Cu^0 crystal phase obtained via the spray pyrolysis have not been reported. Thus, this

present study is the first report on the fabrication of metallic Cu thin films via the spray-coating or any related aqueous solution-based techniques.

By this present study, the importance of designing and mixing different Cu(II) complexes involved in the solution in order to control the crystal structure and surface morphology of the resultant film was clearly illustrated. By varying the ratio of the Cu(II) complexes in the coating solution, films with different crystal structures, morphologies, and electrical properties could be obtained. And this is the advantage of the MPM which enables to design metal complexes in coating solutions, at the molecular level.

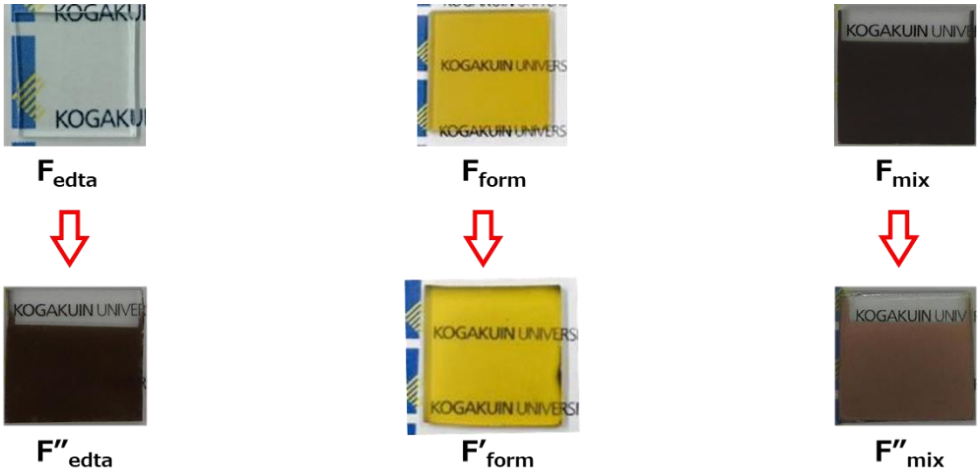

Figure 14. images of the resultant films from the solutions **S_{edta}**, **S_{form}**, and **S_{mix-4}**. The ration of Cu-edta:Cu(II) formate in **S_{mix-4}** was 1:4.

Finally, the spray method employing this aqueous precursor solution has the potential as a promising technique for the fabrication of metallic Cu thin films for various applications. From the environmental friendliness point of view, the use of aqueous solutions is of great advantage for industrial handling safety.

References

1. *Copper and Copper Alloys*; Davis, J.R., Ed.; ASM international: Ohio, USA, 2001; ISBN 0-87170-726-8.

2. Messner, F. Towards a sustainable copper industry? In *Sustainable Metals Management*; 206AD; pp. 113–139 ISBN 978-1-4020-4539-4.

3. Giurco, D.; Petrie, J.G. Strategies for reducing the carbon footprint of copper: New technologies, more recycling or demand management? *Miner. Eng.* **2007**, *20*, 842–853, doi:10.1016/j.mineng.2007.04.014.

4. Auty, R.; Warhurst, A. Sustainable development in mineral exporting economies. *Resour. Policy* **1993**, *19*, 14–29, doi:10.1016/0301-4207(93)90049-S.

5. Ghotbi, M.Y.; Rahmati, Z. Nanostructured copper and copper oxide thin films fabricated by hydrothermal treatment of copper hydroxide nitrate. *Mater. Des.* **2015**, *85*, 719–723, doi:10.1016/j.matdes.2015.07.081.

6. Lee, S.; Kim, J.Y.; Lee, T.-W.; Kim, W.-K.; Kim, B.-S.; Park, J.H.; Bae, J.-S.; Cho, Y.C.; Kim, J.; Oh, M.-W.; et al. Fabrication of high-quality single-crystal Cu thin films using radio-frequency sputtering. *Sci. Rep.* **2015**, *4*, 6230, doi:10.1038/srep06230.

7. Gordon, P.G.; Kurek, A.; Barry, S.T. Trends in copper precursor development for cvd and ALD applications. *ECS J. Solid State Sci. Technol.* **2015**, *4*, N3188–N3197, doi:10.1149/2.0261501jss.

8. Kaelin, M.; Zogg, H.; Tiwari, A.N.; Wilhelm, O.; Pratsinis, S.E.; Meyer, T.; Meyer, A. Electrosprayed and selenized Cu/In metal particle films. *Thin Solid Films* **2004**, *457*, 391–396, doi:10.1016/S0040-6090.

9. Han, S.; Lee, T.L.; Yang, C.J.; Shih, H.C. Trench gap-filling copper by ion beam sputter deposition. *Mater. Chem. Phys.* **2006**, *97*, 19–22, doi:10.1016/j.matchemphys.2005.05.042.

10. Abhinav K, V.; Rao R, V.K.; Karthik, P.S.; Singh, S.P. Copper conductive inks: synthesis and utilization in flexible electronics. *RSC Adv.* **2015**, *5*, 63985–64030, doi:10.1039/C5RA08205F.

11. Park, B.K.; Kim, D.; Jeong, S.; Moon, J.; Kim, J.S. Direct writing of copper conductive patterns by ink-jet printing. *Thin Solid Films* **2007**, *515*, 7706–7711, doi:10.1016/j.tsf.2006.11.142.

12. Magdassi, S.; Grouchko, M.; Kamyshny, A. Copper nanoparticles for printed electronics: routes towards achieving oxidation stability. *Materials (Basel).* **2010**, *3*, 4626–4638, doi:10.3390/ma3094626.

13. Nagai, H.; Mita, S.; Takano, I.; Honda, T.; Sato, M. Conductive and semi-transparent Cu thin film fabricated using molecular precursor solutions. *Mater. Lett.* **2015**, *141*, 235–237, doi:10.1016/j.matlet.2014.11.056.

14. Nagai, H.; Suzuki, T.; Hara, H.; Mochizuki, C.; Takano, I.; Honda, T.; Sato, M. Chemical fabrication of p-type Cu_2O transparent thin film using molecular precursor method. *Mater. Chem. Phys.* **2012**, *137*, 252–257, doi:10.1016/j.matchemphys.2012.09.016.

15. Axelevitch, A.; Gorenstein, B.; Golan, G. Investigation of optical transmission in thin metal films. *Phys. Procedia* **2012**, *32*, 1–13, doi:10.1016/j.phpro.2012.03.510.

16. Knisley, T.J.; Ariyasena, T.C.; Sajavaara, T.; Saly, M.J.; Winter, C.H. Low temperature growth of high purity, low resistivity copper films by atomic layer deposition. *Chem.*

Mater. **2011**, *23*, 4417–4419, doi:10.1021/cm202475e.

17. Kalutarage, L.C.; Clendenning, S.B.; Winter, C.H. Low-Temperature atomic layer deposition of copper films using borane dimethylamine as the reducing co-reagent. *Chem. Mater.* **2014**, *26*, 3731–3738, doi:10.1021/cm501109r.

18. Nagai, H.; Suzuki, T.; Nakano, T.; Sato, M. Embedding of copper into submicrometer trenches in a silicon substrate using the molecular precursor solutions with copper. *Mater. Lett.* **2016**, *182*, 206–209, doi:10.1016/j.matlet.2016.06.123.

19. Nagai, H.; Suzuki, T.; Mochizuki, C.; Takano, I.; Honda, T.; Sato, M. Formation mechanism of *p*-type Cu_2O thin films via intermediate Cu^0 Species derived from cu(ii) complex of Ethylenediamine-*N*,*N*,*N*′,*N*′-Tetraacetic Acid. *Sci. Adv. Mater.* **2014**, *6*, 603–611, doi:10.1166/sam.2014.1788.

20. Mittal, K.L. Adhesion measurement of thin films. *Electrocompon. Sci. Technol.* **1976**, *3*, 21–42, doi:10.1155/APEC.3.21.

21. Lim, J.D.; Lee, P.M.; Rhee, D.M.W.; Leong, K.C.; Chen, Z. Effect of surface treatment on adhesion strength between magnetron sputtered copper thin films and alumina substrate. *Appl. Surf. Sci.* **2015**, *355*, 509–515, doi:10.1016/j.apsusc.2015.07.141.

22. Lukaszkowicz, K.; Kriz, A.; Sondor, J. Structure and adhesion of thin coatings deposited by PVD technology on the X6CrNiMoTi17-12-2 and X40CrMoV5-1 steel substrates. *Arch. Mater. Sci. Eng.* **2011**, *51*, 40–47.

23. Ito, T.; Yamaguchi, H.; Okabe, K.; Masumi, T. Single-crystal growth and characterization of Cu_2O and CuO. *J. Mater. Sci.* **1998**, *33*, 3555–3566, doi:10.1023/A:1004690809547.

24. Rakhshani, A.E. Preparation, characteristics and photovoltaic properties of cuprous oxide-a review. *Solid State Electron.* **1986**, *29*, 7–17, doi:10.1016/0038-1101(86)90191-7.

25. Wang, J.-P.; Cho, W.D. oxidation behavior of pure copper in oxygen and/or water vapor at intermediate temperature. *ISIJ Int.* **2009**, *49*, 1926–1931, doi:10.2355/isijinternational.49.1926.

26. Kosugi, T.; Kaneko, S. Novel spray-pyrolysis deposition of cuprous oxide thin films. *J. Am. Ceram. Soc.* **1998**, *81*, 3117–3124, doi:10.1111/j.1151-2916.1998.tb02746.x.

27. Pattanasattayavong, P.; Thomas, S.; Adamopoulos, G.; McLachlan, M.A.; Anthopoulos, T.D. p-channel thin-film transistors based on spray-coated Cu_2O films. *Appl. Phys. Lett.* **2013**, *102*, 163505, doi:10.1063/1.4803085.

CHAPTER 4: THIN FILM FABRICATION OF A LAYERED-ROCK-SALT $LiCoO_2$ A QUARTZ GLASS SUBSTRATE BY SPRAY-COATING AN AQUEOUS SOLUTION INVOLVING METAL ACETATES

CHAPTER 4: THIN FILM FABRICATION AND CHARACTERIZATION OF LAYERED-ROCK-SALT $LiCoO_2$ ON QUARTZ GLASS SPRAY-COATED WITH AN AQUEOUS SOLUTION INVOLVING METAL ACETATES

4.1. Introduction on lithium-ion batteries and lithium cobalt(II) oxide

The development and commercialization of portable electronic devices let to the advancements of rechargeable batteries as their re-usable power sources. Generally, in a single battery, a series and/ or parallel connection of electrochemical cells is constructed in order to obtain the required voltage and capacity, respectively [1]. Each electrochemical cell is then composed of three main components as follows. The (1) positive and (2) negative electrodes are the sources of chemical reactions, and they are referred to as the cathode and anode, respectively. The third component is the electrolyte solution separating the two electrodes and containing dissociated salts which enable ion transfer between the electrodes.

Extensive research on the electrode materials has been carried out. For example, the early rechargeable batteries referred to as Lithium-batteries utilized Li metal or Li-compounds for anode material [1, 2]. The application of Li in batteries is preferable due to the fact that Li is the most electropositive (–3.04 V versus standard hydrogen electrode) as well as the lightest (equivalent weight M =6 94 g mol^{-1} and specific gravity ρ = 0.52 g cm^{-3}) metal. Thus facilitating the design of storage systems with high energy density [1]. However, it was discovered that after each subsequent charge-discharge cycle, Li-metal is replated from the anode into the electrolyte solution. Such Li-metal/ electrolyte combination is an explosion hazard. This led to the invention of lithium-ion batteries (LIBs) by replacing the Li metal with a Li-intercalation compound, usually, a carbon compound and, several Li-intercalation anode materials have been developed.

For the cathode materials, LIBs have historically used lithiated transition metal oxides due to their high capacity for Li intercalation and suitable chemical and physical properties required

for Li electrodes [3]. These transition metal oxides serve as host structures into which Li^+ ions can be inserted reversibly and charge-compensated by reduction/oxidation of the host. The cost and electrochemical performance of a specific LIB are highly dependent on the cathode material. Therefore, LIBs are commonly identified by the names of the transition metal insertion compound and, there are several classes of these materials such as the MnO_2, $LiCoO_2$, $LiCo_{1-y-z}Ni_yAl_zO_2$, $LiMn_2O_4$, etc [3, 4]. A schematic representation of a Li-ion cell is given in Figure 1.

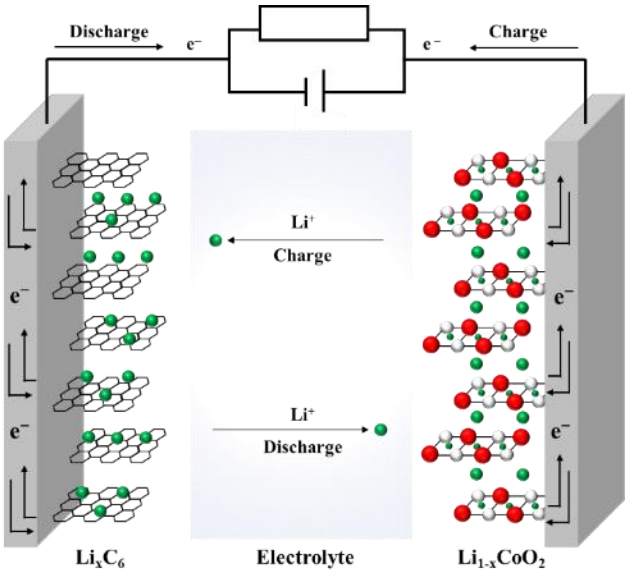

Figure 1. Schematic representation of a Li-ion cell utilizing carbon and $LiCoO_2$ as the anode and cathode active material, respectively [5]. During operation, the Li-ions are shuffled between the two electrodes in a rocking-chair principle.

Progress in the development of LIBs was marked by the manufacturing of the $C/LiCoO_2$ rocking-chair battery which was commercialized by Sony Corporation in June 1991 [1]. Lithium cobalt(III) oxide ($LiCoO_2$, LCO) has been extensively studied and successfully applied as a Li-intercalation compound in LIBs due to the high energy density and voltage of the $Li/LiCoO_2$ system. Generally, two distinct phases of $LiCoO_2$ are known and, they are frequently referenced by the temperature required for their synthesis [6]. The standard or high-

temperature phase, HT-$LiCoO_2$ is hexagonal while the low-temperature phase, LT-$LiCoO_2$ has a spinel structure. In both structures, the oxygen sublattice is the same, with distinguishable partial arrangements of the Li^+ and Co^{3+}. The relation between the HT-$LiCoO_2$ structure and the HT-$LiCoO_2$ structure is shown in Figure 2.

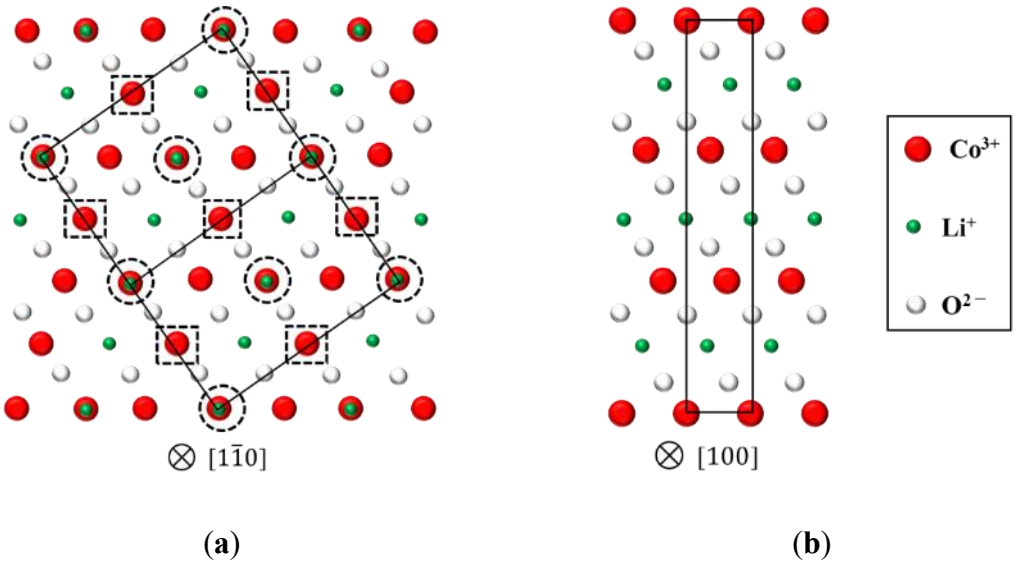

Figure 2. The relation between the LT-$LiCoO_2$ (a) and the HT-$LiCoO_2$ (b) structures [7].

The HT-$LiCoO_2$ which is also referred to as layered-rock-salt $LiCoO_2$ is characterized by a slightly higher voltage than the LT-$LiCoO_2$ and high structural stability that promotes extended battery cycle-ability [8–13]. The crystal structure of HT-$LiCoO_2$ is shown in Figure 3. In addition to the hexagonal unit cell which has been assigned to the $R\bar{3}m$ space group, the crystal structure shows an additional rhombohedral structure composed of Li^+ ions only. Because HT-$LiCoO_2$ is more preferable over the low-temperature phase for applications in LIBs, usage of the term LCO in the subsequent sections of this chapter will be in reference to the HT-$LiCoO_2$.

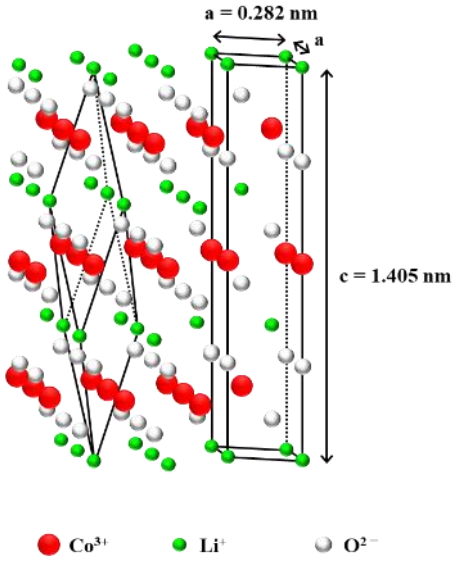

Figure 3. Crystal structure of the HT-$LiCoO_2$

4.2. Thin films of LCO

In the past two decades, there has been significant progress toward the development of smaller-scale and portable electronic devices, such as autonomous microelectronic sensors, microelectromechanical (MEMs), and portable personal electronics such as implantable medical devices [14, 15]. Therefore, parallel miniaturization of LIBs is very important for the development of power sources required to operate such microscale devices. The LIBs with electrodes employing thin films of active materials, which include LCO, are preferred over their bulk counterparts due to the much improved electronic and ionic conductivity, increased specific surface area and the ease of controlling the morphology. Additionally, the thin film electrodes are free from impurities such as binders and carbon fillers used in the fabrication of bulk electrodes.

Techniques such as magnetron sputtering and pulsed laser deposition (PLD) are capable of depositing high-quality thin films of LCO [9, 16]. However, they are associated with expensive and complicated experimental setups, requiring ultrahigh vacuum systems. On the other hand, thin films of LCO have been fabricated *via* the sol-gel method [16–19] at high temperatures

and prolonged annealing conditions, which are likely to lead to moderate lithium loss and compromise the electrochemical properties of the materials [11, 13].

Recently, our group reported the fabrication of a novel thin-film lithium-ion battery (LIB) which can be charged by light irradiation and thus functioning as a photovoltaic LIB (PV-LIB) [20]. The cathodic active material for this PV-LIB was a thin film of LCO deposited on fluorinated tin oxide (FTO) pre-coated glass substrate by the MPM. Very recently, our group attained to fabricate a thin film of LCO on a (0001) oriented sapphire substrate by heat-treating a spin-coated precursor film at 500°C for 0.5h in the air, a temperature 300°C or more, lower than the annealing temperatures reported for the sol-gel method [21]. However, the LCO thin films were successfully deposited on only crystallized materials such as FTO and phase-oriented sapphire, because Co3O4 was preferentially formed on a quartz glass substrate.

The fabrication of LCO thin films on a quartz glass substrate, *via* wet chemical processes is quite limited as abovementioned in the cases of MPM. In this study, we attempted to fabricate and characterize an LCO thin film on a quartz glass substrate by heat-treating a spray-coated precursor film by using an aqueous precursor solution and the results are presented here.

4.3. Preparation of the coating solutions and thin film fabrication

Two coating solutions whose solvents are different from each other were prepared as follows: The coating solution $\mathbf{S_{aq}}$ was prepared by mixing lithium acetate dihydrate (0.12 g, 1.21 mmol) with cobalt(II) acetate tetrahydrate (0.30 g, 1.21 mmol) in 10 g of deionized water, and followed by the addition of 28% NH_4OH (1.65 g, 24.20 mmol NH_3). The mixture was then stirred on a magnetic stirrer for 1 h at room temperature.

The coating solution $\mathbf{S_{EtOH}}$ was prepared according to the procedures previously reported[20], with a slight modification as follows [21]: Firstly, a lithium oxide precursor solution (S_{Li}) was prepared by reacting 0.64 g (6.2 mmol) of lithium acetate dihydrate and 1.83 g (25.0 mmol) of butylamine in 10 g of ethanol by stirring for 1 h at room temperature. The

concentration of Li^+ ions was adjusted to 0.50 mmol g^{-1} and then, 1.47 g of molecular sieves 4A was added to the solution. Secondly, the cobalt oxide precursor solution (S_{Co}) was prepared by reacting 1.90 g (7.6 mmol) of cobalt(II) acetate tetrahydrate and 3.35 g (45.7 mmol) of butylamine in 10 g of ethanol by stirring for 1 h at room temperature. The concentration of Co^{2+} ions was adjusted to 0.50 mmol g^{-1} and then, 3.63 g of molecular sieves 4A was added to the solution. Finally, the **S_{EtOH}** coating solution was prepared by mixing 0.50 g of S_{Li} and 0.50 g of S_{Co}. The mixed solution was stirred at ambient temperature for 20 min, and 0.16 g of molecular sieves 4A was added

All solutions were used with no further modifications.

Using the earlier-mentioned spray-coating and heat-treating procedures, 3.00 g of the solution, **S_{aq}** was spray-coated onto the preheated substrate. In this chapter, the fabricated films are denoted as follows: **$F_{as\text{-}spray}$** and **F_{spray}** refer to the precursor film obtained after spray-coating a quartz glass with the S_{aq} and the resultant film obtained after heat-treating the precursor film at 500°C for 30 min h in air.

A precursor film of $LiCoO_2$ was formed onto a 20 × 20 mm^2 quartz glass substrate by spin-coating 100 μL of the **S_{EtOH}**, using the spin-coating conditions previously mentioned in chapter 2. The precursor film was then heat-treated at 500°C for 30 min, in the air. The resultant film is denoted as **F_{spin}**.

Another film was fabricated by spin-coating 100 μL of **S_{EtOH}** onto the **F_{spray}** film. A double-step process identical to the abovementioned one was employed for the spin-coating. The spin-coated film formed on top of the **F_{spray}** film was then heat-treated at 500°C for 0.5 h in air. Hereinafter, the resultant film is denoted as **F_{ss}**.

4.4. Results and discussions

4.4.1. UV-vis absorption properties of the prepared precursor solutions

The UV-vis absorption spectra of two precursor solutions are shown in Figure 4. The spectra of **S_{aq}** and **S_{EtOH}** show broad peaks at around 520 and 580 nm, respectively. These broad peaks are characteristic to the d-d band of a Co^{2+} complex thus confirming the presence of a Co^{2+} in the precursor solutions.

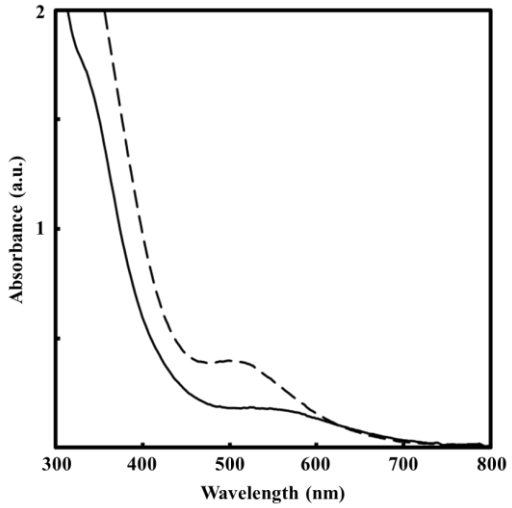

Figure 4. Absorption spectra of **S_{aq}** and **S_{EtOH}**. The spectrum of each solution is represented as follows: **S_{aq}** (– – – –), **S_{EtOH}** (———).

4.4.2. Structural characterization of the resultant thin films

XRD and Raman spectroscopy analyses

The XRD patterns of all films obtained in the present study are presented in Figure 5. Figure 5(a) shows the XRD patterns of **$F_{as\text{-}sprayed}$** and **F_{spray}**. The XRD pattern of **$F_{as\text{-}sprayed}$** indicated that the film is amorphous because only a hollow band could be observed in the 2θ range of 15–35°. In the XRD pattern of **F_{spray}**, nine peaks at 19.0, 37.4, 39.3, 45.2, 49.5, 59.6, 65.6, 66.6 and 69.7° are assignable to the (003), (101), (012), (104), (015), (107), (018), (110) and (113) crystal phase of LCO, respectively (ICDD card no. 00-050-0653). Additional two peaks can be observed in the pattern of **F_{spray}** at 31.5 and 37.1°, and they are assignable to the (220) and

(311) crystal phases of the spinel-type Co_3O_4, respectively (ICDD card no. 01-073-1701). Figure 5(b) presents the XRD patterns of $\mathbf{F_{spin}}$ and $\mathbf{F_{ss}}$. In the XRD pattern of $\mathbf{F_{spin}}$, only peaks assignable to the (111), (220), (311), (400), (511) and (440) crystal phase of the spinel-type Co_3O_4 appeared at 19.1, 31.3, 37.0, 45.0, 59.7 and 65.3°, respectively (ICDD card no. 01-073-1701). For the $\mathbf{F_{ss}}$ thin films, nine peaks at 19.0, 37.4, 39.3, 45.2, 49.5, 59.6, 65.6, 66.6 and 69.7° are assignable to the (003), (101), (012), (104), (015), (107), (018), (110) and (113) crystal phase of LCO, respectively (ICDD card no. 00-050-0653). In addition to the peaks assignable to LCO, the additional two peaks at 31.5 and 37.1° are assignable to the (220) and (311) crystal phases of the spinel-type Co_3O_4, respectively (ICDD card no. 01-073-1701).

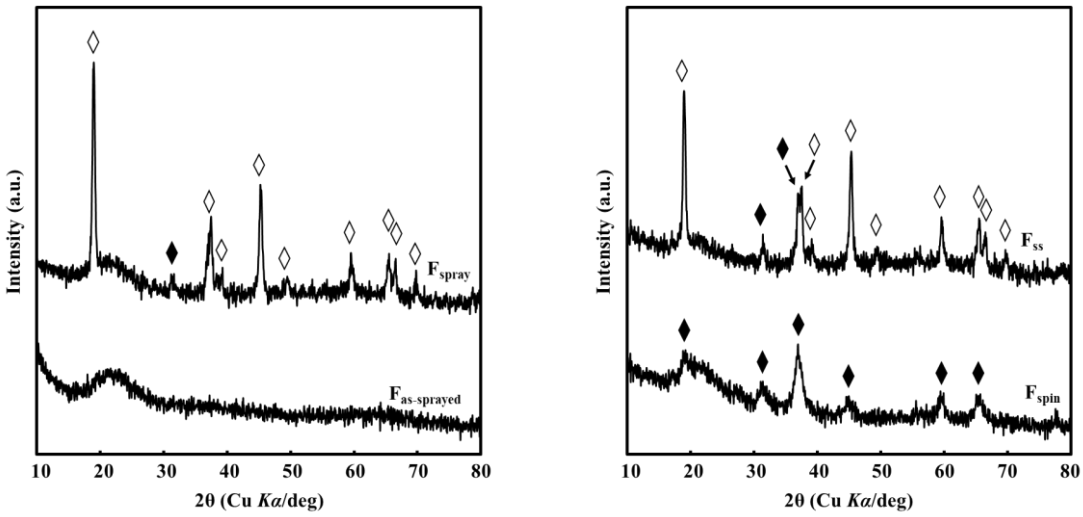

(**a**) (**b**)

Figure 5. (a) XRD patterns of $\mathbf{F_{as\text{-}sprayed}}$ and $\mathbf{F_{spray}}$. (b) XRD patterns of $\mathbf{F_{spin}}$ and $\mathbf{F_{ss}}$. The peaks assignable to the LCO and the spinel-type Co_3O_4 are denoted by ◊ and ♦, respectively.

The Raman spectra of $\mathbf{F_{spray}}$, $\mathbf{F_{spin}}$, and $\mathbf{F_{ss}}$ are given in Figure 6. The Raman spectra of $\mathbf{F_{spray}}$ and $\mathbf{F_{ss}}$, figure 6 (a) and (c), respectively, are identical. Two peaks at 485 and 595 cm^{-1} in both spectra are assignable to the layered-rock-salt LCO [10, 22, 23]. The additional broad peak at 1169 cm^{-1} is assignable to the overtone of the A_{1g} mode of layered-rock-salt LCO [24]. Four additional peaks assignable to the vibrational modes of spinel-type Co_3O_4 are observed in both

spectra at 194, 522, 619 and 690 cm^{-1} [25]. On the other hand, the Raman spectrum of $\mathbf{F_{spin}}$ shows only peaks assignable to the vibrational modes of spinel-type Co_3O_4 at 194, 483, 522, 619 and 690 cm^{-1}.

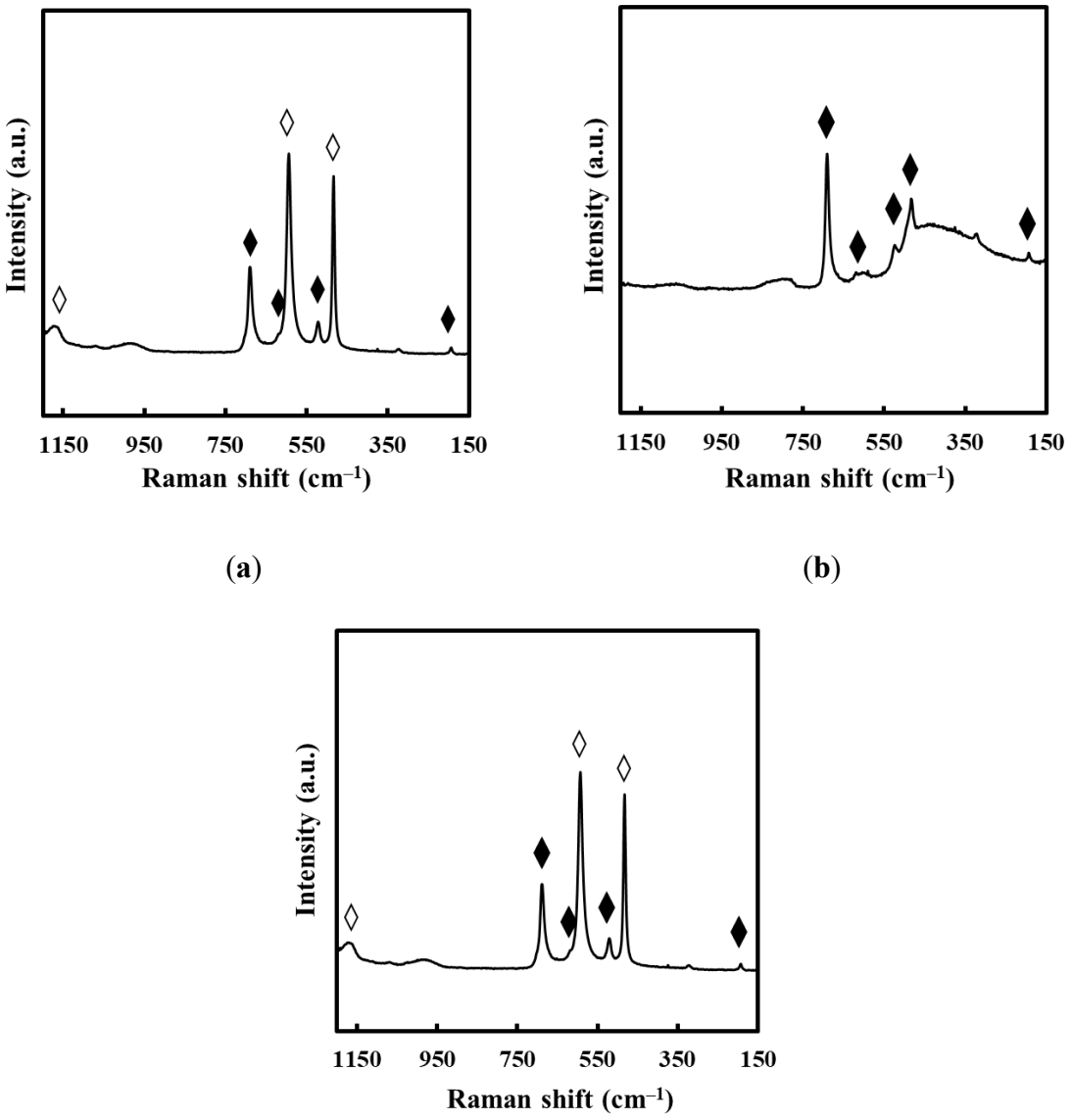

Figure 6. Raman spectra of (a) $\mathbf{F_{spray}}$, (b) $\mathbf{F_{spin}}$ and (c) $\mathbf{F_{ss}}$. The peaks assignable to the vibration modes for layered-rock-salt LCO and the Co_3O_4 are represented by using ◊ and ♦, respectively.

Figure 7 (a–b) shows the fitted peaks for the spectra of $\mathbf{F_{spray}}$ and $\mathbf{F_{spin}}$. The percentage of Co_3O_4 in each thin film was then calculated as the area ratio of the fitted peaks assignable to the F_{2g} and E_g modes of Co_3O_4 and layered-structure LCO, respectively. Using these percentages, the mole ratio of Co_3O_4 in each thin film was then determined from the calibration curve given in figure 7 (c).

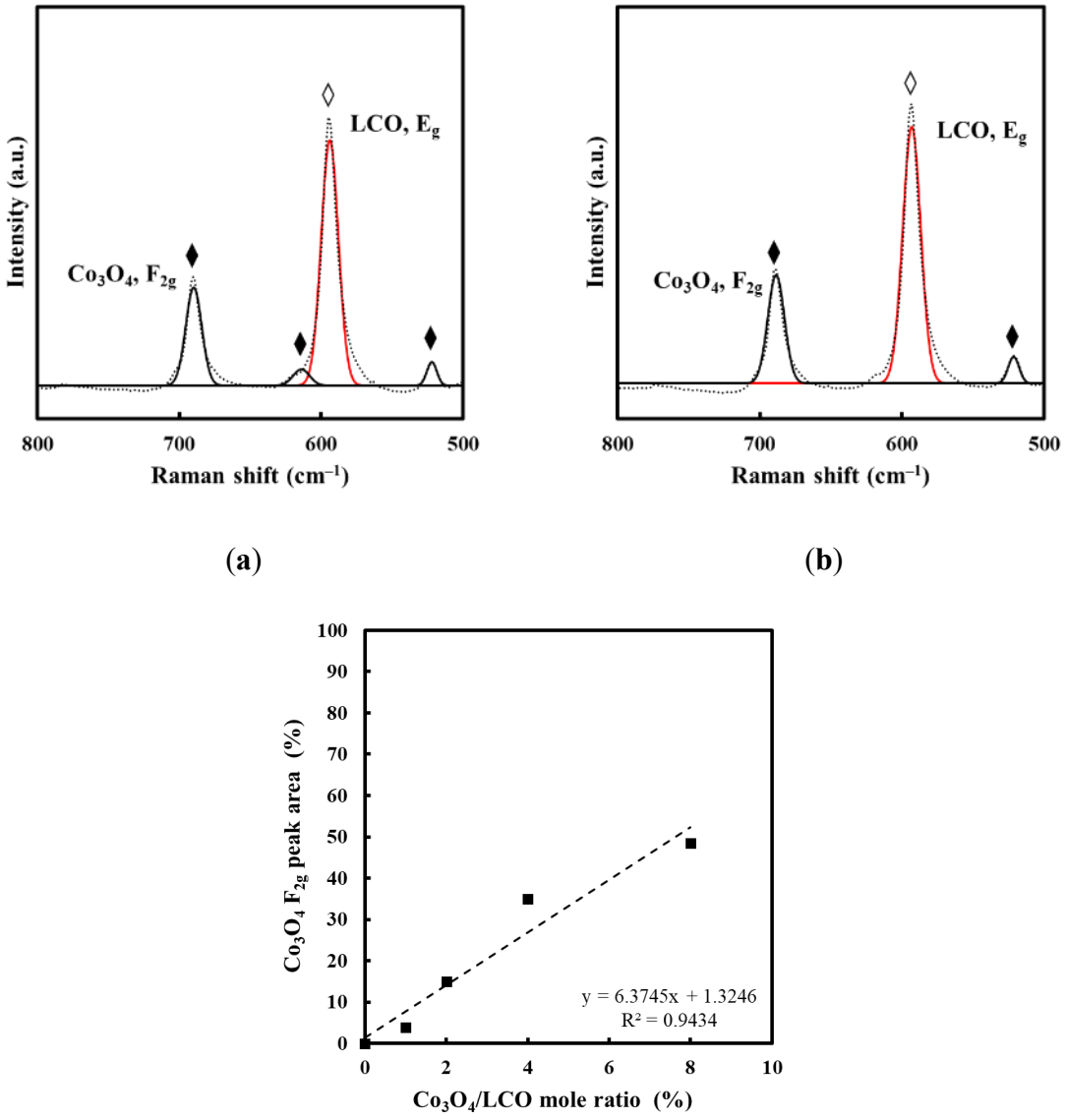

Figure 7. Fitted peaks for the Raman spectra of (a) $\mathbf{F_{spray}}$ and (b) $\mathbf{F_{ss}}$. The peaks assignable to the vibration modes for layered-rock-salt LCO and the Co_3O_4 are

represented by using ◊ and ♦, respectively. (c) The calibration curve for determining the Co_3O_4/LCO mole ratio.

To calculate the peak area ratio for the peak assignable to the F_{2g} mode of Co_3O_4, equation (1) was used as follows.

$$Co_3O_{4\,\text{peak area ratio}} = \frac{Co_3O_4,F_{2g}{}_{\text{peak area}}}{Co_3O_4,F_{2g}{}_{\text{peak area}} + \text{LCO, } E_g{}_{\text{peak area}}} \times 100 \quad (1)$$

To determine the mole ratio of Co_3O_4 in each thin film, equation (2) obtained from the calibration curve was used as follows.

$$y = 6.3745x + 1.3246 \quad (2)$$

where y and x represent the peak area ratio for the peak assignable to the F_{2g} mode of Co_3O_4 and the mole ratio of Co_3O_4 in the thin film, respectively, both in percentage. The values of y and x for the thin films $\mathbf{F_{spray}}$ and $\mathbf{F_{ss}}$ are given in table 1.

Table 1. Peak area ratio and the mole ratio of Co_3O_4 in $\mathbf{F_{spray}}$ and $\mathbf{F_{ss}}$

	Co_3O_4, F_{2g} peak area ratio (%)	**Co_3O_4, mole ratio (%)**
F_{spray}	27	4.1
F_{ss}	28	4.2

Fabrication of LCO on the quartz glass substrate via spray-coating

It is generally suggested that the nature of the substrate is vital in determining the microstructure and surface morphology of the thin film deposited on the substrate [26]. For example, in the fabrication of LCO thin films by a sol-gel method, the annealing temperatures and heating times depend on the crystalline substrates, a Si substrate (800°C, 0.5 h) or a (0001) oriented sapphire substrate (700°C, 5 h) [17, 18]. Very recently, it was clarified that an LCO thin film on a (0001) oriented sapphire substrate can be fabricated at a lower annealing

temperature of 500°C for 0.5 h, *via* the MPM, in contrast to the sol-gel method [21]. The LCO formation at low annealing temperature in the MPM is attributable to the fast appearance of fine LCO crystals, associated with the simultaneous nucleation of metal oxides and the elimination of the ligands during the heat-treatment procedure [15, 16] and this is a vital benefit of the MPM over other wet chemical methods such as the sol-gel method.

It is, however, important to note that, in all the previous studies employing wet chemical processes, crystalline substrates were used. In the present study, the LCO on a quartz glass substrate can be fabricated by the spray-coating technique. It can be accepted that during the spray-coating procedure at a preheated substrate in the temperature range of 150–180°C, the evaporation of the solvent in the vicinity of the hot substrate is accompanied by the formation of very-fine, rigid and concentrated precursors having the Li/Co ratio of LCO. The layer-by-layer accumulation of these LCO precursors continues during the subsequent spraying cycles, thus forming an amorphous precursor film on the quartz substrate. In fact, the $\mathbf{F_{as\text{-}sprayed}}$ film before the heat treatment at 500°C, showed no peak in its XRD pattern (Figure 5(a)). This accumulation process of the LCO precursor film by the low-temperature spray-coating can prevent from the undesirable reactions between Li^+ ion and the quartz glass substrate, because the precursor film spin-coated with $\mathbf{S_{EtOH}}$ could not be converted to the LCO film due to the possible reaction of Li^+ ion with the quartz glass leading to the formation of a film with Co_3O_4 crystal phase only, as shown by the XRD pattern of $\mathbf{F_{spin}}$ in Figure 5(b).

Both the evaporation of solvent and deposition of fine and dry precursors are the basic mechanism of the spray-deposition method[28, 29]. In the case of molecular precursor solutions involving metal complexes, the accompanied elimination of ligands, i.e. ammonia in this present case, plays an important role to form the amorphous precursor films of the desired compound, LCO in the Li/Co ratio of 1. Therefore, heat-treating at 500°C for 0.5 h readily transforms the amorphous LCO phase into the LCO one, without the co-presence of the low-

temperature spinel-type of LCO (Figure 6 (a, c)). From the peak fitting (Figure 7 (a, b)) and the calibration curve (Figure & (c)), the content of the spinel-type Co_3O_4 phase in both thin films was determined to be less than 5 mol%.

4.4.3. Surface morphologies and the electrical properties of the resultant thin films

The surface morphologies of $\mathbf{F_{spray}}$ and $\mathbf{F_{ss}}$ are given in Figure 8. On the surface of $\mathbf{F_{spray}}$, a uniform distribution of cylindrical grains, ca. 0.1 μm in size and rounded grains can be observed. The surface morphology of the $\mathbf{F_{spray}}$ film (Figure 8(a)) shows grains formed on top of each other, which is in agreement with the formation of rigid and fine particles of amorphous LCO during the spray-coating procedure, as proposed in the discussion of the previous section. From the surface morphology of $\mathbf{F_{spin}}$, the thin film appears to be composed much smaller and well-connected grains than $\mathbf{F_{spray}}$. The surface morphology of $\mathbf{F_{ss}}$ reveals a combination of round grains, ca. 10 nm in size, on top of extruding large and elongated grains of ca. 0.2 μm in length. The thicknesses and electrical properties of $\mathbf{F_{spray}}$ and $\mathbf{F_{ss}}$ are given in table 2. The Hall-effect measurements indicated that the resultant thin film is a *p*-type semiconductor

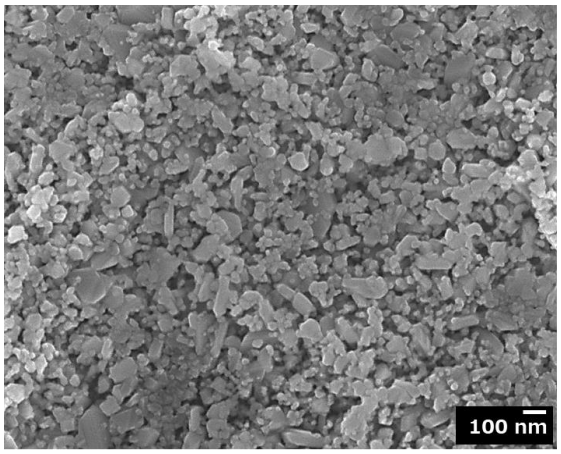

(**a**)

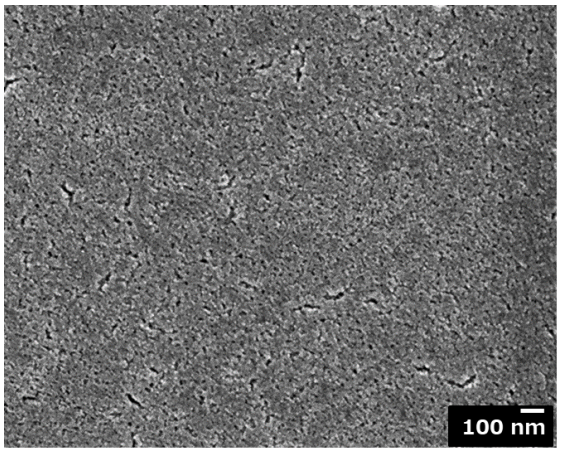

(**b**)

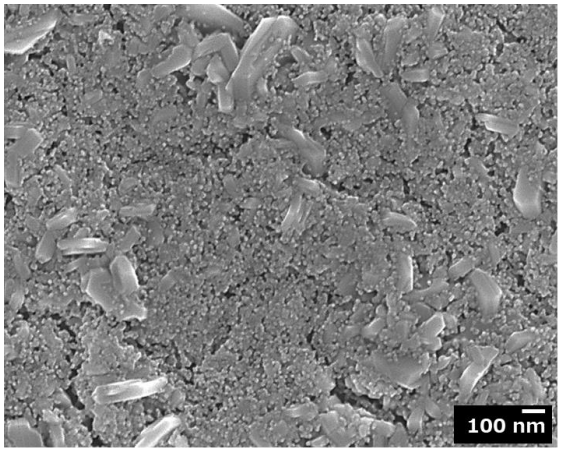

(**c**)

Figure 8. FE-SEM images showing the surface morphologies of (a) $\mathbf{F_{spray}}$, (b) $\mathbf{F_{spin}}$ and (c) $\mathbf{F_{ss}}$.

Table 2. Thicknesses and electrical properties of $\mathbf{F_{spray}}$ and $\mathbf{F_{ss}}$.

	Thickness	**Electrical resistivity**	**Carrier concentration**	**Carrier mobility**
	nm	**Ω cm**	**cm^{-3}**	**$cm^{-2}\ V^{-1}\ s^{-1}$**
$\mathbf{F_{spray}}$	120	$> 3 \times 10^{6}$	–	–
$\mathbf{F_{spin}}$	90	40(20)	$2(1) \times 10^{17}$	0.5(3)
$\mathbf{F_{ss}}$	210	35(2)	$8(2) \times 10^{16}$	2(1)

The standard deviations are presented in parentheses (n = 3).

The versatility of MPM in fabricating an electrically conductive thin film of LCO on a quartz glass substrate

Generally, the electrical conductivity of LCO can be promoted by the diffusion of lithium ions. Although the results of the XRD and Raman measurements for the $\mathbf{F_{spray}}$ thin film reveal features attributable to the LCO, Hall-effect measurements of this thin film were unsuccessful due to high electrical-resistivity. This implies that the lithium ions in the matrix were immobile to ensure electrical conductivity, and it was confirmed by the surface morphology of the thin film (Figure 8(a)) owing to the limited grain connection. The formation of LCO thin films on a crystalline substrate by annealing for a short duration, at low annealing temperatures has been emphasized in our previous study [21]. In the present study, because a film of LCO has been

already formed on the quartz glass substrate during the heat-treatment of the precursor film obtained *via* spray-coating, the heat-treatment of a film spin-coated onto the $\mathbf{F_{spray}}$ film results in the nucleation of much smaller grains of LCO, co-existing with the earlier formed LCO grains as has been observed from the surface morphology of the film (Figure 8(c)). The formation of these smaller grains can be anticipated based on the basis of the surface morphology of $\mathbf{F_{spin}}$ (Figure 8 (b)). As a result, the lithium ions can diffuse easily within the matrix and the resultant thin film ($\mathbf{F_{ss}}$) is electrically conductive, with a carrier concentration and carrier mobility of $8(2) \times 10^{16}$ cm^{-3} and 2(1) cm^{-2} V^{-1} s^{-1}, respectively. Although the $\mathbf{F_{ss}}$ film consists of the Co_3O_4 phase (Figure 5, 6) which may affect the electrical conductivity of the film, the presence of excess amount of Li^+ ions in the matrix would lead to improved carrier mobility.

One of the many identified benefits of the MPM is the ability to prepare coating solutions ideal for various appropriate coating techniques. In the present study, it was clearly revealed how various coating techniques can be used in combination to successfully achieve the fabrication of the desired functional thin film, on a specific substrate.

4.5. Summary

The aqueous coating solutions containing lithium and cobalt acetates, nitrates or hydroxides have been utilized in the preparations of gels [30] and LCO precipitates [31], in order to fabricate LCO thin films and powders. In those cases, the LCO phases were obtained after annealing at 550°C for 10 h and 850°C for 5 h in the order, respectively. In the present study, an aqueous ammonia solution $\mathbf{S_{aq}}$ containing both lithium and cobalt acetates was newly prepared and used to spray-coat onto a quartz glass preheated at 180°C, in the air. The solution was stable and could be easily used without forming any precipitate nor clogging the nozzle of the airbrush. Additionally, the solution was suitable for coating a uniform precursor film onto

a preheated quartz glass substrate with no powdery product. Heat-treating the precursor film at 500°C for 0.5 h, a thin film of LCO was facilely obtained as the major product.

The fabrication of a thin film of LCO on an amorphous quartz glass substrate was facilely achieved at low-temperature and short annealing duration. The spray-coating technique was useful in obtaining an intermediate thin film of LCO on the quartz glass substrate after heat-treating the spray-coated precursor film at 500°C for only 0.5 h. As a result, it was possible to form a thin film of LCO by spin-coating the precursor solution on top of the film obtained *via* spray-coating and, the Hall-effect measurements of the resultant thin film were successful.

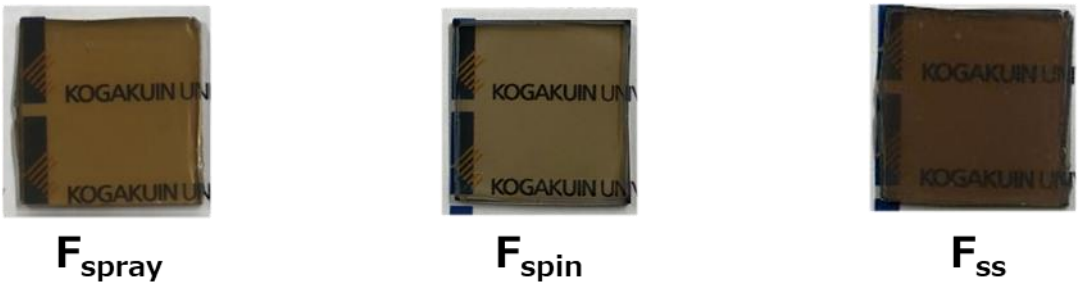

Figure 9. Images of the fabricated thin films.

By combining the abovementioned processes, it was, therefore, possible to control the formation of an LCO thin film on a quartz glass substrate. The present study serves as an indication that the spin-coating and spray-coating methods can be effectively combined in the MPM to achieve the fabrication of desired functional thin films.

References

1. Tarascon, J.-M.; Armand, M. Issues and challenges facing rechargeable lithium batteries. *Nature* **2001**, *414*, 359.

2. Nagai, H.; Sato, M. Highly Functionalized Lithium-Ion Battery. In *Alkali-ion Batteries*; InTech, 2016.

3. Julien, C.; Camacho-Lopez, M.A.; Escobar-Alarcon, L.; Haro-Poniatowski, E. Fabrication of $LiCoO_2$ thin-film cathodes for rechargeable lithium microbatteries. *Mater. Chem. Phys.* **2001**, *68*, 210–216.

4. Ohnishi, T.; Takada, K. High-rate growth of high-crystallinity $LiCoO_2$ epitaxial thin films by pulsed laser deposition. *Appl. Phys. Express* **2012**, *5*, 055502, doi:10.1143/APEX.5.055502.

5. Hausbrand, R.; Cherkashinin, G.; Ehrenberg, H.; Gröting, M.; Albe, K.; Hess, C.; Jaegermann, W. Fundamental degradation mechanisms of layered oxide Li-ion battery cathode materials: Methodology, insights and novel approaches. *Mater. Sci. Eng. B Solid-State Mater. Adv. Technol.* **2015**, *192*, 3–25, doi:10.1016/j.mseb.2014.11.014.

6. Antaya, M.; Cearns, K.; Preston, J.S.; Reimers, J.N.; Dahn, J.R. In situ growth of layered, spinel, and rock-salt $LiCoO_2$ by laser ablation deposition. *J. Appl. Phys.* **1994**, *76*, 2799–2806, doi:10.1063/1.357514.

7. Yamazaki, K.; Okabe, T. The structural study of lithium cobalt oxide. *Annu. Rep. Hydrog. Isot. Res. Center*, **2001**, *2500*, 45–52, doi:10.1016/j.immuni.2015.06.013.

8. Mizushima, K.; Jones, P.C.; Wiseman, P.J.; Goodenough, J.B. A new cathode material for batteries of high energy density. *Mater. Res. Bull.* **1980**, *15*, 783–789,

doi:10.1016/0025-5408(80)90012-4.

9. Nitta, N.; Wu, F.; Lee, J.T.; Yushin, G. Li-ion battery materials: Present and future. *Mater. Today* **2015**, *18*, 252–264, doi:10.1016/j.mattod.2014.10.040.

10. Porthault, H.; Baddour-Hadjean, R.; Le Cras, F.; Bourbon, C.; Franger, S. Raman study of the spinel-to-layered phase transformation in sol-gel $LiCoO_2$ cathode powders as a function of the post-annealing temperature. *Vib. Spectrosc.* **2012**, *62*, 152–158, doi:10.1016/j.vibspec.2012.05.004.

11. Mendiboure, A.; Delmas, C.; Hagenmuller, P. New layered structure obtained by electrochemical deintercalation of the metastable $LiCoO_2$ (O_2) variety. *Mater. Res. Bull.* **1984**, *19*, 1383–1392, doi:10.1016/0025-5408(84)90204-6.

12. Reimers, J.N.; Dahn, J.R. Electrochemical and In Situ X-Ray Diffraction Studies of Lithium Intercalation in Li_xCoO_2. *J. Electrochem. Soc.* **1992**, *139*, 2091, doi:10.1149/1.2221184.

13. Bak, T.; Nowotny, J.; Rekas, M.; Sorrell, C.C.; Sugihara, S. Properties of the electrode material Li_xCoO_2. *Ionics (Kiel).* **2000**, *6*, 92–106.

14. Mihailescu, I.N.; Caricato, A.P. *Pulsed Laser Ablation: Advances and Applications in Nanoparticles and Nanostructuring Thin Films*; Pan Stanford Publishing, 2018; ISBN 9781351733526.

15. Ohnishi, T.; Hang, B.T.; Xu, X.; Osada, M.; Takada, K. Quality control of epitaxial $LiCoO_2$ thin films grown by pulsed laser deposition. *J. Mater. Res.* **2010**, *25*, 1886–1889, doi:10.1557/jmr.2010.0250.

16. Porthault, H.; Baddour-Hadjean, R.; Le Cras, F.; Bourbon, C.; Franger, S. Raman study

of the spinel-to-layered phase transformation in sol-gel $LiCoO_2$ cathode powders as a function of the post-annealing temperature. *Vib. Spectrosc.* **2012**, *62*, 152–158.

17. Kushida, K.; Kuriyama, K. Sol–gel growth of $LiCoO_2$ films on Si substrates by a spin-coating method. *J. Cryst. Growth* **2002**, *237–239*, 612–615.

18. Kwon, T.; Ohnishi, T.; Mitsuishi, K.; Ozawa, T.C.; Takada, K. Synthesis of $LiCoO_2$ epitaxial thin films using a sol-gel method. *J. Power Sources* **2015**, *274*, 417–423.

19. Aziz, N.A.A.; Abdullah, T.K.; Mohamad, A.A. Synthesis of $LiCoO_2$ prepared by sol–gel method. *Procedia Chem.* **2016**, *19*, 861–864, doi:10.1016/j.proche.2016.03.114.

20. Nagai, H.; Suzuki, T.; Takahashi, Y.; Sato, M. Photovoltaic lithium-ion battery fabricated by molecular precursor method. *Funct. Mater. Lett.* **2016**, *9*, 1650046-1–4, doi:10.1142/S1793604716500466.

21. Suzuki, T.; Nagai, H.; Lu, L.; Sato, M. Electrical properties of partially nitrided $LiCoO_2$ thin films with an equivalent amount of Li and Co, involving small amounts of amorphous or crystallized Co_3O_4. Manuscript submitted for publication.

22. Kosuril, Y.R.; Penki, T.R.; Nookala, M.M.; Morgen, P.; Gowravaram, M.R.; Rao Kosuri, Y.; Rao Penki, T.; Nookala, M.M.; Morgen, P.; Rao Gowravaram, M. Investigations on sputter deposited $LiCoO_2$ thin films from powder target. *Adv. Mater. Lett.* **2013**, *4*, 615–620, doi:10.5185/amlett.2012.12479.

23. Inaba, M.; Todzuka, Y.; Yoshida, H.; Grincourt, Y.; Tasaka, A.; Tomida, Y.; Ogumi, Z. Raman spectra of $LiCo_{1-y}Ni_yO_2$. *Chem. Lett.* **1995**, *24*, 889–890, doi:10.1246/cl.1995.889.

24. Gross, T.; Hess, C. Raman diagnostics of $LiCoO_2$ electrodes for lithium-ion batteries. *J.*

Power Sources **2014**, *256*, 220–225, doi:10.1016/j.jpowsour.2014.01.084.

25. Hadjiev, V.G.; Iliev, M.N.; Vergilov, I. V. The Raman spectra of Co_3O_4. *J. Phys. C Solid State Phys.* **1988**, *21*, L199–L201, doi:10.1088/0022-3719/21/7/007.

26. Lee, J.K.; Lee, S.J.; Baik, H.K.; Lee, H.Y.; Jang, S.W.; Lee, S.M. Substrate effect on the microstructure and electrochemical properties in the deposition of a thin film $LiCoO_2$ electrode. *Electrochem. Solid State Lett.* **1999**, *2*, 512–515, doi:10.1149/1.1390887.

27. Nagai, H.; Sato, M. treatment in molecular precursor method for fabricating metal oxide thin films. In *Heat Treatment—Conventional and Novel Applications*; Czerwinski, F., Ed.; InTech: Rijeka, Croatia, 2012; pp. 297–322.

28. Mochizuki, C.; Hara, H.; Takano, I.; Hayakawa, T.; Sato, M. Application of carbonated apatite coating on a Ti substrate by aqueous spray method. *Mater. Sci. Eng. C* **2013**, *33*, 951–958, doi:10.1016/j.msec.2012.11.027.

29. Hsu, H.-W.; Liu, C.-L. Spray-coating semiconducting conjugated polymers for organic thin film transistor applications. *RSC Adv.* **2014**, *4*, 30145–30149, doi:10.1039/c4ra03726j.

30. Peng, Z.; Wan, C.; Jiang, C. Synthesis by sol–gel process and characterization of LiCoO2 cathode materials. *J. Power Sources* **1998**, *72*, 215–220, doi:10.1016/S0378-7753(97)02689-X.

31. Liao, D.Q.; Xi, X.M. Study on the preparation of $LiCoO_2$ by multiphase redox method. *Powder Technol.* **2014**, *253*, 146–151, doi:10.1016/j.powtec.2013.11.012.

CHAPTER 5: MWCNT/CU COMPOSITE THIN FILMS VIA SPRAY-COATING OF AN AQUEOUS SOLUTION CONTAINING COPPER(II) COMPLEXES AND MWCNT

CHAPTER 5: FABRICATION AND CHARACTERIZATION OF MWCNT/Cu COMPOSITE THIN FILMS VIA SPRAY-COATING OF AN AQUEOUS SOLUTION CONTAINING COPPER(II) COMPLEXES AND MWCNT

5.1. Introduction

Copper is already being used as an interconnecting material of choice over aluminum in the fabrication of Ultra-Large-Scale-Integrated (ULSI) devices, due to its lower electrical resistivity and power dissipation, and high resistance to electro-migration [1]. As the miniaturization of various basic device elements continues, the electronics' industry is faced with a challenge on how to maintain the functionality of the conducting materials even at the nanoscale [2, 3]. For this reason, carbon nanotubes/cooper (CNT/Cu) composite materials are promising candidates to replace pure copper as an electrical conductor. There is a potential to improve the current capacity of copper in nanoelectronics by incorporating carbon nanostructures into the copper lattice [4] and, the fabrication of a CNT/Cu composite with an increased current carrying capacity has been reported [5].

Multi-walled carbon nanotubes (MWCNT) are promising materials for the development of nano-electronics due to their outstanding properties such as ballistic electron transfer, huge current carrying capacity [6–8]. Additionally, it has been reported that the electrical resistivity of MWCNT films remains constant at high temperatures [9] and this an advantage for applications in high temperature operating nano-devices. Techniques such as electroplating and electroless plating have been identified as some of the ideal, wet chemical processes for the fabrication of CNT/Cu composite films [10, 11]. The electroplating technique involves the electroplating Cu ions into a pre-deposited CNT forest on a conducting substrate [5]. On the other hand, electroless plating has been identified as a promising deposition technique to fabricate CNT/Cu composite films on insulating substrates by using CNT-Cu ions dispersions

[12, 13]. However, the use of $PdCl_2$ or, $SnCl_2$ to activate the surface of the specimens is required and might remain as a compromising factor to the quality of the thin films [14].

In this chapter, the fabrication and characterization of MWCNT/Cu composite thin films using an aqueous solution containing Cu(II) complexes and MWCNT *via* the MPM are reported. To the best of our knowledge, up-to-date, there is no report on the fabrication of MWCNT/Cu composite thin films by spray-coating an aqueous solution containing Cu(II) complexes and MWCNT.

5.2. Preparation of the coating solutions and thin film fabrication

The coating solution containing Cu(II) complexes of EDTA and NH_3 was prepared according to the procedures in chapter 3. Hereinafter, this solution is denoted as $\mathbf{S_{Cu}}$. Coating solutions containing Cu(II) complexes and MWCNTs were then prepared by mixing 6.00 g of $\mathbf{S_{Cu}}$ with varying amounts of the 2 mass% MWCNT ink. Hereinafter, the prepared precursor solutions containing Cu(II) complexes with MWCNT are denoted as $\mathbf{S_{MWCNT/Cu\_}}_{\boldsymbol{x}}$ whereby the subscript $\boldsymbol{x}$ represents the MWCNT volume percent calculated using Eq. (1), where V_{MWCNT} and V_{Cu} represent the volume of MWCNT derived from the quantity of MWCNT ink used and the volume of metallic copper obtainable from 6.00 g of the used solution containing Cu(II) complexes, respectively. A density value of 2.10 g cm^{-3} for the MWCNT [15] was used to calculate the volume of MWCNT in each prepared solution and four solutions with 10, 20, 30 and 50 vol% were prepared. For comparison, another solution containing MWCNT only was prepared by mixing 0.50 g of the MWCNT ink with 6.00 g of water and this solution is hereinafter referred to as $\mathbf{S_{MWCNT}}$. The mixtures were stirred on a magnetic stirrer for 1 h at room temperature and used with no further modifications.

$$\boldsymbol{x} = \frac{V_{MWCNT}}{V_{MWCNT} + V_{Cu}} \times 100 \qquad \text{Eq. (1)}$$

Using the earlier-mentioned spray-coating and heat-treating procedures, 6.00 g of the respective precursor solution was spray-coated onto the preheated substrate. In this chapter, the

fabricated films are denoted as follows: **F_{Cu}**, **F_{MWCNT}**, and **F_{MWCNT/Cu_x}** refer to the precursor films obtained after spray-coating the preheated quartz glass substrates with the **S_{Cu}**, **S_{MWCNT}** and **S_{MWCNT/Cu_x}** solutions, respectively. The resultant films obtained by heat-treating **F_{Cu}**, **F_{MWCNT}** and **F_{MWCNT/Cu_x}** at 350°C for 50 min under Ar gas with a flow rate of 1.5 L min^{-1} are denoted as **F'_{Cu}**, **F_{MWCNT/Cu_x}**, and **F'_{MWCNT}**, respectively. Finally, the films obtained from the post-annealing of **F'_{Cu}**, **F_{MWCNT/Cu_x}**, and **F'_{MWCNT}** are denoted as **F''_{Cu}**, **F''_{MWCNT/Cu_x}**, and **F''_{MWCNT}**, respectively.

5.3. Results and discussions

5.3.1. Crystal structures of the resultant thin films

Figure 1a shows the XRD patterns of **F_{Cu}** and **F_{MWCNT/Cu_x}**. The XRD pattern of **F_{Cu}** shows peaks at 43.5, 50.7 and 74.3° are assignable to the (111), (200) and (220) crystal phase of metallic Cu, respectively (ICDD card no. 00-004-0836). In the XRD patterns of **F_{MWCNT/Cu_10}** and **F_{MWCNT/Cu_20}**, in addition to the peaks at 43.4, 50.5 and 74.2° assignable to the (111), (200) and (220) crystal phase of metallic Cu, respectively, two additional peaks assignable to the (111) and (220) crystal phase of Cu_2O can be observed at 36.5 and 61.5°, respectively (ICDD card no. 01-071-3645). The XRD pattern of **F_{MWCNT/Cu_30}** is identical to those of **F_{MWCNT/Cu_10}** and **F_{MWCNT/Cu_20}** with additional peaks at 42.3 and 73.7° assignable to the (200) and (311) phase of Cu_2O, respectively. In the XRD pattern of **F_{MWCNT/Cu_50}**, a peak assignable to the (002) phase of graphite (derived from the MWCNT) can be observed at 25.7° (ICDD card no. 00-056-0159). Additionally, peaks assignable to the (110), (111), (200), (220) and (311) crystal phase of Cu_2O can be observed at 29.7, 36.5, 42.3, 61.4 and 73.7°, respectively.

In figure 1(b), the XRD patterns of **F'_{Cu}** and **F'_{MWCNT/Cu_x}** are shown. In all patterns, the three peaks at 43.4, 50.5 and 74.3° are assignable to the (111), (200) and (220) crystal phase of metallic Cu, respectively. In the XRD pattern of **F'_{Cu}**, two additional peaks assignable to the (111) and (220) crystal phase of Cu_2O can be observed at 36.5 and 61.5°, respectively. The

XRD pattern of **F'$_{MWCNT/Cu\_10}$** is identical to that of **F'$_{Cu}$** with additional peaks assignable to the (110) and (200) phase of Cu_2O at 29.6 and 42.44°, respectively. In the XRD patterns of **F'$_{MWCNT/Cu\_20–50}$**, an additional peak at 77.4° assignable to the (222) phase of Cu_2O can be observed. Also, the XRD pattern of **F'$_{MWCNT/Cu\_50}$** has a peak at 25.7° assignable to the (002) phase of graphite.

Figure 1(c) shows the XRD patterns of **F''$_{Cu}$** and **F''$_{MWCNT/Cu\_x}$**. In the patterns of **F''$_{Cu}$** and **F''$_{MWCNT/Cu\_10–30}$**, only peaks assignable to the (111), (200) and (220) crystal phase of metallic Cu can be observed at 43.4, 50.6 and 74.2°, respectively. The XRD pattern of **F''$_{MWCNT/Cu\_50}$** has additional peaks at 25.94 and 29.60° assignable to the (002) phase of graphite and (111) phase of Cu_2O, respectively.

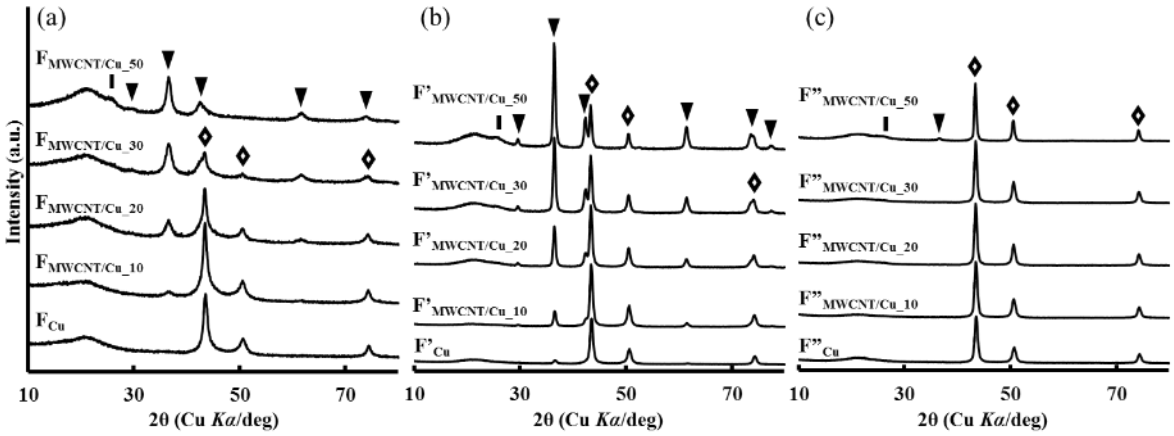

Figure 1. XRD patterns of the fabricated films. (a) Right after spray-coating, (b) After heat-treating the spray-coated films and, (c) After post-annealing. The peaks are denoted as follows; ◊ Cu, ▼ Cu_2O and ▌Graphite.

The relationship between the coating solution's MWCNT ink content and the crystallized Cu species in the resultant thin films

It has been established from our previous study that spray-coating of **S$_{Cu}$** onto a quartz glass substrate preheated to 180°C, a precursor film with crystallized Cu^0 phase can be obtained (**F$_{Cu}$**, Figure 1(a)). On the other hand, when **S$_{Cu}$** is mixed with an MWCNT dispersion, the

appearance of the oxidized Cu phase is observed and increases with the MWCNT volume fraction (Figure 1(a)). In our previous work (in chapter 3), we have discussed how the identity of the crystallized Cu species in the as-sprayed film depends on the ratios of the Cu(II) complexes in the coating solution. In the present study, the used MWCNT ink contains an added amount of surfactant and its influence on the chemical identity of the coating solution is evident from the formation of the Cu_2O phase with increased MWCNT volume percent.

The oxidation of the precursor films during the heat-treatment procedure under Ar gas containing less than 10 ppm of air as its impurity, has been discussed in our previous studies [16]. Therefore, the formation of the Cu_2O phase in the films after heat-treating at 350°C under an Ar gas flow of 1.5 L min^{-1} for 50 min (Figure 1(b)), is expected. However, the extent of oxidation of each respective composite film is dependent on the amount of MWCNT ink used which modifies the chemical identity of the coating solution as a result. In the fabrication of Cu thin films *via* the MPM, the carbon atoms derived from the ligands that remain within the heat-treated films have been utilized to reduce the previously formed Cu_2O species. On the same basis, the Cu_2O species formed as a result of heat-treating the composite precursor films at 350°C under an Ar gas flow of 1.5 L min^{-1} for 50 min, were successfully reduced to the Cu^0 phase (Figure 1(c)) through the post-annealing procedure as described in the experimental section above. At high MWCNT ink contents, it might be possible that because the extent of oxidation is too high during the heat-treating procedure, carbon derived from the MWCNT might be used for the reduction of the Cu_2O phase during the post-annealing procedure as observed in the XRD pattern of $\mathbf{F''_{MWCNT/Cu\_20\text{-}50}}$ (Figure 1(c)).

5.3.2. Surface morphologies and electrical properties of the resultant thin films

The FE-SEM images of the top and cross-section views of the $\mathbf{F''_{Cu}}$ and $\mathbf{F''_{MWCNT}}$ are given in figure 2(a–b) and (c–d), respectively. The top view of $\mathbf{F''_{Cu}}$ (figure 2(a)), reveals a crack-free surface with well-connected and closely packed grains of Cu grains. Random networks of

the deposited MWCNT can be observed in the top view of **F''$_{MWCNT}$** (figure 2(b)). The cross-sectional image of **F''$_{Cu}$** (figure 2(a)) reveals that the thin film is homogeneously and densely deposited on the quartz glass substrate whereas that of **F''$_{MWCNT}$** (figure 2(b)) indicates a less dense mass of MWCNT on the substrate.

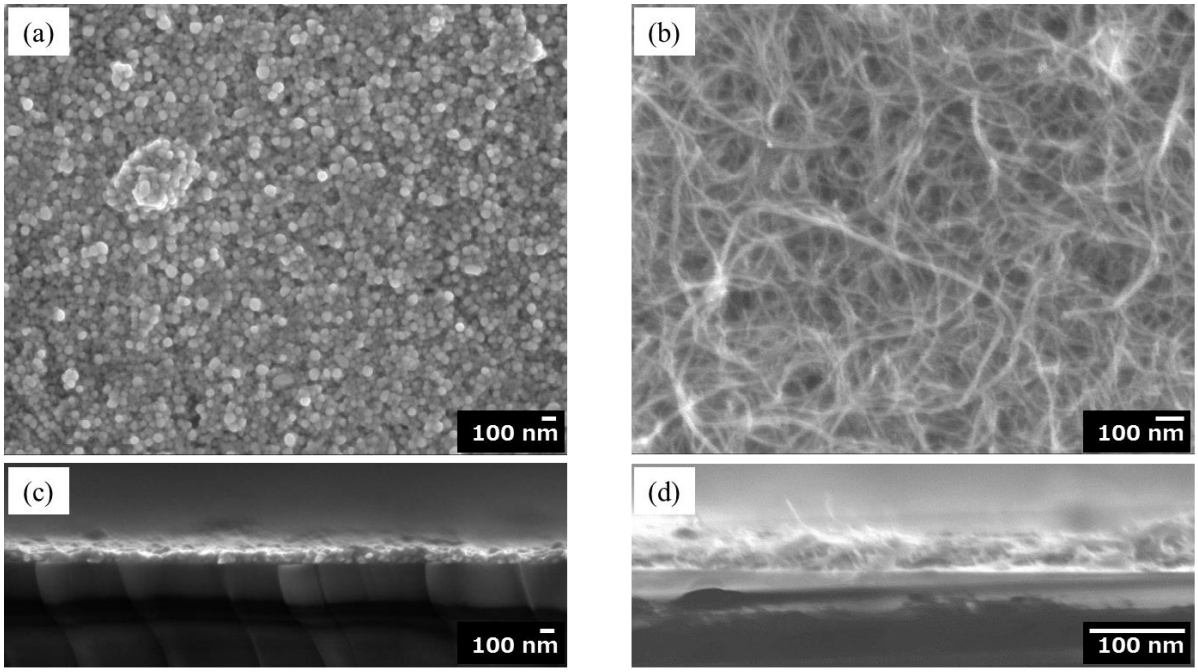

Figure 2. FE-SEM images of **F''$_{Cu}$** and **F''$_{MWCNT}$** on quartz glass substrates. (a) and (c) show the top view and cross-section view of **F''$_{Cu}$**, respectively. (b) and (d) show the top view and cross-section view of **F''$_{MWCNT}$**, respectively

The FE-SEM images of the resultant composite thin film are given in figure 3. From the top views (figure 3 (a, b, e and d)), the mixture of the Cu grains and MWCNT can be observed. The cross-sectional image of the **F''$_{MWCNT/Cu\_10}$** (figure 3(c)) shows a densely deposited film on the quartz glass substrate. For **F''$_{MWCNT/Cu\_20–50}$** (Figure 3(d, g and h)), the films appear as less compact masses of the MWCNT/Cu composites with MWCNT structures clearly observable in random directions.

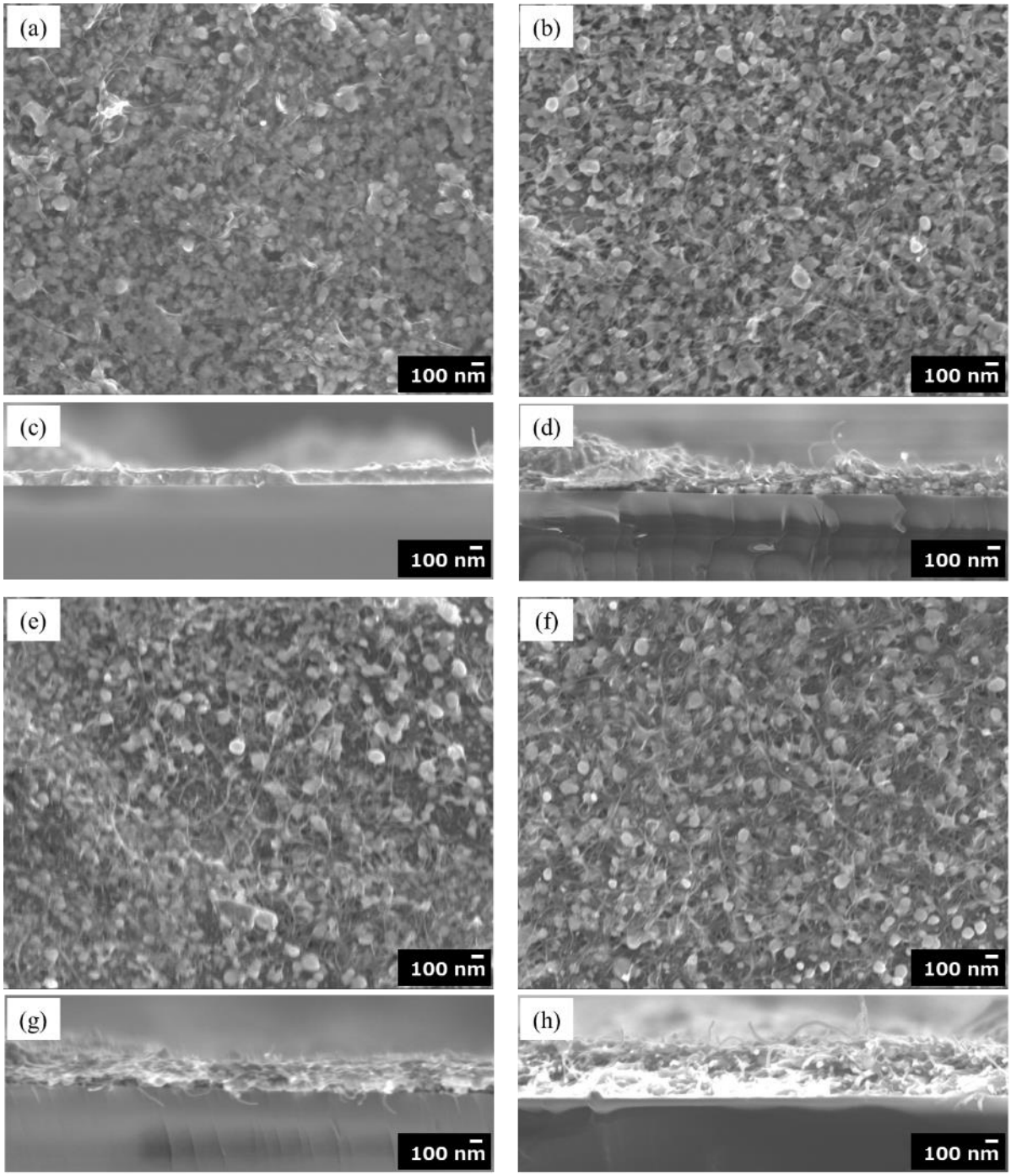

Figure 3. FE-SEM images of MWCNT/Cu composite thin films fabricated on quartz glass substrates. The top view of **F''$_{MWCNT/Cu\_10}$**, **F''$_{MWCNT/Cu\_20}$**, **F''$_{MWCNT/Cu\_30}$,** and **F''$_{MWCNT/Cu\_50}$** are given in (a), (b), (e) and (f), respectively, while the cross-section views are given below the top view of the corresponding thin film (c, d, g, and h).

The thickness of the resultant thin films and their electrical resistivity are tabulated in Table 1below.

Table 1. The thickness and electrical resistivity of the resultant films

Thin film	Thickness (nm)	Electrical resistivity (Ω cm)
$\mathbf{F''_{Cu}}$	100	$3.8(6) \times 10^{-5}$
$\mathbf{F''_{MWCNT/Cu\_10}}$	110	$4.8(1) \times 10^{-5}$
$\mathbf{F''_{MWCNT/Cu\_20}}$	160	$1.14(1) \times 10^{-4}$
$\mathbf{F''_{MWCNT/Cu\_30}}$	200	$1.9(1) \times 10^{-4}$
$\mathbf{F''_{MWCNT/Cu\_50}}$	350	$1.31(4) \times 10^{-2}$
$\mathbf{F''_{MWCNT}}$	360	$3.16(2) \times 10^{-2}$

The standard deviations are given in parenthesis

Influence of the Cu(II) complexes in the coating solution on the surface morphologies and electrical conductivities of the resultant thin films

As references, the morphologies of $\mathbf{F''_{Cu}}$ and $\mathbf{F''_{MWCNT}}$ (Figure 2(a) and (b), respectively) could give a clear understanding of a typical Cu thin film and MWCNT film, respectively, fabricated by heat-treating films obtained through spray-coating using the present method. The electrical resistivity of $\mathbf{F''_{Cu}}$ and $\mathbf{F''_{MWCNT}}$ (3.8×10^{-5} Ω cm and 3.2×10^{-2} Ω cm, respectively) also formed vital indicative tools on understanding the electrical resistivity of the expected composite thin films, depending on whether the resultant composite thin film is predominantly Cu or MWCNT. At an MWCNT volume fraction of 10% in the coating solution, the resultant composite thin film is densely deposited on the quartz glass substrate (Figure 3(a, c)) and its electrical resistivity is 4.8×10^{-5} Ω cm. It is important to note that at this MWCNT volume fraction, the MWCNT nanostructures are observable on the FE-SEM images, however, the electrical conductivity of the resultant composite thin film is not disrupted and its electrical resistivity is equivalent to that of $\mathbf{F''_{Cu}}$. However, when the MWCNT volume fraction has been increased to 20 and 30%, the increase in the MWCNT nanostructures is evident from the FE-

SEM images of **F''$_{MWCNT/Cu\_20}$** and **F''$_{MWCNT/Cu\_30}$** (Figure 3(b, d and e, g, respectively). Their electrical resistivity is of × 10^{-4} Ω cm order, with a thickness of 160 and 200 nm for **F''$_{MWCNT/Cu\_20}$** and **F''$_{MWCNT/Cu\_30}$**, respectively. For these resultant composite films, the influence of both the Cu and the MWCNT on their morphologies and electrical resistivity is not negligible, producing a composite material with mixed properties.

At a 50% MWCNT volume fraction in the coating solution, the properties of the resultant composite thin film do not represent a 50/50 influence of Cu and MWCNT. Although the top view of the FE-SEM image (Figure 3(f)) shows the co-presence of Cu grains and MWCNT nanostructures, the cross-section image (Figure 3 (h)) shows how the MWCNT content extensively dictates the morphology of this composite thin film. Random and solid nanostructures can be observed from the image and the film is not so compact. Implying a decreased contact between the Cu grains within the composite and as a result, the electrical resistivity of this composite thin film is 1.3 × 10^{-2} Ω cm, which is of the same order as the electrical resistivity of **F''$_{MWCNT}$**. In the present study, we have revealed how the electrical resistivity of the resultant composite thin films can change from that identical to a highly conductive Cu thin film to that of an MWCNT film with random MWCNTs on a quartz glass substrate, by changing the volume fraction of MWCNT in the coating solutions.

5.3.3. Reflectance spectra and adhesion strength of **F"$_{Cu}$** and **F"$_{MWCNT/Cu\_10}$**

Figure 4 shows the reflectance spectra of the resultant films. The reflectance of **F''$_{Cu}$** approaches over 90% in the far infrared region while that of **F''$_{MWCNT/Cu\_10}$** approaches over 70% in the identical region. The adhesion strength of the thin film **F''$_{Cu}$** and the composite thin film **F''$_{MWCNT/Cu\_10}$** onto the quartz glass substrates was found to be 37(7) and 21(7) MPa, respectively. It's also worth noting here that has **F''$_{MWCNT}$** no adhesion onto the quartz glass and can be easily wiped off the quartz glass substrate by any contact.

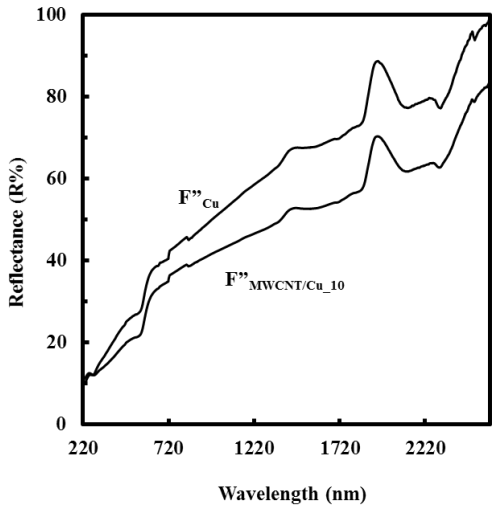

Figure 4. Reflectance spectra of **F''$_{Cu}$** and **F''$_{MWCNT/Cu\_10}$**.

The adhesion-strength of any conductive thin film onto the substrate represents an important mechanical characteristic that determines the applicability of such material [17] and, various techniques have been established to modify the surfaces of the substrates and ensure acceptable adherence [13,18]. Copper/MWCNT composite films fabricated onto resin substrates roughened by etching with a chromic acid solution had an adhesion-strength of 25 MPa and it is attributable to the anchor effect [13]. Noting that **F''$_{MWCNT}$** does not form any adhesion while **F''$_{Cu}$** has strongly adhered onto the substrate with an adhesion strength of 37 MPa, it is conclusive that the 21 MPa adhesion-strength of the composite thin film **F''$_{MWCNT/Cu\_10}$** is the result of the formation of an interface having bonds between Cu and O^{2-} belonging to the quartz glass substrate [19]. The decrease in adhesion-strength of the composite thin film can be related to the influence of the MWCNT structures within the composite's matrix. In **F''$_{Cu}$,** it is easy to form a homogeneous and continuous interface between the film and the substrate. On the other hand, in **F''$_{MWCNT\_10}$** due to the random orientation of the MWCNT, the interface between the substrate and the film is not homogenous resulting in a reduced thin film adhesion-strength.

5.4. Summary

Homogenous solutions containing both the Cu(II) complexes and MWCNTs with MWCNTs' volume fractions of 10, 20, 30 and 50%, could be easily prepared in the present study by mixing the stable and volatile organic compounds (VOC)-free solution, $\mathbf{S_{Cu}}$ with an MWCNT dispersion. Importantly, no colloids or any solid particles was formed upon the mixing and the mixture could be successfully spray-coated onto a quartz glass substrate preheated to 180°C, without clogging the nozzle tip and precursor films were obtained. Heat-treating the obtained precursor films, on the basis of our previous procedures, produced conductive MWCNT/Cu composite thin films. From a coating solution with 10% MWCNT volume fraction, the resultant composite thin film of 110 nm thickness has an electrical resistivity of 4.8×10^{-5} Ω cm which is identical to that of a Cu thin film fabricated by using $\mathbf{S_{Cu}}$ only, and an adhesion-strength onto the quartz glass substrate of 21 MPa.

The fabrication of copper/MWCNT composite films using a plating technique referred to as composite plating, which involves both electrolytic plating [20,21] and electroless plating [13,22] has been reported. However, because electrolytic plating requires the use of conductive substrates, the fabrication of MWCNT/Cu thin film on glass and other insulating substrates would be impossible. On the other hand, the electroless plating technique requires roughening of the substrate in order to improve the adhesion of the film, followed by sensitization and activation to ensure deposition and reduction of the copper ions, using $SnCl_2$ and $PdCl_2$, respectively. Tin is highly toxic and the electroless plating technique is generally an uncontrollable process resulting in the waste of Pd and plating failure [23]. Therefore, the fabrication of MWCNT/Cu composite thin films via a method that does not require substrate modification and uses safer and affordable chemical reagents is of great advantage.

In addition, even though the deposition of MWCNT films onto various substrates has achieved *via* the spray-coating with MWCNT inks [24, 25], the simultaneous spray-coating of

a mixture of MWCNT and Cu precursors has not been reported. This can be attributed to the fact that there were no suitable coating solutions of Cu precursors that can be used to fabricated Cu thin films *via* methods employing spray-coating at ambient conditions, and also can be mixed with MWCNT dispersions to yield homogenous solutions suitable for spray-coating. This present study is the first report on the fabrication of MWCNT/Cu composite thin films on an insulating substrate by using the combination of an aqueous solution made up of Cu(II) complexes and without substrate pre-treatment.

The use of aqueous solutions and rather simple fabrication methods to fabricate functional materials cannot be understated. In this study, we further explored the applicability of the MPM to fabricate composite thin films. Therefore, this work serves as a contribution to the fabrication of MWCNT/Cu composite materials *via* methods that do not require complicated experimental set-ups and coating can be done at ambient laboratory conditions.

References

1. Murarka, S.P.; Hymes, S.W. Copper metallization for ULSI and beyond. *Crit. Rev. Solid State Mater. Sci.* **1995**, *20*, 87–124, doi:10.1080/10408439508243732.

2. Lotey, G.S.; Kumar, S.; Verma, N.K. Fabrication and electrical characterization of highly ordered copper nanowires. *Appl. Nanosci.* **2011**, *2*, 7–13, doi:10.1007/s13204-011-0034-z.

3. Li, B.; Sullivan, T.D.; Lee, T.C.; Badami, D. Reliability challenges for copper interconnects. *Microelectron. Reliab.* **2004**, *44*, 365–380, doi:10.1016/j.microrel.2003.11.004.

4. Isaacs, R.A.; Zhu, H.; Preston, C.; Mansour, A.; Lemieux, M.; Zavalij, P.Y.; Jaim, H.M.I.; Rabin, O.; Hu, L.; Salamanca-Riba, L.G. Nanocarbon-copper thin film as transparent electrode. *Appl. Phys. Lett.* **2015**, *106*, doi:10.1063/1.4921263.

5. Subramaniam, C.; Yamada, T.; Kobashi, K.; Sekiguchi, A.; Futaba, D.N.; Yumura, M.; Hata, K. One hundred fold increase in current carrying capacity in a carbon nanotube-copper composite. *Nat. Commun.* **2013**, *4*, 2202, doi:10.1038/ncomms3202.

6. Li, H.J.; Lu, W.G.; Li, J.J.; Bai, X.D.; Gu, C.Z. Multichannel ballistic transport in multiwall carbon nanotubes. *Phys. Rev. Lett.* **2005**, *95*, 1–4, doi:10.1103/PhysRevLett.95.086601.

7. Byeon, J.H.; Hwang, J. Morphology of metallic nanoparticles as a function of deposition time in electroless deposition of metal on multi-walled carbon nanotubes. *Surf. Coatings Technol.* **2008**, *203*, 357–363, doi:10.1016/j.surfcoat.2008.09.017.

8. Wei, B.Q.; Vajtai, R.; Ajayan, P.M. Reliability and current carrying capacity of carbon

nanotubes. *Appl. Phys. Lett.* **2001**, *79*, 1172–1174, doi:10.1063/1.1396632.

9. Zhang, H.-L.; Li, J.-F.; Zhang, B.-P.; Yao, K.-F.; Liu, W.-S.; Wang, H. Electrical and thermal properties of carbon nanotube bulk materials: Experimental studies for the 328–958 K temperature range. *Phys. Rev. B* **2007**, *75*, 205407, doi:10.1103/PhysRevB.75.205407.

10. Bakshi, S.R.; Lahiri, D.; Agarwal, A. Carbon nanotube reinforced metal matrix composites - a review. *Int. Mater. Rev.* **2010**, *55*, 41–64, doi:10.1179/095066009X12572530170543.

11. Silvestre, N. State-of-the-art Review on Carbon Nanotube Reinforced Metal Matrix Composites. *Int. J. Compos. Mater.* **2013**, *3*, 28–44, doi:10.5923/s.cmaterials.201309.04.

12. Arai, S.; Osaki, T.; Hirota, M.; Uejima, M. Fabrication of copper/single-walled carbon nanotube composite film with homogeneously dispersed nanotubes by electroless deposition. *Mater. Today Commun.* **2016**, *7*, 101–107, doi:10.1016/j.mtcomm.2016.04.009.

13. Arai, S.; Kanazawa, T. Electroless deposition and evaluation of Cu/multiwalled carbon nanotube composite films on acrylonitrile butadiene styrene resin. *Surf. Coatings Technol.* **2014**, *254*, 224–229, doi:10.1016/j.surfcoat.2014.06.017.

14. Han, S.; Lee, T.L.; Yang, C.J.; Shih, H.C. Trench gap-filling copper by ion beam sputter deposition. *Mater. Chem. Phys.* **2006**, *97*, 19–22, doi:10.1016/j.matchemphys.2005.05.042.

15. Lehman, J.H.; Terrones, M.; Mansfield, E.; Hurst, K.E.; Meunier, V. Evaluating the characteristics of multiwall carbon nanotubes. *Carbon N. Y.* **2011**, *49*, 2581–2602,

doi:10.1016/j.carbon.2011.03.028.

16. Nagai, H.; Suzuki, T.; Mochizuki, C.; Takano, I.; Honda, T.; Sato, M. Formation Mechanism of *p*-Type Cu_2O Thin Films via Intermediate Cu^0 Species Derived from Cu(II) Complex of Ethylenediamine-*N*,*N*,*N*′,*N*′-Tetraacetic Acid. *Sci. Adv. Mater.* **2014**, *6*, 603–611, doi:10.1166/sam.2014.1788.

17. Mittal, K.L. Adhesion Measurement of Thin Films. *Electrocompon. Sci. Technol.* **1976**, *3*, 21–42, doi:10.1155/APEC.3.21.

18. Lim, J.D.; Lee, P.M.; Rhee, D.M.W.; Leong, K.C.; Chen, Z. Effect of surface treatment on adhesion strength between magnetron sputtered copper thin films and alumina substrate. *Appl. Surf. Sci.* **2015**, *355*, 509–515, doi:10.1016/j.apsusc.2015.07.141.

19. Nagai, H.; Mita, S.; Takano, I.; Honda, T.; Sato, M. Conductive and semi-transparent Cu thin film fabricated using molecular precursor solutions. *Mater. Lett.* **2015**, *141*, 235–237, doi:10.1016/j.matlet.2014.11.056.

20. Arai, S.; Endo, M. Carbon nanofiber-copper composites fabricated by electroplating. *Electrochem. Solid-State Lett.* **2004**, *7*, C25, doi:10.1149/1.1644354.

21. Arai, S.; Endo, M. Various carbon nanofiber-copper composite films prepared by electrodeposition. *Electrochem. commun.* **2005**, *7*, 19–22, doi:10.1016/j.elecom.2004.10.008.

22. Arai, S.; Osaki, T. Fabrication of copper/multiwalled carbon nanotube composites containing different sized nanotubes by electroless deposition. *J. Electrochem. Soc.* **2014**, *162*, D68–D73, doi:10.1149/2.0971501jes.

23. Song, D.; Zhou, J.; Jiang, W.; Zhang, X.; Yan, Y.; Li, F. A novel activation for

electroless plating on preparing Ni/PS microspheres. *Mater. Lett.* **2009**, *63*, 282–284, doi:10.1016/j.matlet.2008.10.011.

24. Tuukkanen, S.; Välimäki, M.; Lehtimäki, S.; Vuorinen, T.; Lupo, D. Behaviour of one-step spray-coated carbon nanotube supercapacitor in ambient light harvester circuit with printed organic solar cell and electrochromic display. *Sci. Rep.* **2016**, *6*, 1–9, doi:10.1038/srep22967.

25. Zhou, W.; Belay, A.B.; Davis, K.; Sorloaica-Hickman, N. Transparent conductive film fabrication by carbon nanotube ink spray coating and ink-jet printing. In *2012 38th IEEE Photovoltaic Specialists Conference*; IEEE, 2012; pp. 002324–002327.

CHAPTER 6: CONCLUDING REMARKS AND RECOMMENDATIONS

CHAPTER 6: CONCLUDING REMARKS AND RECOMMENDATIONS

In this thesis, the spray-coating method was successfully integrated into the MPM to achieve the fabrication of metallic copper and the metal oxide LCO. In both cases, aqueous solutions involving metal complexes were facilely prepared and required no additional modifications to improve their applicability. The stable solutions could be stored for over six months without the formation of precipitates and could be easily spray-coated without forming any clogging solids in the nozzle of the airbrush. The advantages of using aqueous precursor solutions cannot be understated. Currently, industries and researchers around the world are putting more effort in limiting the introduction of volatile organic compounds (VOCs) into the ecosystem and reduce the health risk and fire hazards associated with the use of VOCs. Therefore, the use of aqueous-based precursor solutions to fabricate functional thin films is very important.

The spray-coating procedures were easily carried out using a simple setup involving an airbrush, a hot plate, and an air compressor. Therefore, the use of such cheap and uncomplicated experimental setups is not only an advantage for the industries as they try to minimize production-cost, but also a representation that the MPM could be used as the functional thin films' fabrication method of choice in any part of the world, without the state-of-the-art facilities. This is a practical example of a potential application of the MPM in developing countries such as Namibia and I believe that this work will contribute to the industrialization of Namibia.

The results for the studies of this thesis are briefly summarized in the subsequent sections of this chapter.

Fabrication of a highly-conductive and well-adhered thin film of copper

The fabrication of a highly-conductive and well-adhered copper thin film was successfully fabricated for the first time by heat-treating a precursor film obtained by the spray-coating

method utilizing an aqueous precursor solution involving Cu(II) complexes. The spray-coating was done in air at ambient temperatures and pressures. By selectively designing the Cu(II) complexes in the coating solution, the fabrication of a highly conductive thin film of copper could be facilitated *via* the simultaneous thermal decomposition of the organic materials derived from the ligands and the reduction of the Cu^{2+} to metallic copper, without the application of any reducing atmospheres such as the use of H_2 gas. However, because metallic copper is easily oxidized, the heat-treatment of the precursor film needs to be carried out under a non-oxidizing atmosphere. In this study, the precursor film that formed on the substrate at 180°C in the air was heat-treated at 350°C and post-annealed at 400°C by placing an identical-sized glass on top, under Ar gas flow in a tubular furnace.

The resultant thin **F"$_{mix}$** of 100 nm thickness has an adhesion strength and electrical resistivity of 37(7) MPa and 3.8(6) × 10^{-5} Ω cm, respectively, and it was obtained on an insulating quartz glass substrate without substrate activation. In addition, the reflectance of the thin film is more than 90% in the far-infrared region. Pending additional investigations, the copper thin films fabricated *via* the current procedure can be useful as excellent electrical conductors, glass coatings for electromagnetic shielding, and coatings for thermal collectors, heat evacuators etc. Therefore, the coupling of the spray-coating method to the MPM has great potential as a simple and effective procedure for the fabrication of thin films for metallic copper on a thermally-stable substrate.

Recommendations

The fabrication of a highly-conductive and well-adhered thin film of copper right after the spray-coating procedure is an interesting future prospect of this study. Therefore, it is highly recommended that the subsequent studies in the line of this work must focus on minimizing the involved annealing temperatures.

Thin film fabrication of layered-rock-salt $LiCoO_2$ on a non-crystalline quartz glass substrate

To the best of our knowledge, the fabrication of an LCO thin film on a quartz glass substrate has not been reported up-to-date. Based on the unavailability of reports on this procedure, we suspect that fabrication of LCO on a quartz substrate by a wet-chemical process is challenging due to a possible undesirable reaction between the Li^+ ion and the quartz glass, as proved results for the $\mathbf{F_{spin}}$ film. In this thesis, the principle of the spray-coating method has been elaborated in the first chapter. The modifications of the atomized droplets during a flight between the atomizer and the substrate leads to the deposition of a partially dried precursor on the substrate. Therefore, using this knowledge, if we can limit the Li^+ ion/ quartz glass interaction by forming a partially dried LCO precursor during the spray-coating procedure, fabrication of an LCO thin film on a quartz glass substrate will be a success.

By spray-coating an aqueous ammonia solution containing $LiCH_3COO$ and $Co(CH_3COO)_2$ onto a quartz glass preheated to 180°C, the XRD measurement revealed that the deposited precursor film was amorphous in nature. Heat-treating the precursor film at 500°C for a short period of 0.5 h led to the formation of an LCO thin film $\mathbf{F_{spray}}$. XRD and Raman analyses revealed that the formed LCO has a layered-rock-salt structure which is usually characterized by prolonged annealing procedures at temperatures as high as 900°C. Therefore, the employed procedure was effective in the fabrication a thin film of HT-LCO at a relatively lower temperature and, on a non-crystalline quartz glass substrate.

The SEM image of $\mathbf{F_{spray}}$ showed that that the LCO grains in the film are isolated and this might be the contributing factor to the non-conductivity of the film. However, because a thin film of LCO has been formed on the quartz substrate *via* utilizing the spray-coating procedure, a film of LCO could be facilely fabricated by employing spin-coating, improving grain connectivity and therefore promoting Li^+ ion diffusion in the matrix. Hall-Effect measurements

indicated that the resultant film $\mathbf{F_{ss}}$ showing an electrical resistivity of 35(2) Ω cm, has properties of a *p*-type semiconductor with a carrier concentration and carrier mobility of 8(2) × 10^{16} cm^{-3} and 2(1) cm^{-2} V^{-1} s^{-1}, respectively.

The above results presented another superiority of the spray-coating method and its incorporation in the MPM to effectively fabricate LCO thin films on a quartz glass substrate, which proves to be challenging by using other coating methods such as the spin-coating.

Recommendations

The formation of poorly-connected LCO grains in the $\mathbf{F_{spray}}$ film can be attributed to the high surface-roughness of films obtained *via* the spray-coating method. Therefore, in future studies, the variation of spray-coating parameters introduced in chapter 1 must be investigated in order to achieve the fabrication of a conductive LCO thin film without employing spin-coating.

Fabrication of MWCNT/Cu thin films and recommendations

The fabrication of MWCNT/Cu composite thin films is another promising area attempted in this thesis. With a simple addition of the MWCNT to the solution $\mathbf{S_{mix}}$ used to fabricate the highly-conductive and well-adhered film of copper, composite thin films of multi-walled carbon nanotubes (MWCNTs) and Cu on quartz glass substrates could be easily fabricated onto quartz glass substrates. The crystal structures of the resultant composite films were successfully analyzed by XRD and, the co-presence of MWCNTs and Cu grains was confirmed from the FE-SEM images. From the coating solution with an MWCNT volume fraction of 10%, the resultant film of 110 nm thickness has an adhesion strength and electrical resistivity of 21(7) MPa and 4.8(1) × 10^{-5} Ω cm, respectively. This composite thin film has a reflectance of more than 70% in the far-infrared region.

This result showed the potential of the spray-coating method to be used for the fabrication of MWCNT/Cu composite thin films. However, further investigation for the functionality of these thin films such as in the measurements for electrical resistivity versus temperature needs to be conducted in the near future.

Fabrication of functional thin films from Namibian natural resources, in Namibia

The work presented in this thesis outline how the spray method can be successfully utilized for the fabrication of the Cu and LCO thin films and the MWCNT/Cu composite thin film. In conclusion of this thesis, the direct link between the application of spray-coating in Namibia will be discussed in term of Scheme 1 given below, using copper as an example.

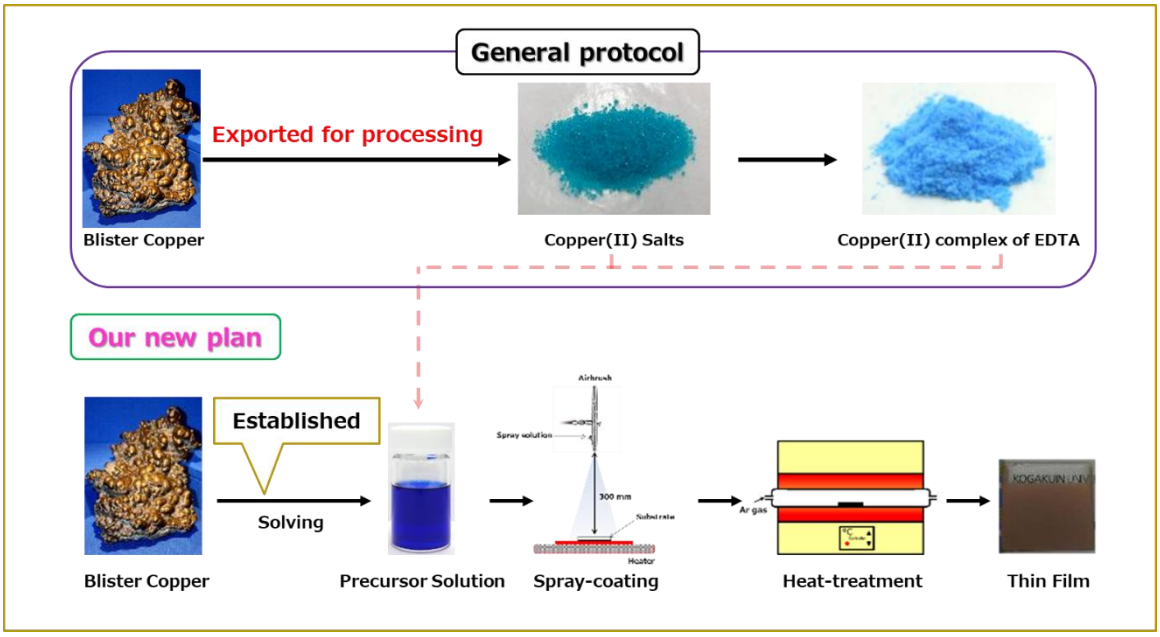

Figure 1. Proposed new route for the fabrication of a copper thin film. The general protocol involves the preparation of Cu(II) salts and complexes from processed copper. This means that the blister copper produced in Namibia are always exported to other countries for final processing. However, with the new plan by our research group, the method to directly convert blister copper into the precursor solution involving Cu(II) complexes has been established. This will significantly reduce the exportation of raw materials from Namibia.

研 究 業 績 書

Ⅰ．審査付論文
番号を付して、著書名(学位申請者にアンダーライン)、論文名、学協会誌名、巻(号)、最初と最後のページ、発表年(西暦)を記載すること。
Ⅱ．その他の研究論文(著書、学術雑誌,研究機関への研究報告,解説など)
番号を付して、著書名(学位申請者にアンダーライン)、論文名、学協会誌名、巻(号)、最初と最後のページ、発表年(西暦)を記載すること。
Ⅲ．口頭研究発表
国外と国内に分けて、番号を付して、研究者名(学位申請者にアンダーライン)、学会名、開催地、発表年月日を記載すること。
Ⅳ．学会（委員会関係も含む）および社会における活動状況等
活動期間と学会、委員会名を記載すること。
Ⅴ．その他の業績（特許・資格・賞罰も含む）
年月日と業績内容を記載すること。

Ⅰ．審査付論文

Publications

1. Philipus N. Hishimone, Hiroki Nagai, Masato Morita, Tetsuo Sakamoto and Mitsunobu Sato
Highly-Conductive and Well-Adhered Cu Thin Film Fabricated on Quartz Glass by Heat Treatment of a Precursor Film Obtained Via Spray-Coating of an Aqueous Solution Involving Cu(II) Complexes. *Coatings*, **8(10)**, **352** (**2018**).

2. Philipus N. Hishimone, Kenta Watarai, Hiroki Nagai and Mitsunobu Sato
Thin Film Fabrication and Characterization of a Layered rock salt $LiCoO_2$ on a Quartz Glass Spray-coated with an Aqueous Ammonia Solution Involving Metal Acetates. *Coatings*, **9(2)**, **97** (**2019**).

3. Enos M. R. Kiremire,Likius S. Daniel and Philipus N. Hishimone
Numerical assignment of shapes and symmetries of borane molecules and ions. *Oriental Journal of Chemistry*, **30(3)**, **923-932** (**2014**).

Ⅱ．その他の研究論文(著書)

Book chapter

1. Philipus N. Hishimone, Hiroki Nagai, and Mitsunobu Sato
Methods of fabricating thin films for energy materials and devices. Lithium-ion Batteries - Thin Film for Energy Materials and Devices. Intech, ISBN 978-953-51-6313-8 (Accepted, 18 March 2019).

研 究 業 績 書

Ⅲ. 口頭研究発表

Oral presentations

International conferences

1. Philipus N. Hishimone, Hiroki Nagai, and Mitsunobu Sato: “Fabrication of a MWCNT/Cu composite Thin-Film From an Aqueous Solution Containing Copper(II) Complexes and MWCNT by the Molecular Precursor Method.” Global Young Investigator Forum. The 12th International Conference on Ceramic Materials and Components for Energy and Environmental Applications (CMCEE 2018). Suntec Convention & Exhibition Centre, Singapore. (22-27 July 2018)

2. Philipus N. Hishimone, Hiroki Nagai, Tomohiro Yamaguchi, Takeyoshi Onuma, Tohru Honda and Mitsunobu Sato: “Fabrication of Cu(I) Oxide Thin Film by Using a Spray Method of an Aqueous Solution Containing a Cu(II) Complex.” The 23rd International SPACC Symposium. Okayama University of Science, Okayama, Japan. (21-23 November 2016)

Domestic conferences

1. Philipus N. Hishimone, Hiroki Nagai, Mitsunobu Sato: “Fabrication of Copper Thin Films by Using a Spray Method of Aqueous Solutions Involving Copper(II) Complexes.” The 66th Conference of Japan Society of Coordination Chemistry. Fukuoka University, Fukuoka, Japan. (10-12 September 2016)

Poster presentations

International conferences

1. Philipus N. Hishimone, Hiroki Nagai, Norio Baba and Mitsunobu Sato: “Electrical Resistance of a MWCNT/Cu Composite Thin-Film Fabricated From an Aqueous Precursor Solution Containing Cu(II) Complexes and MWCNT.” The 16th International Symposium on Advanced Technology. Kogakuin University, Tokyo, Japan. (01-02 November 2017)

2. Philipus N. Hishimone, Enos M. R. Kiremire and Likius S. Daniel: “On the synthesis and characterization of Zn(II) and Cd(II) complexes of bis(2-acetylpyridine)- thiocarbohydrazone for biological evaluation against the malaria parasite.” The joint symposia of the 1st IFAEE and the 21st International SPACC symposium. Kogakuin University (Tokyo Urban Tech.), Tokyo, Japan. (31 October-03 November 2014)

研 究 業 績 書

Ⅴ．その他の業績

Academic awards

1. Best Student Award. Certificate of Recognition for Social Contribution Activities, 2018 Academic Year (Award Ceremony: 22 January 2019). Education Support Section, Science Education Center, Kogakuin University, Tokyo, Japan.

2. Best Poster Presentation Certificate (01 November 2017). The 16th International Symposium on Advanced Technology. Kogakuin University, Tokyo, Japan.

3. Research Student Certificate (October 2015-March 2016). Kogakuin University, Tokyo, Japan.

4. Japanese Language Intensive Training Certificate (April 2015-September 2015). University of Electrocommunication (UEC), Chofu, Tokyo, Japan.

5. Ministry of Education, Culture, Sports, Science and Technology (MEXT) Scholarship. (April 2015-March 2019). UEC and Kogakuin University, Tokyo, Japan.

ACKNOWLEDGMENTS

Firstly, I would like to offer my gratitude to the government of Japan through the Ministry of Education, Culture, Sports, Science, and Technology (**MEXT)** for granting me the opportunity to further my studies in Japan. I would like to offer my sincere appreciation to my supervisor **Prof. Mitsunobu Sato** for his great vision, support and guidance in all aspects of my studies. Many thanks for the advice in the field of Science and technology and patience with my progress. I would also like to extend my gratitude to **Prof. Hiroki Nagai** for his advice, revision of my work and encouragement. Thank you for being a great role model. Many thanks to **Dr. Chihiro Mochizuki** for her invaluable support. I would like to thank the professors at Kogakuin University (**KU**) for their support and kind words of encouragement. Particularly, **Prof.Tetsuo Sakamoto** and **Prof. Masato Morita** for their valuable input to my first publication, **Prof. Tohru Honda**, **Prof. Yamaguchi**, **Prof. Takeyoshi Onuma**, **Prof. Ichiro Takano** and **Prof. Norio Baba** for allowing me to use the various advanced instruments at their Laboratories. I Would like to thank the examiners **Prof. Toshinori Okura**, **Prof. Hidetaka Asoh** and **Prof. Kazuaki Kudo** for their valuable time and very important comments during the reviewing stages of my thesis. My sincere gratitude to **Prof. Koji Kazuma** for introducing me to the Japanese culture through Kendo. I would like to thank the **Student Support Section of KU** for their support and assistance with the procedures and lots of paperwork required for a comfortable settling in Japan.

I would like to express my sincere gratitude to my senior **Dr. Daniel Shipwiisho Likius** for introducing me to Japan and the Japanese academic life, his continued support and motivation during my Ph.D. studies. Many thanks to all members of our laboratory during my 4 years period in Japan (2015 –2018). Specifically, I would like to thank **Mr. Tatsuya Suzuki**, **Mr. Hsiang-Jung Wu** and **Mr. Kenta Watarai** for their assistance with some measurements and discussions. To my fellow Namibian students, **Mr. Paulus Shigwedha**, **Ms. Alina Uusiku,**

and **Natague H. Shafudah**, many thanks for the support, encouragement and the shared vision to succeed in our academic work and uplift the Namibia society through Science and technology. During my stay in Japan, I have experienced memories of a lifetime, with many great friends. Many thanks to **Ms. Mariko Mori**, **Ms. Kumi Yamamoto**, and the **Akimoto family**.

I would like to thank my Mentor **Prof. E. M. R. Kiremire** for his great vision, encouragement and full support from my early years in the academic field. I would like to thank the former VC of the University of Namibia (UNAM), **Prof. Lazarus Hangula**, the current VC **Prof. Kenneth Matengu** for their support and words of encouragement. Many thanks to **Dr. Erold Naomab**, **Prof. Frednard Gideon**, **Dr. Veikko Uahengo**, **Prof. Edet Archibong**, **Dr. Petrina Kapewangolo**, **Mr. Song Wei** and all staff members of the **Department of Chemistry and Biochemistry**, The UNAM's **Staff Development** and **HR Office** for their support during my study leave.

I would like to wholeheartedly thank my beloved family for a great sense of patience and understanding, the support and encouragement during my time in Japan. Many thanks to my late grandmother **Fulasina yaVaminauka** for the love and support with my studies. Muchas gracias to my mother, **Ufemia Kafute. N. Josef** for your great vision, strength, and determination to get me into school and ensure that I achieve the best of academic success. Because of your humbleness and being a people's person, great family friends became important contributors to my long but fruitful journey in the academic field. Many thanks to **Mee Frieda yaNghipetwa**, **Mr. Nicolaus Gabriel and his family**, and **Mr. Jesaya Hangula his family.** My sincere gratitude to **Mr. Paulus Hangula** and **Ms. Sonia Pius** for their inspiration during my early years of University-life. Many thanks to **Margareth M. A. Heita**, **Jonas Lungameni**, **Moses Pius**, **Albert Shikongo**, **Jesaya Shilunga**, **Natalia Ananias** and **Celine Mukakalisa** for the support and encouragements.